Technical Report Documentation Page

1. Report No	2 Government Accession No	3 Recipient's Catalog No
CR-145108		

4 Title and Subtitle	5 Report Date
AN AVIONICS SENSITIVITY STUDY, VOLUME II, Evaluation of Airborne Navigation System Performance During RNAV/MLS Transition	SEPTEMBER 1976
	6 Performing Organization Code
7 Author(s) Heine, Walter	8 Performing Organization Report No
9. Performing Organization Name and Address SYSTEMS CONTROL, INC. (Vt) 1801 Page Mill Road Palo Alto, CA 94304	10 Work Unit No (TRAIS) 11 Contract or Grant No NAS 1-14144
12 Sponsoring Agency Name and Address LANGLEY RESEARCH CENTER National Aeronautics and Space Administration Hampton, VA 23365	13 Type of Report and Period Covered Final August 1975-September 1976 14 Sponsoring Agency Code

15 Supplementary Notes

16 Abstract

A computer simulation developed by Systems Control, Inc. (Vt) [SCI (Vt)], was modified to generate a suitable data base for performance of an avionics sensitivity study during RNAV/MLS transition. The avionics sensitivity data provides information necessary to establish requirements for additional guidance law design during transition and to establish airspace requirements for maneuvering to null out any residual RNAV errors upon MLS transition. The data base is also beneficial as planning information for subsequent flight testing.

The parameters varied during the generation of the data base include flight profile, error source content and magnitude, ground facility location, runway/flight path orientation and navigation mode (INS updated with DME/DME or INS updated with VOR/DME). The avionics, autopilots and aircraft dynamics corresponded to the existing TCV-737 aircraft. Significant transients were observed during MLS transition, primarily in the vertical channel. The transients are dependent on RNAV delivery errors, MLS filter initialization and magnitude of range-dependent MLS errors (azimuth and elevation). These transients have a significant impact on airspace requirements and operational procedures in the RNAV/MLS environment.

17. Key Words	18. Distribution Statement
AREA NAVIGATION RNAV/MLS TRANSITION TERMINAL AREA CURVED APPROACH MICROWAVE LANDING SYSTEM	

19 Security Classif. (of this report)	20. Security Classif. (of this page)	21. No. of Pages	22. Price
Unclassified	Unclassified	111	

Form DOT F 1700.7 (8-72) Reproduction of completed page authorized

ACKNOWLEDGEMENTS

This study, performed for the National Aeronautics and Space Administration, Langley Research Center, is the second part of a three-part study entitled, "An Avionics Sensitivity Study." Appreciation is extended to all the Langley Research Center personnel who provided assistance and insight into the individual components of the TCV avionics. Appreciation is particularly extended to Thomas M. Walsh and his staff.

Particular acknowledgement is given to the following Systems Control, Inc. (Vt) staff members for their contributions:

- Ed Jones (Analysis/Program Debugging)
- Jennifer Mohr (Computer Program Development and Debugging)
- Deborah Buenz and Clare Walker (Report Preparation, Editing and Publication)

Appreciation is also extended to Rick Tompkins who performed the original program development and analysis.

TABLE OF CONTENTS

I. INTRODUCTION

In recent years, several new advancements have been made in the area of navigation to enable the pilot to navigate more accurately and with greater efficiency. These advancements have arisen because of the requirement for improved enroute navigation and landing systems to provide increased safety and greater capability for instrument flight rule (IFR) flights in adverse weather conditions. The desire for flight capability during IFR conditions arises from increased demand for air travel under all weather conditions. Furthermore, increased air traffic densities place greater demands on safety which has a potential impact on improved navigation accuracy requirements.

The equipment modifications to provide the navigation improvements range from airframe avionics changes for implementation of new enroute navigation techniques, to modified landing systems which provide greater precision in final approach and landing. Two such systems that this report is concerned with are the area navigation (RNAV) concept and the Microwave Landing System (MLS). Both of these concepts are elements of the National Airspace Systems (NAS) Upgraded Third Generation Plan. The area navigation system concept allows for flight between predetermined navigation waypoints not necessarily coincident with VOR/DME ground stations utilized if, in fact, the RNAV support is supplied by the VOR/DME navigation system. RNAV can also be supported by other navigation systems such as LORAN-C, Omega, and GPS which are more amenable to the point-to-point navigtion concept associated with RNAV. The Microwave Landing System is an improved landing aid which can provide 4-D guidance with accuracies sufficient to provide Category III-C landings. With suitable avionics the MLS mode of navigation can be utilized as a highly accurate RNAV system in the terminal area.

To date, many studies have been performed that concentrate on either the area navigation concept or the Microwave Landing System. However, very little has been done in the way of examining the aircraft transition from the RNAV region to the MLS region. Although both systems are capable of providing three-dimensional position

information, the accuracies of the two systems are quite different. These differences may produce considerable transients, or the RNAV delivery accuracies at the MLS coverage boundary may be unacceptably large, under certain conditions. These potential problems provide the motivation for the study documented in this report.

Another motivating factor is to provide analytical support to the on-going terminal configured vehicle (TCV) program being conducted at the NASA Langley Research Center. This study includes evaluation of the RNAV/MLS transition problems. The TCV aircraft is a Boeing 737 equipped with an inertial RNAV system updated with VOR/DME or DME/DME. Sensors and software are also available onboard to provide MLS guidance.

These motivating factors form the basis in establishing the objectives of this avionics sensitivity study. The primary objective is to generate statistical data regarding aircraft position errors in the RNAV/MLS transition region. This data is to be generated for the TCV aircraft with the navigation components aboard this particular aircraft. The statistical data is to be generated such that the sensitivity to navigation errors and flight geometries can be determined.

The primary purpose for generating the data is to provide insight into the behavior of the aircraft in the RNAV/MLS transition region. Knowledge of aircraft behavior in this region due to navigation errors is desirable for subsequent guidance law and airspace design. The avionics sensitivity data will provide the information necessary to establish requirements for additional control law design during transition and to establish airspace requirements for maneuvering to null out any residual RNAV errors upon MLS transition. Availability of the statistical data will also provide insight into the evaluation of the feasibility of RNAV/MLS transition for various geometries, flight profiles and error parameter magnitudes. Feasibility of the various profiles and geometries aid in the establishment of guidelines for route design in the RNAV/MLS transition region. Finally, the data base is beneficial for providing insight into the development of subsequent flight test plans.

To meet the stated objectives, a computer simulation developed by Systems Control, Inc. (Vt) [SCI (Vt)] was appropriately modified. The digital simulation provides data regarding the expected aircraft position errors along any route or route position for the TCV aircraft in both the RNAV and MLS regions. It is possible, with the digital

simulation, to evaluate navigation system performance for any operational scenario and range of error parameters. In this manner, the feasibility of proposed navigation and facility locations and approach path/runway configurations can be evaluated in a cost-effective manner.

The flight profiles of the current evaluation of navigation system performance are restricted to flight paths typical of conventional take-off and landing (CTOL) aircraft. However, navigation facility locations are selected to give worst-case error possibilities. The error sources have been selected to be compatible with the recommended error budget values as discussed in AC 90-45A [1]. The relative amount of random bias and noise contained within the error budget values, however, is varied so that it is possible to evaluate the effect of each.

Through judicious quantification of the variables in the study, a data base is generated for subsequent applications and analysis. The data is basically presented in the form of plots and graphs. The organization of the report is as follows. The second section presents the motivation for implementing an ensemble or covariance type digital simulation as opposed to a Monte Carlo type. This discussion includes a presentation of the advantages and disadvantages of each of the simulation techniques. The discussion leads into the presentation of the RNAV and MLS simulations. Supporting analysis is presented in Appendix A. Chapter II ends with a discussion of the simulation capabilities.

The analytical approach is presented in Chapter III. The section begins with a discussion of the application of the ensemble simulation to meet the study objectives as stated in this chapter. To meet the study objectives it is necessary to carefully design a suitable experimentation test plan. The test plan for the study documented in this report is presented in the remainder of Chapter III with supporting details presented in Appendix B.

The analytical results of the sensitivity study are presented in Chapter IV. The primary quantities of interest are the cross-track and vertical deviation time histories through the RNAV/MLS transition as a function of the various study parameters. These time histories are presented in the form of plots with corresponding narrative discussing the contents of each.

The study conclusions are presented in Chapter V with corresponding recommendations presented in Chapter VI.

"Page missing from available version"

p.4, p.5

Generally, two techniques are associated with simulation experimentation. These are Monte Carlo analysis and ensemble analysis (covariance propagation). The former represents the occurrence of a single random event whereas the latter represents an ensemble of events occurring simultaneously. For example, in a Monte Carlo simulation, a single aircraft is executing a simulated flight along a prescribed flight path driven by errors representative of a single source. In the ensemble simulation, an ensemble of aircraft are traversing the prescribed flight path driven by errors representing the ensemble average of a particular source. The primary difference between these two techniques is that the analytical models of the Monte Carlo simulation can be either linear or nonlinear, whereas the analytical models of the ensemble simulation must be linearized. Hence, the Monte Carlo simulation can be utilized to evaluate all effects whether linear or nonlinear. Judicious modelling must be employed for the linearized ensemble simulation to retain realism. The primary advantage of the ensemble simulation is that statistical data is achievable through a single simulation execution, whereas, similar statistical data is achievable from the Monte Carlo simulation only through a large number of computer runs. The level of confidence in the Monte Carlo generated statistics is directly dependent on the sample size. Hence, this approach is potentially more costly than using covariance propagation techniques, especially for the generation of preliminary statistical data.

For this study the linearized ensemble approach was utilized to generate the desired statistical data. For the system under investigation the linearization assumption is not overly restrictive. This is due to the fact that suitable linear navigation error models exist and the navigation filters and the controls already exist in linear form. Furthermore, since this is essentially a navigation system evaluation, the aircraft dynamics and autopilots can be represented by simplified linear models. The primary nonlinearities omitted in the analysis are the control bounds. However, these nonlinearities will not appreciably affect the ensemble results.

The sensitivity analysis of this study is concerned with aircraft performance during transition from an area navigation (RNAV) environment to the Microwave Landing System (MLS) coverage region. The ensemble simulation

development therefore involves a separate analysis for the RNAV and MLS avionics. Transition is achieved by retaining those elements of the covariance matrix common to both systems (aircraft dynamics, autopilot, and so on) at MLS lock-on and substituting the RNAV-related elements with MLS-related elements. In this manner the covariance propagation across the MLS coverage boundary will represent the actual situation. This approach precludes any potential blending of RNAV and MLS signals. Therefore the discussion regarding simulation development is presented in two parts - RNAV and MLS simulation development.

Generally, the analytical models were derived from existing literature on the TCV-737 aircraft system [1-4]. Where insufficient information was available to derive adequate analytical models other suitable sources were consulted [5-7](INS, VOR, DME, MLS). As indicated previously, almost all of the navigation filter and the control equations (except for control bounds) appear in linear form, hence, simplifying the linearization process. The aircraft dynamics are assumed to represent simple point mass motion and are represented by second order equations of motion in both the vertical and lateral directions.

The section organization is as follows. Section 2.2 presents a detailed discussion of the simulation model development. This includes the models of the RNAV and MLS portions of the simulation. Block diagrams are presented to indicate information flow in these two systems. The assumptions and derivation of the covariance propagation equations are then presented. Section 2.3 describes in detail the features of the simulation design. These features include run time waypoint and station specification, interactive control logic, free format input, printer and CALCOMP plotting capabilities and others. Finally, Section 2.4 presents a summary of the overall simulation capabilities.

2.2 SIMULATION MODELS

2.2.1 RNAV Simulation

As indicated in Section 2.1, the basic TCV-737 linear ensemble simulation consists of two parts. The first is the RNAV simulation and the second is the MLS simulation. The purpose of this subsection is to present, with the aid of a block diagram, the details of the RNAV simulation. The details with regard to mathematical expressions for each component of the simulation are presented in Appendix A.

Figure 2.1 is the block diagram describing the RNAV simulation. The components of this particular simulation include an Inertial Navigation System (INS), second order lateral and vertical complementary filters, lateral and vertical autopilots, barometric altimeter and aircraft dynamics. The lateral inertial velocity, δV_{N_I} and δV_{E_I}, and vertical inertial acceleration, α_z, serve as inputs which complement the second order lateral and vertical filters respectively. The filter estimated north and east position errors, $\hat{X}_N$ and $\hat{X}_E$, are transformed to station-referenced range, $\Delta\rho_c$, and bearing, $\Delta\theta_c$, to yield the computed measurement errors. The geometry depicting the range and bearing measurements is shown in Figure 2.2. The computed measurement errors are subtracted from the actual measurement errors and this differenced quantity is filtered after a coordinate transformation into the second order lateral complementary filter. The filter estimated lateral position and velocity states are used to compute the indicated cross-track deviation $\hat{CTD}$ and heading error, $\hat{\psi}$. $\hat{CTD}$ and $\hat{\psi}$ are used to compute the roll command ϕ which is input to the aircraft dynamics.

In the vertical channel the input to the complementary filter is the measured altitude and altitude rate as output from the barometric altimeter model. This model includes bias and noise input to a first order lag to represent the time lag characteristic of altimeters. The output is a commanded altitude rate which, together with the measured altitude form the basic input into the vertical autopilot. For 3D RNAV systems the along-track error propagates into the vertical channel as shown in Figure 2.3. The primary impact of the along-track error is to shift the vertical profile. This error source can be significant for 3D RNAV systems, especially when executing steep descent profiles (for example, a 6° STOL approach). This is due to the fact that the vertical error is proportional to the glideslope according to

$$VD = ATD \tan \gamma \qquad (2.1)$$

Hence, for an along-track error of 2780 meters (which is reasonable for RNAV systems) and a glideslope of 3°, the vertical deviation due to along-track alone is 146 meters. The output of the vertical autopilot is commanded vertical acceleration (pitch rate) which is fed into the vertical dynamic equations.

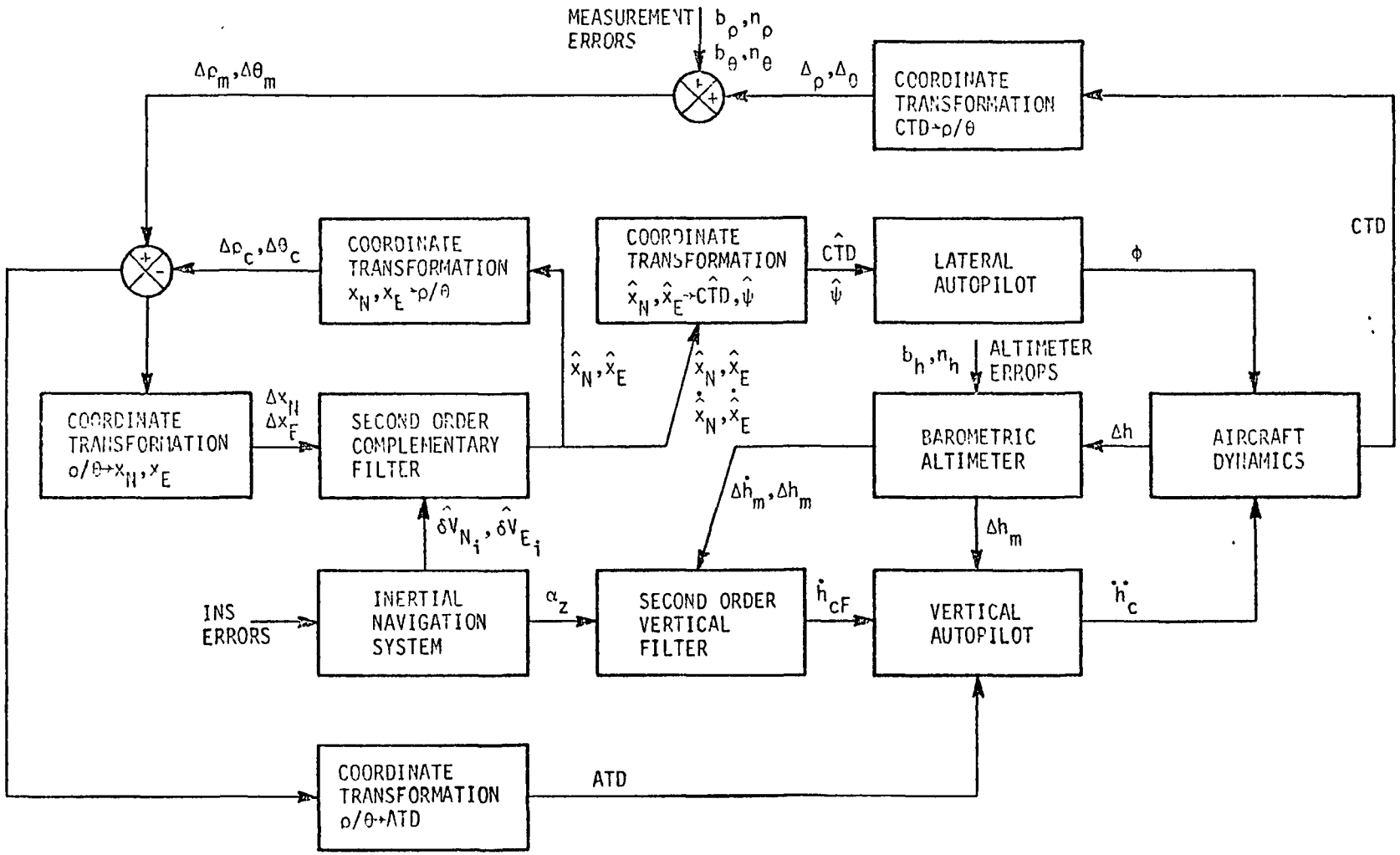

Figure 2.1 VOR/DME RNAV Simulation Block Diagram

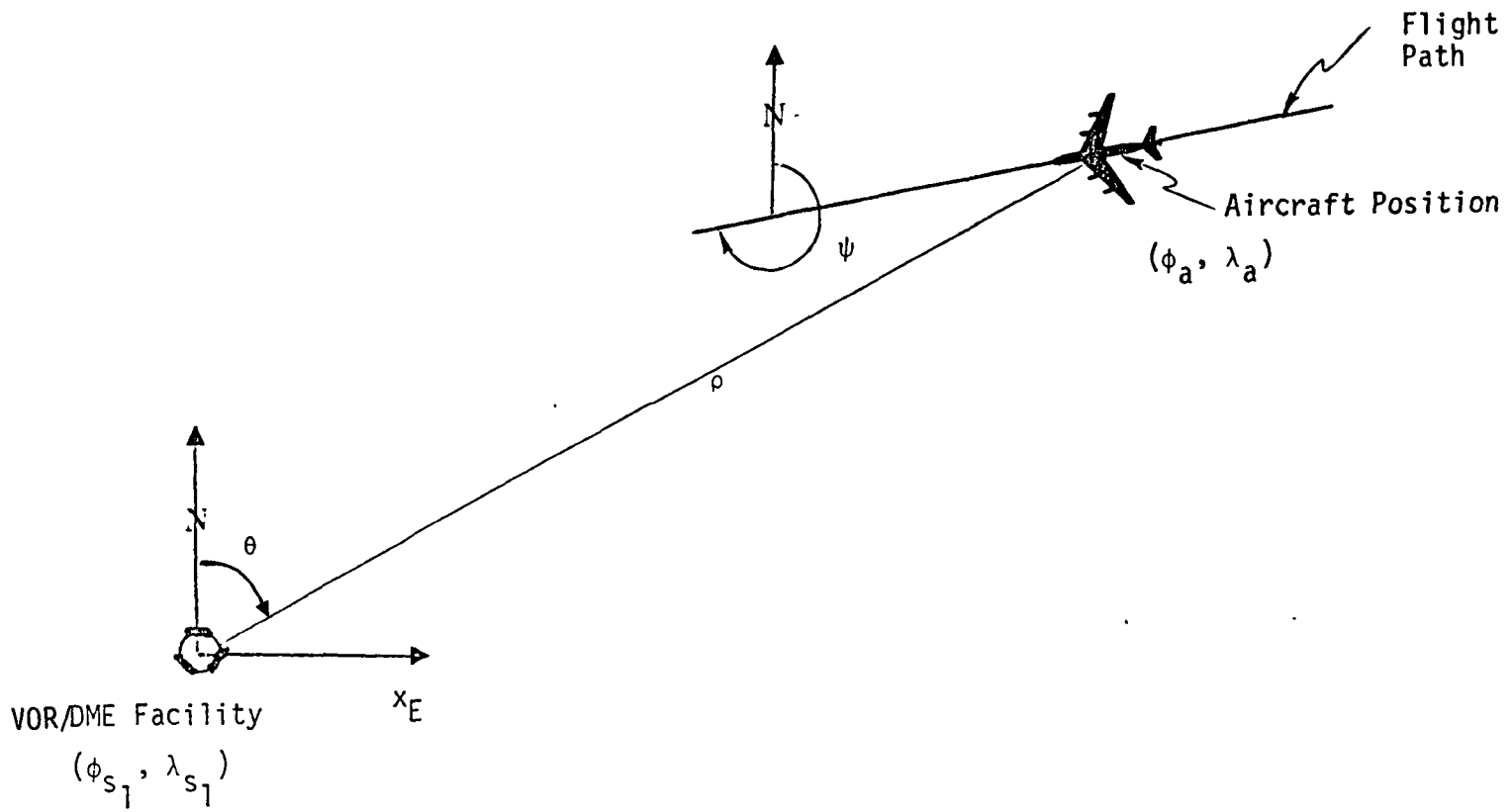

Figure 2.2 VOR/DME Facility Geometry

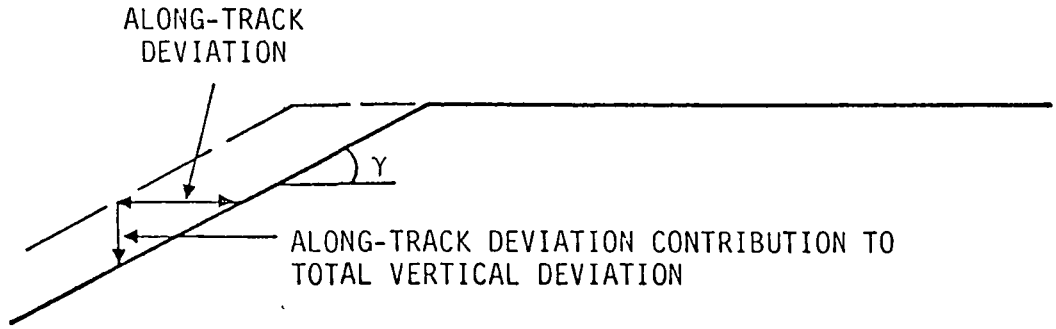

Figure 2.3 Along-Track Deviation Contribution to Total Vertical Deviation

For the current simulation the lateral autopilot and dynamics and the vertical autopilot and dynamics are each represented by second-order equations. The aircraft dynamic output is the actual cross-track and vertical deviation which is fed back to evaluate the measurements.

The error sources for the RNAV simulation consist of range and bearing noise and bias, altimeter noise and bias and INS error (platform tilt errors, accelerometer biases and drifts). For this effort the INS and altimeter errors will be fixed.

2.2.2 MLS Simulation

The flow chart depicting the MLS simulation is shown in Figure 2.4. The lateral and vertical autopilot and the aircraft dynamics are essentially the same as those of the RNAV simulation. The primary difference in the two simulations is the manner in which the guidance computations are computed from which appropriate steering commands can be generated.

The guidance computations are based on MLS-derived position measurements. The MLS measurements differ from the RNAV measurements in that they consist of range, azimuth angle and elevation angle measured with respect to a runway fixed coordinate system. Figure 2.5 schematically depicts the MLS coverage region and Figure 2.6 the corresponding measurements. Hence, several coordinate transformations are required to properly perform the guidance computations.

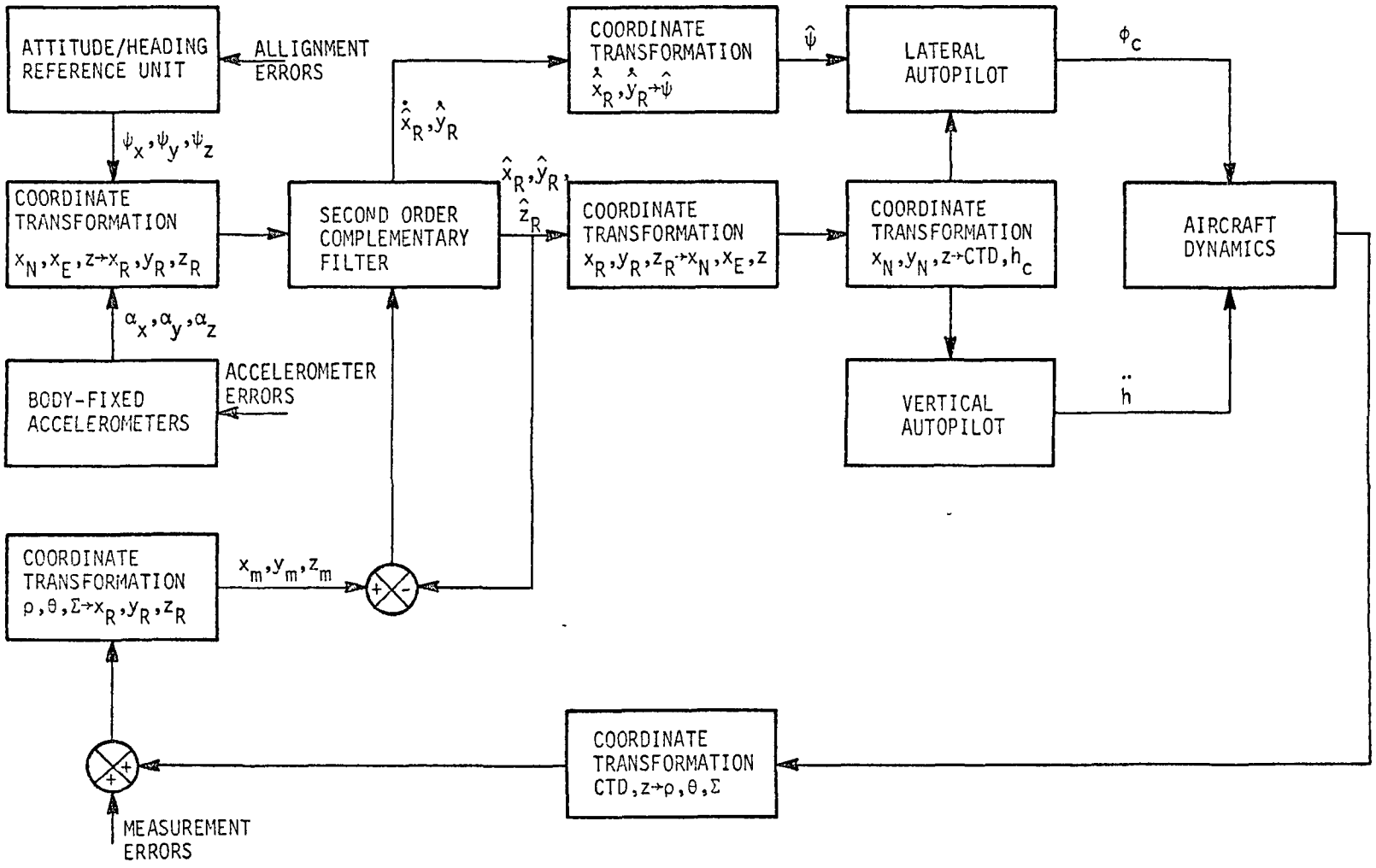

Figure 2.4 MLS Simulation Block Diagram

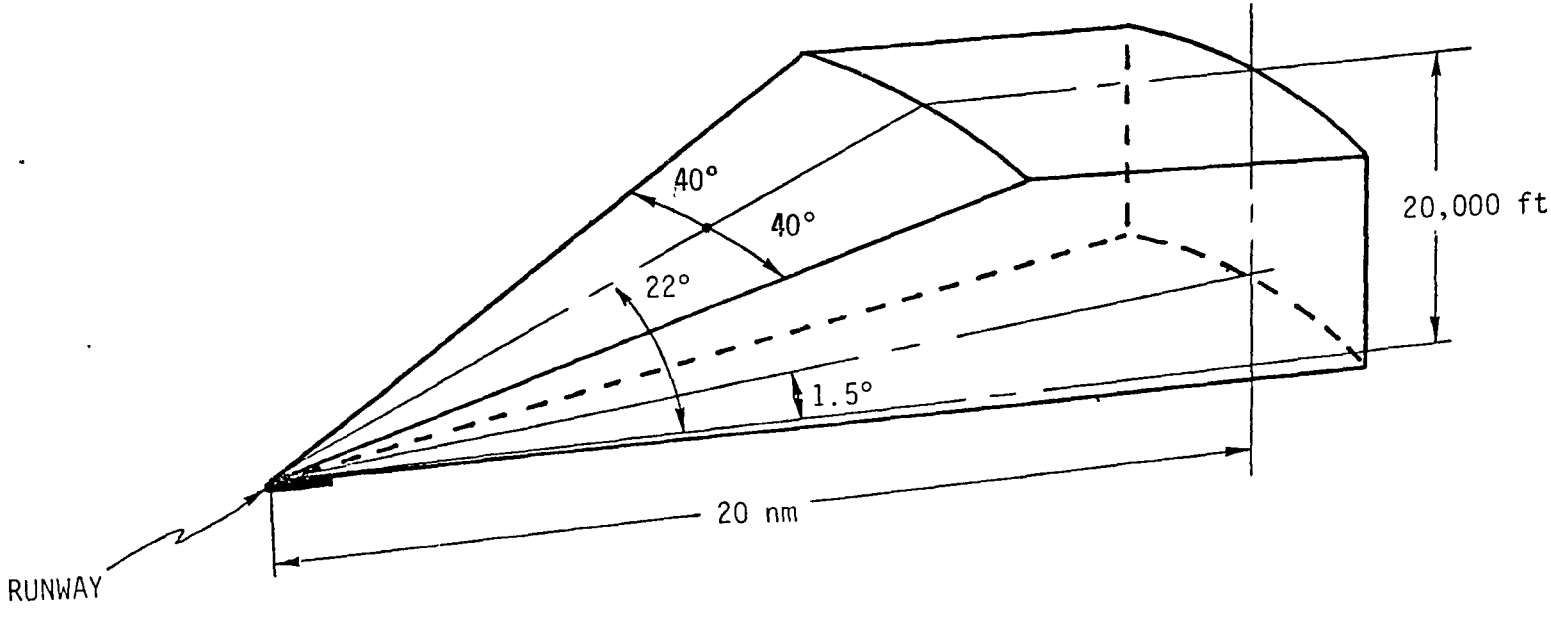

Figure 2.5 MLS Coverage Region

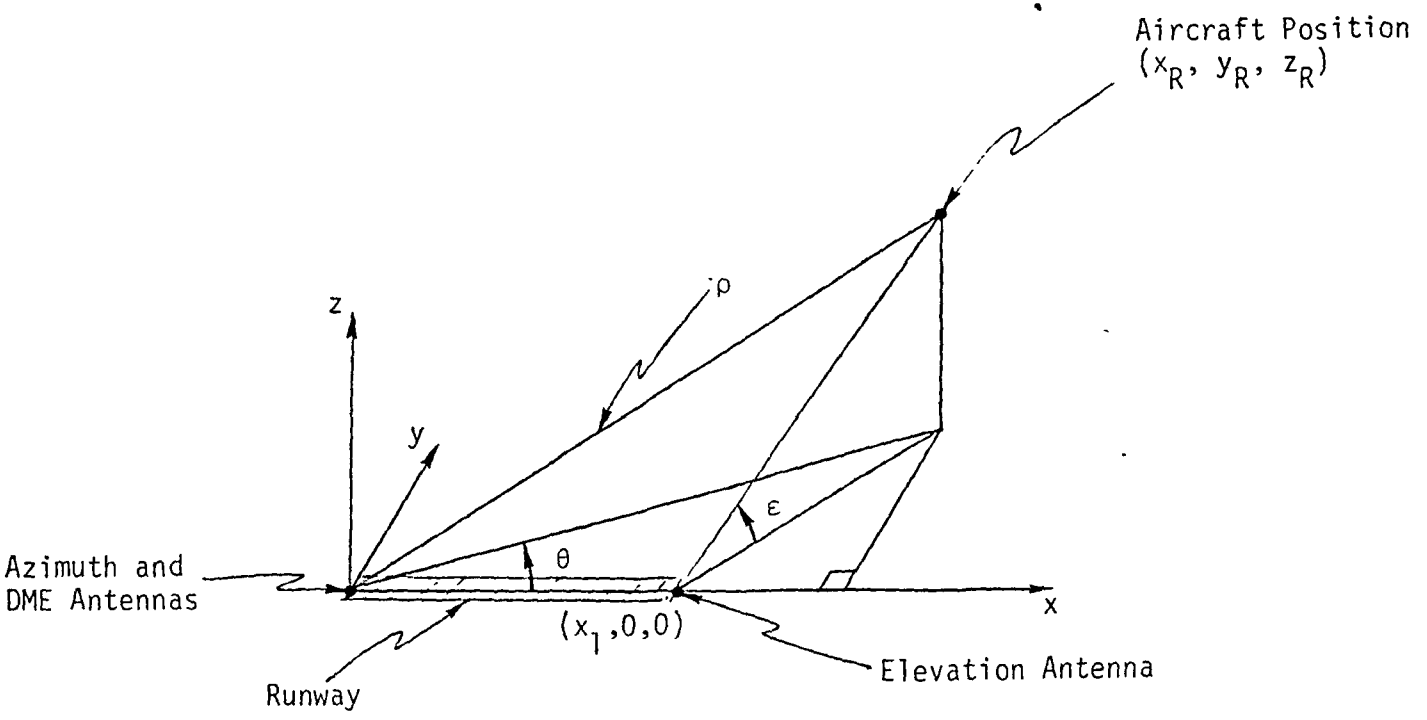

Figure 2.6 MLS Antenna Coordinate System

In the MLS mode, the second order complementary filter has as input the three acceleration components. The accelerations are derived from body fixed accelerometers. Runway-referenced accelerations are derived using aircraft attitude information derived from the attitude/heading reference unit to transform the accelerometer acceleration components. The filtered estimated position errors, $\hat{x}_R$, $\hat{y}_R$, and $\hat{z}_R$ (computed measurements) are subtracted from the MLS-derived measurements to form the second input to the second-order filter.

The filter estimated velocities are used to compute heading errors. Similarly, the filtered estimated positions are used to compute course deviations. The heading error and course deviations are then used to generate the appropriate steering commands.

The error sources for the MLS mode of operation consist of the measurement errors and errors associated with the acceleration measurements. The MLS measurement errors consist of range, azimuth and elevation bias and noise. Similarly, the alignment and accelerometer errors are represented by bias and random noise.

Currently, blending between the RNAV and MLS measurements is not envisioned. Hence, at the MLS boundary the navigation mode is assumed to transfer discretely from RNAV to MLS. The reason for this is that not much is known about blending techniques and it is uncertain what effects are to be expected at MLS transition from RNAV. The purpose of this study is to provide more insight into this problem area so that subsequent analysis can be performed with regards to the development of appropriate blending techniques.

2.2.3 Covariance Propagation

The previous two subsections have discussed the two basic simulations that make up the overall ensemble simulation for this study. Appendix A has presented the equations describing the various components of the RNAV and MLS simulations. These equations are presented in linearized form suitable for ensemble simulation implementation. The linearity assumption is the most important one regarding covariance propagation yet it is this very assumption that limits the applicability of ensemble analysis. This assumption eliminates the evaluation of system performance due to inherent nonlinearities unless these nonlinearities can be linearized without destroying realism or if they can be represented by such techniques as

describing functions. However, ensemble techniques do provide the capability of generating desirable statistical data in a cost effective manner. It is this cost effectiveness that provides the motivation for utilizing this approach.

For a dead-reckoning navigation system, such as an inertial or air data system, updated with external measurements, VOR/DME or DME/DME, the covariance propagation can be performed in one of two ways. First of all the covariance matrix can be propagated between ground-based measurement updates using the dynamics associated with the dead-reckoning system, autopilot and aircraft. The covariance would then be updated at the measurement interval using the appropriate measurement updating techniques. The covariance propagation for this approach is represented by (in discrete form) [8]

$$\text{State:} \quad x_k = \phi_{k-1}\, x_{k-1} + W_{k-1}, \; W_k \sim N(0,Q_k) \tag{2.2}$$

$$\text{Measurement:} \quad z_k = H_k\, x_k + v_k, \; v_k \sim N(0,R_k) \tag{2.3}$$

$$\text{State Estimate Extrapolation:} \quad \hat{x}_k(-) = \phi_{k-1}\, \hat{x}_{k-1}(+) \tag{2.4}$$

$$\text{Covariance Extrapolation:} \quad P_k(-) = \phi_{k-1}\, P_{k-1}(+)\, \phi_{k-1}^T + Q_{k-1} \tag{2.5}$$

$$\text{State Estimate Update:} \quad \hat{x}_k(+) = \hat{x}_k(-) + K_k[z_k - H_k\hat{x}_k(-)] \tag{2.6}$$

$$\text{Covariance Update:} \quad P_k(+) = [I-K_kH_k]P_k(-)[I-K_kH_k]^T + K_kR_kK_k^T \tag{2.7}$$

where:

x - actual state

ϕ - state transition matrix

W - process noise

The states, x, state transition matrix, ϕ, and process noise matrix, Q, are presented explicitly in Appendix A.

2.3 BASIC SIMULATION DESIGN

The simulation developed for this study was intentionally made comprehensive and flexible. It is comprehensive in that complete guidance, navigation, and control systems are included, along with models of the full complement of radio and inertial navigation sensors. Flexibility is achieved through modularity of design in conjunction with a sophisticated executive structure and user interface, which had previously been developed and verified. The executive structure provides for employing multiple iteration rates of the simulator functions (guidance, navigation, control, covariance propagation, output recording, etc.) and for accommodating large simulator core requirements in an efficient manner. The user interface permits free-format input/output. The simulation also has an interactive feature whereby the engineer may monitor, stop, correct, and resume simulation computations from a remote terminal; this feature was used extensively in the simulation development process as an efficient debugging aid.

The simulation has been designed to operate in two modes. The first is a nonlinear Monte Carlo mode which provides the capability for evaluation of nonlinear effects on a case-by-case basis. The second is the covariance propagation (ensemble) mode which provides the capability of evaluating the ensemble statistics on a single computer run basis. Execution of a large number of Monte Carlo runs will approach the statistics generated by the ensemble simulation for the same error source inputs.

2.4 SIMULATION CAPABILITIES

The purpose of this subsection is to summarize the ensemble simulation capabilities. As indicated in the introduction the primary objective for this study is to propagate aircraft position errors in the RNAV/MLS transition region. This objective is the primary driving force in the determination of the specific simulation capabilities listed here.

Although the primary application for this study is the ensemble mode it is necessary to generate the nominal trajectory. For this study the nominal is generated as an error free Monte Carlo simulation. Hence, by adding errors it is possible to determine the mean three-dimensional position errors from constant or repetitive error sources. This part of the simulation includes such nonlinearities as

z - measurements

H - measurement matrix

v - measurement noise

x - state estimate

P - error covariance matrix

Q - diagonal matrix representing process noise

K - weighting matrix

I - identity matrix

R - diagonal matrix representing measurement noise

For this particular study the errors associated with the inertial navigation system and altimeter would appear as process noise. The measurements would be VOR/DME, DME/DME or MLS. The errors associated with each of the measurements would be represented as measurement noise, for the random component, and as additional states for the bias or correlated noise component.

In the TCV-737 navigation system the inertial navigation system is updated every second with external position fixes. In the interest of conserving computation time it is desirable to integrate with a step size of at least one second or, if the system time constants permit, at a larger step size. This can be accomplished by including the measurements as part of the state and their associated noise components as process noise. Hence, the covariance extrapolation is reduced to

$$P_k = \phi_{k-1} P_{k-1} \phi_{k-1}^T + \Gamma Q_{k-1} \Gamma^T \qquad (2.8)$$

where Q_{k-1} now includes inertial navigation system, altimeter, VOR, DME, or MLS noise components as applicable. Note that the block diagrams for the RNAV and MLS simulations of the previous sections have been configured in a form suitable for application of the above covariance extrapolation. Utilizing this particular formulation negates the capability of examining the effect of update rate. However, for the current study this disadvantage is insignificant compared to the advantage gained by reduced computation time.

control bounds. The ensemble portion of the simulation provides the capability of generating the standard deviation of the position errors due to random errors about the mean. The ensemble simulation, due to the inherent linearity assumptions in the development of this type of simulation, provides the capability of evaluating the statistical behavior for a larger range of parameters through application of the root-sum-squaring (RSS) technique to the simulation-generated results.

The error propagation capabilities provide the analytical tool necessary to determine the sensitivity of position errors to variations in several key parameters. The first parameter of interest is the error source type and magnitude. The type can be, for example, bias, correlated or random noise and the magnitude can represent current navigation accuracy requirements or proposed requirements. In this manner, hypothetical navigation system performance can be evaluated by appropriately varying the simulation inputs.

The next parameter of interest, especially for angle measurement or range-dependent navigation systems, is the flight configuration (speed and geometry). The simulation has the capability to have as input and prespecified three-dimensional route with arbitrary ground facility locations. This provides the ability to evaluate navigation system performance for any operational scenario. This flexibility is important for the avionics sensitivity study since the design of RNAV/MLS approach paths and the allocation of airspace depend to a great extent on the potential RNAV delivery errors at the MLS boundary and the capability to deal with them upon MLS transition. These errors are geometry-dependent and therefore it becomes necessary to evaluate the impact of geometry on the achievable position accuracies.

The capabilities of the navigation simulation can be summarized as:

(1) determination of the mean three-dimensional position error from constant or repetitive error sources;

(2) determination of the standard deviation of the position errors due to random error sources about the mean;

(3) combination of (1) and (2) to obtain the "mean square error";

(4) error distribution using RSS technique;

(5) sensitivity of position errors to variations in error source types and magnitudes;

(6) sensitivity of position errors to variations in flight configuration (speed and geometry);

(7) response of the system to nonlinear error sources;

(8) comparison of filters for error attenuation;

(9) comparison of RNAV and MLS system mechanizations;

(10) performance of the system using real navigation aid data;

(11) determination of RNAV and MLS system performance along any prespecified route; and

(12) propagation of non-Gaussian error probability distributions through typical RNAV and MLS systems.

III. ANALYTICAL APPROACH

3.1 INTRODUCTION

The basis of an avionics sensitivity study is the generation of a suitable statistical data base. The primary objective is to evaluate the propagation of navigation error statistics through the system and assess the impact on aircraft position performance. Several analytical approaches can be taken to generate the desired data base. The first approach is using Monte Carlo type simulations and the second is the use of covariance propagation (ensemble simulation). The difference between these two simulation techniques has been discussed in Section 2.1. The purpose of the discussion in this section is to indicate the manner in which the ensemble simulation is applied to the current avionics sensitivity study.

The ensemble simulation (covariance propagation) essentially generates the time history of the variances and covariances of the states along a prespecified nominal trajectory. The covariance time history generated in this manner eliminates the necessity to generate a large number of Monte Carlo runs. The limitation, as discussed previously, is the requirement to linearize the appropriate system equations. For this study the primary nonlinearities exist in the equations of motion for the aircraft and in the control bounds. However, the focus here is on avionics sensitivities to navigation errors, hence, the aircraft dynamics play a minor role and can be simplified to linear form.

The primary objective for implementation of the ensemble simulation is to generate as broad a statistical data base as feasible in the most cost effective manner. Through judicious selection of states and the equations governing their motion this objective can be achieved. Where the equations are not in linear form, a linearization process is executed such that the appropriate covariance propagation form is achieved while retaining adequate physical representation.

Following the development of the appropriate covariance propagation equations, it is necessary to generate a simulation test plan designed to include a sufficiently broad scope of parameters and broad range of variation of these parameters. The purpose of the data generated is to provide increased insight into the transient behavior of

navigation-induced errors in the RNAV/MLS transition region. Therefore, the test plan should include at least potentially worst case geometries and error parameter magnitudes and other geometries providing data of general interest. The test plan cannot be all encompassing, hence, the parameters and geometries for the sensitivity analysis must be judiciously selected.

Application of the ensemble simulation developed for the avionics sensitivity analysis will yield expected aircraft position error time histories in the terminal area where navigation support is provided by RNAV and MLS. Of special interest is the expected transient at the MLS boundary due to the known error differences between the two navigation systems. The error differences are observed by comparing Tables 3.1 and 3.2. Table 3.1 indicates the MLS error specifications and Table 3.2 shows the VOR/DME errors. The VOR/DME system is currently the basic means of navigation support for RNAV. Other systems, such as LORAN-C, Omega and GPS, for example, are also typical RNAV systems. However, evaluation of aircraft position error due to these systems is beyond the scope of the current study.

The primary purpose for the data base generated under this study is to provide appropriate information for guidance law development and airspace design. More specifically the data will, first of all, aid in establishing the feasibility of RNAV/MLS transition for various geometries, flight profiles and error parameter magnitudes. Having established the feasibility of RNAV/MLS transition the data provides information to establish requirements for additional control laws during transition and to establish airspace requirements for maneuvering to null out RNAV errors. The airspace requirements would also include guidelines for route design in the RNAV/MLS transition. Finally, the data base can be used to identify potential areas or geometries for additional flight experimentation.

Generation of a suitable data base for the avionics sensitivity analysis requires at the onset the development of a suitable simulation test plan. Because of the inherent flexibility available for simulation experimentation, a broader range of parameters can be varied. For this study, these parameters are: flight profile, ground navigation aid location, runway (MLS) orientation, and error parameter content and magnitudes. These parameters and the range of values associated with each are selected to give as broad a data base as is feasible. They have been selected to yield results providing the greatest amount of information for subsequent analysis.

Table 3.1

RTCA [9] MLS Specifications (1σ)

Configuration Operational Use	D Cat. I	F Cat. II	K Cat. III
DME			
Bias	91.4 m (300 ft.)	30.5 m (100 ft.)	6.1 m (20 ft.)
Random	*	*	*
Total	91.4 m	30.5 m	6.1 m
AZ			
Bias	.125 degrees	.090 degrees	.036 degrees
Random	.065 degrees	.033 degrees	.024 degrees
Total	.141 degrees	.096 degrees	.042 degrees
EL			
Bias	.050 degrees	.050 degrees	.050 degrees
Random	.058 degrees	.035 degrees	.035 degrees
Total	.077 degrees	.061 degrees	.061 degrees

* Random error negligible compared to bias

Table 3.2

AC 90-45A [10] VOR/DME Specifications (2σ)

SOURCE	ERROR MAGNITUDE
VOR:	
Ground	1.9°
Airborne	3.0°
DME:	
Ground	185m (0.1 nmi)
Airborne	926m (0.5 nmi)

3.2 SIMULATION IMPLEMENTATION

The purpose of this subsection is to explain in greater detail the implementation of the simulation and the issues alluded to in the introduction. One of the advantages of computer simulation is the capability to begin and end a particular simulated flight at arbitrary points. Since this study is primarily concerned with RNAV/MLS transition and the evaluation of the expected transients during this transition, it is desirable to initiate the simulation some time prior to the MLS boundary and terminate the simulation after the desired transients have been observed. The simulation must be initiated, however, with sufficient time prior to the MLS boundary to eliminate initial condition transients. Also, the termination of the simulation, for this study, is considered to occur at the initiation of flare in order to observe the behavior of MLS-induced position errors during the entire flight in this navigation mode.

Specific flight profiles and ground navigation facility locations are selected to provide sensitivity data valuable for analysis and inputs for subsequent flight test design. The computer simulation flexibility is again utilized for these parameter variations. Since the flight profile and navigation aid locations are varied by input into the simulation they need not be fixed as they are for actual flight tests. In this manner it is possible to design the flight profile, locate the navigation facilities and orient the runway and MLS antennas in such a manner to produce the most useful results.

An additional degree of flexibility provided by the simulation approach is the capability to vary the error source content and magnitude. Variation of the error parameters yields the ability to evaluate avionics sensitivities to existing navigation errors and hypothetical or proposed navigation errors. Ability to vary the error content and magnitude is significant during navigation system error budget analysis and airspace planning.

The simulation flexibilities described above form the basis of the simulation test plan design. Of primary interest in a preliminary avionics sensitivity analysis are parametric values providing the greatest amount of useful information. During airspace planning or guidance algorithm development it is essential to consider the minimum capabilities of the navigation system. This can be accomplished by generating data for the worst case parameter values. As stated previously, one of the objectives is to generate data for airspace planning and

guidance algorithm development. Hence, the desire for establishing worst case parameter values becomes a motivating factor in the test plan design.

Consideration of worst-case parameter values (flight profiles, geometries, error sources) in the test plan provides data necessary to answer questions regarding airspace requirements, terminal area route design and RNAV/MLS transition control law requirements. Airspace allotments must be made for safe separation assurance between aircraft equipped with minimum navigation systems susceptible to worst case error content and magnitudes. The subsequent route design must also provide the capability for the safe and expeditious passage of aircraft from the enroute RNAV system to final approach and landing. The route design must provide adequate length to execute maneuvers to null out any undesirable RNAV delivery errors detected by the more accurate MLS system. There may also exist some speculation as to the requirement for a guidance policy and/or algorithm to null out the RNAV delivery errors. If the worst case geometries do not require implementation of specialized transition guidance algorithms then it is obvious that less than worst case geometries would not require additional algorithm development.

Additionally, it is desirable to consider other more typical geometries to broaden the scope and, hence, the usefulness of the data. The additional parametric values of the test plan will provide greater insight into aircraft navigation system performance in the transition region, and thereby aid in the route design problem and in the determination of the flexibility of various geometries and flight profile configurations. The broader data base is also useful for any subsequent flight test designs. Generally, flight test profiles are based on knowledge gained through analytical means or good engineering judgment. With knowledge gained from the data base generated by simulation techniques, more judicious selection of actual flight test profiles is possible.

Implementation of the simulation is initiated upon completion of the test plan design. Each of the flight profiles is used to generate the nominal trajectory about which the covariance matrix is propagated. The navigation aid locations, because of the geometry dependence of the navigation errors, and the error parameters drive the error covariance about the nominal. Execution of the test plan using the ensemble simulation provides the data necessary for the avionics sensitivity analysis data base.

3.3 EXPERIMENT-SIMULATION PLAN

The parameters to be considered for the avionics sensitivity study include:

(a) Geometric parameters

- vertical profile
- horizontal profile
- VOR/DME facility location
- DME/DME facility location
- flight path/runway orientation

(b) Navigation systems

- airborne equipment
- ground navigation aids

(c) Error source parameters

- type (bias, correlated, random noise)
- magnitude

The parameters to be held constant for this study are the vertical profile (3° CTOL approach paths) and airborne equipment (INS) to be compatible with the TCV aircraft avionics. The following test plan describes the variations considered for the remaining parameters.

Two sets of horizontal profiles will be considered. The first set consists of the ICAO demonstration profiles as shown in Figures 3.1 and 3.2. Tables 3.3 and 3.4 present the waypoint data for each profile, respectively. Three hypothetical profiles are included in the second set in an attempt to provide more generality to the results and to examine worst-case situations. The three hypothetical profiles include a straight-in approach, a 90°-turn on to final and a 180°-turn on to final.

The ground navigation aids being considered for this study are DME/DME and VOR/DME. The location of the ground facilities have been selected for the ICAO demonstration flights to represent those used during the demonstration. The demonstration flights are to be executed in the INS/DME/DME (IDD) mode only. The airborne system has an autotune feature which selects ground facilities according to specific criteria. The primary facility is fixed (in this case, ACY) and the secondary facility is autotuned from Millville, Coyle or Sea Isle. For the simulation tests the facility providing the best geometry will be selected.

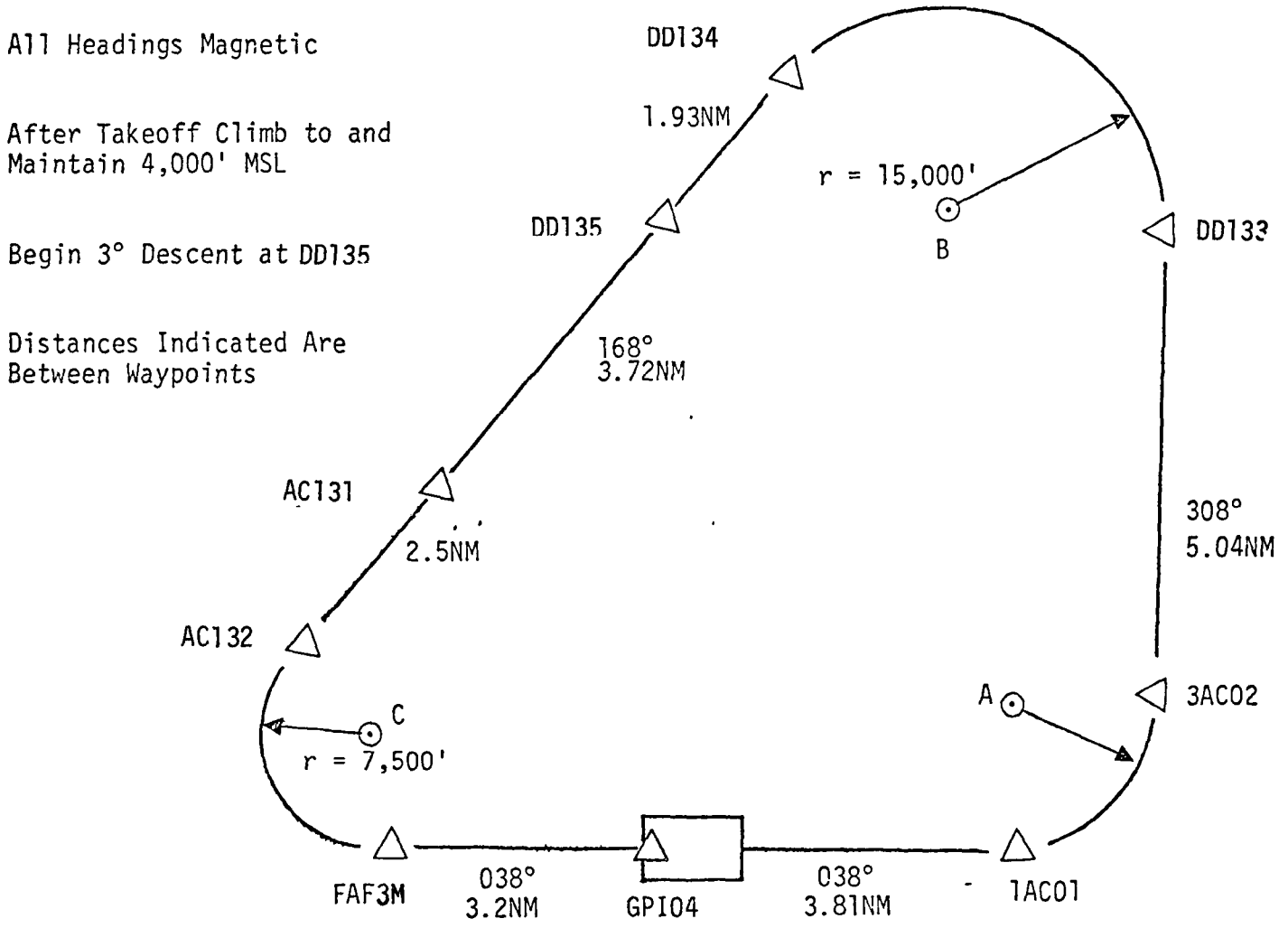

Figure 3.1 ICAO Demonstration Profile 4

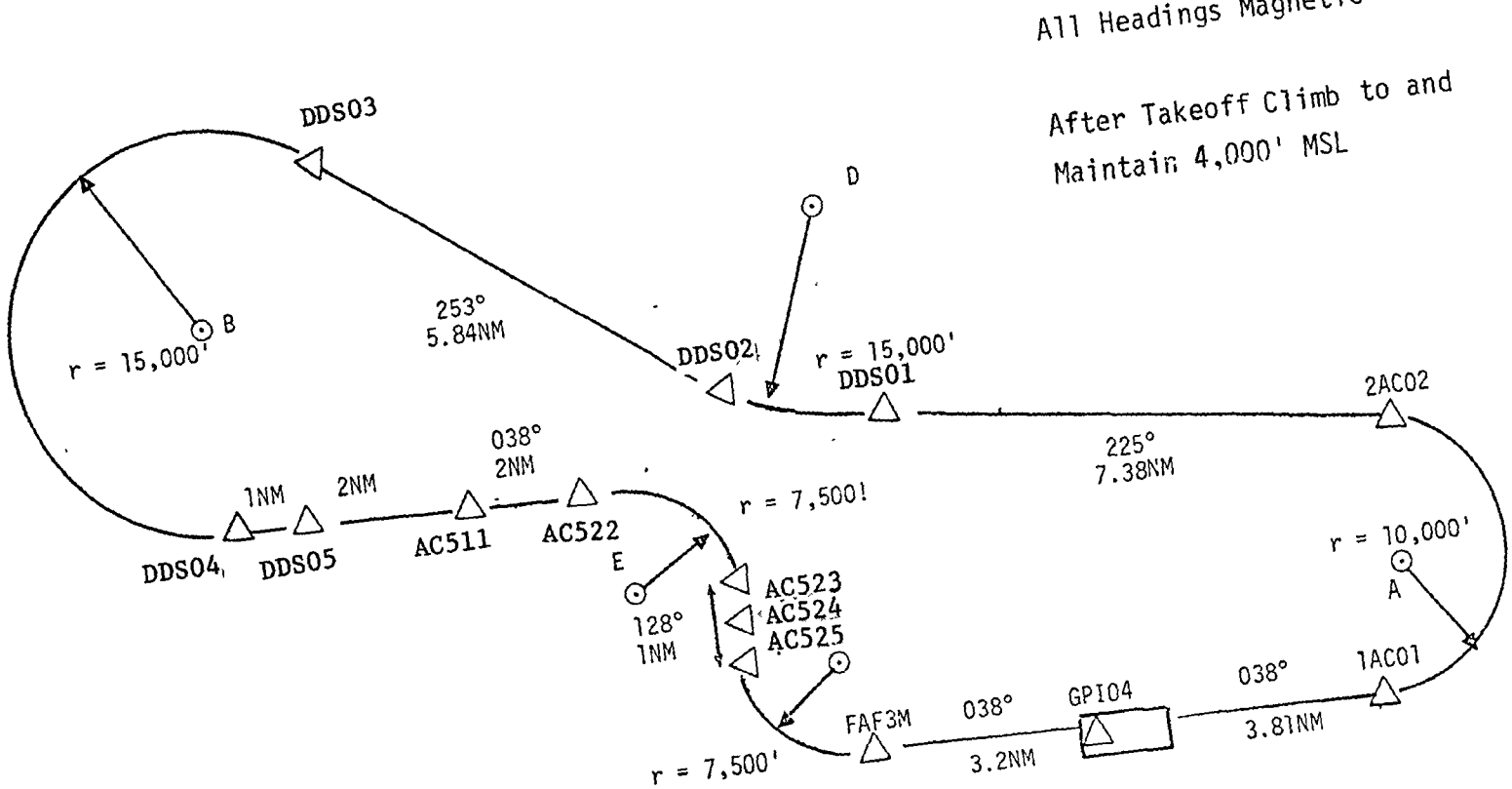

Figure 3.2 ICAO Demonstration Profile Number 2

Table 3.3

Altitude and GPI04 Based Upon A Calculated GPIP Opposite EL1 Antenna

ICAO DEMONSTRATION WAYPOINT LOCATIONS FOR PROFILE 3 (STAR 4AC043)			
WAYPOINT	LATITUDE	LONGITUDE	ALTITUDE, MSL
1AC01	39° 30' 31.00"	74° 32' 42.38"	Climbing
3AC02	39° 32' 44.62"	74° 33' 35.09"	
DD133	39° 35' 06.59"	74° 39' 19.50"	4,000'
DD134	39° 32' 00.20"	74° 43' 46.25"	4,000'
DD135	39° 30' 20.70"	74° 42' 54.6 "	4,000'
AC131	39° 26' 45.79"	74° 41' 02.69"	2,771'
AC132	39° 24' 26.61"	74° 39' 50.17"	1,975'
FAF3M	39° 24' 19.56"	74° 36' 57.14"	1,083'
GP104	39° 27' 07.35"	74° 35' 02.05"	66'
DME ARC CENTERS			
POINT	LATITUDE	LONGITUDE	RADIUS
A	39° 31' 17.42"	74° 34' 34.93"	10,000'
B	39° 32' 55.79"	74° 40' 49.32"	15,000'
C	39° 24' 54.36"	74° 38' 21.55"	7,500'

Table 3.4

Altitude and GPI04 Based Upon A Calculated GPIP Opposite E11 Antenna

ICAO DEMONSTRATION WAYPOINT LOCATIONS FOR PROFILE 3 (STAR 4AC043)			
WAYPOINT	LATITUDE	LONGITUDE	ALTITUDE, MSL
1AC01	39° 30' 31.00"	74° 32' 42.38"	Climbing
2AC02	39° 32' 14.05"	74° 36' 19.34"	
DDS01	39° 26' 10.86"	74° 41' 47.36"	4,000'
DDS02	39° 25' 23.82"	74° 42' 57.17"	4,000'
DDS03	39° 22' 41.51"	74° 49' 47.46"	4,000'
DDS04	39° 19' 22.85"	74° 45' 24.86"	4,000'
DDS05	39° 19' 57.60"	74° 45' 01.10"	4,000'
AC511	39° 22' 00.44"	74° 43' 36.82"	3,273'
AC522	39° 23' 46.48"	74° 40' 24.08"	2,636'
AC523	39° 24' 17.12"	74° 40' 14.80"	2,019'
AC524	39° 24' 03.02"	74° 39' 40.61"	1,860'
AC525	39° 23' 48.93"	74° 39' 06.4 "	1,702'
FAF3M	39° 24' 19.56"	74° 36' 57.14"	1,083'
GPI04	39° 27' 07.35"	74° 35' 02.05"	66'
DME ARC CENTERS			
POINT	LATITUDE	LONGITUDE	RADIUS
A	39° 31' 17.42"	74° 34' 34.93"	10,000'
B	39° 20' 32.37"	74° 48' 13.82"	15,000'
C	39° 24' 54.36"	74° 38' 21.55"	7,500'
D	39° 27' 35.89"	74° 44' 24.08"	15,000'
E	39° 27' 11.65"	74° 40' 59.72"	7,500'

For the hypothetical profiles, both the DME/DME and VOR/DME navigation modes are assumed. The ground facility locations are selected to provide worst-case situations. The most adverse geometries are selected since they provide the most useful information by indicating an upper bound to the expected error magnitudes. For the DME/DME navigation modes the facilities are located such that the relative bearing between the two stations measured at the aircraft is 45° or 135° (the threshold value for the airborne RNAV system) at the intersection of the flight path and MLS coverage boundary. When the relative bearing reaches these threshold values the aircraft position errors due to DME errors is maximum.

The three horizontal profiles and DME facility locations for the DME/DME mode are shown in Figures 3.3 through 3.5. For each profile two sets of DME facility locations are assumed denotes by (a_1,a_2) and (b_1,b_2) in the figures. The facilities (a_1,a_2) will provide the worst-case along-track and the facilities (b_1,b_2) will provide the worst-case cross-track.

The VOR/DME facility locations are shown in Figures 3.6 through 3.8. The facility at a, in each case, represents the worst-case along-track, due to VOR bearing errors. The facility at b represents the worst-case cross-track error due to VOR bearing errors. The worst-case along-track error is of interest, since for 3D RNAV systems, this error propagates into the vertical. All of the geometries are presented explicitly in Appendix B.

The VOR and DME error sources are assumed to consist of random noise and bias. The magnitude of these errors are assumed to be consistent with those specified in Advisory Circular AC90-45A [10]. Although the Advisory Circular does not delineate the amount of bias or noise, it is assumed for the study that this is a variable for VOR, in the case of VOR/DME, and for DME in the case of DME/DME. When studying VOR/DME, the DME noise content does not have the significant effect of VOR noise content, particularly VOR bias. Hence, for VOR/DME the error content and magnitudes to be considered are:

(a) VOR bias = 0.0°; VOR noise = 3.65°
DME bias = 660 meters; DME noise = 660 meters;

(b) VOR bias = 2.51°; VOR noise = 2.57°
DME bias = 660 meters; DME noise = 660 meters;

(c) VOR bias = 3.56°; VOR noise = 0.0°
DME bias = 660 meters; VOR noise = 660 meters.

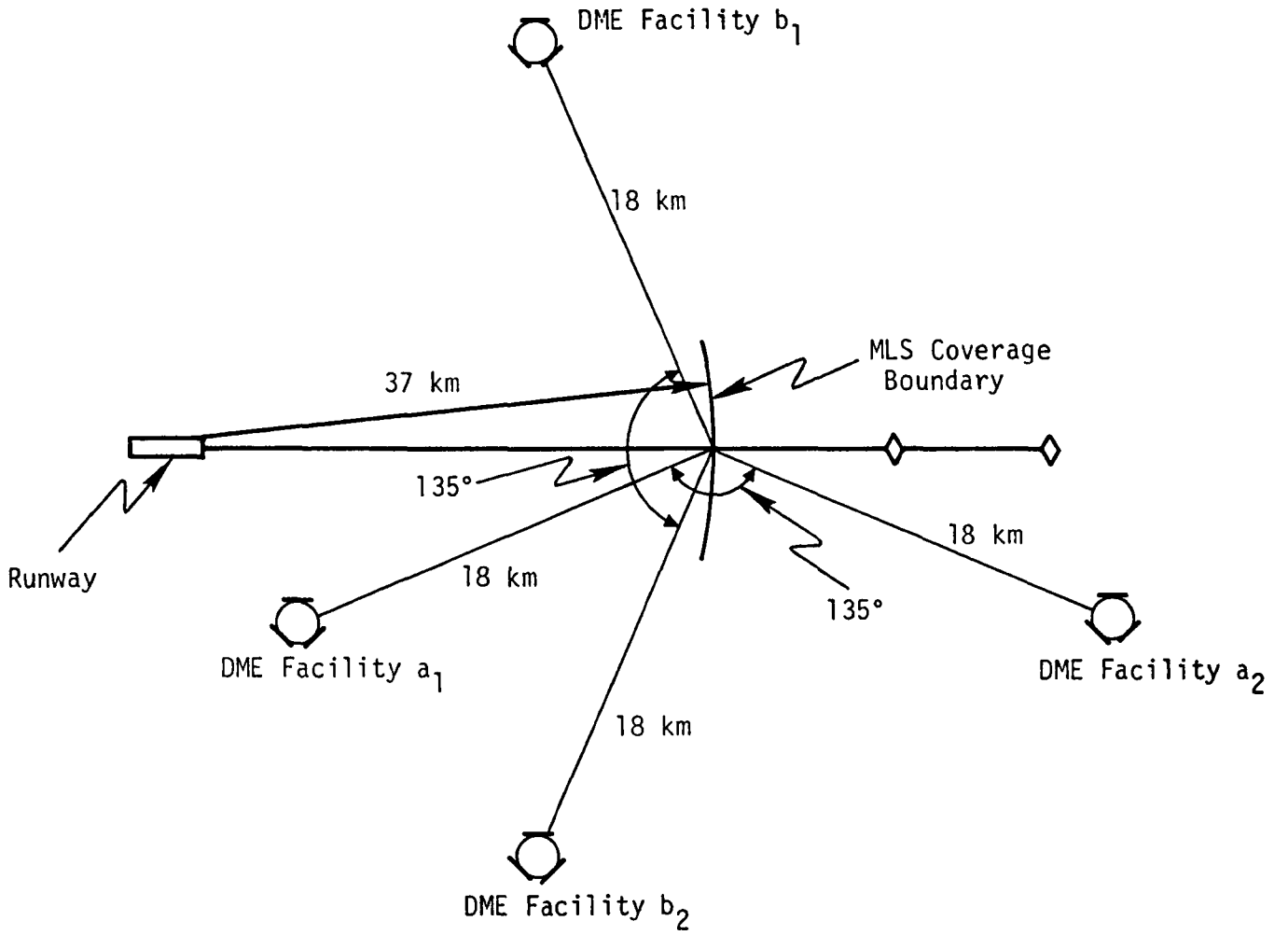

Figure 3.3 Straight-In Approach for DME/DME Navigation Mode

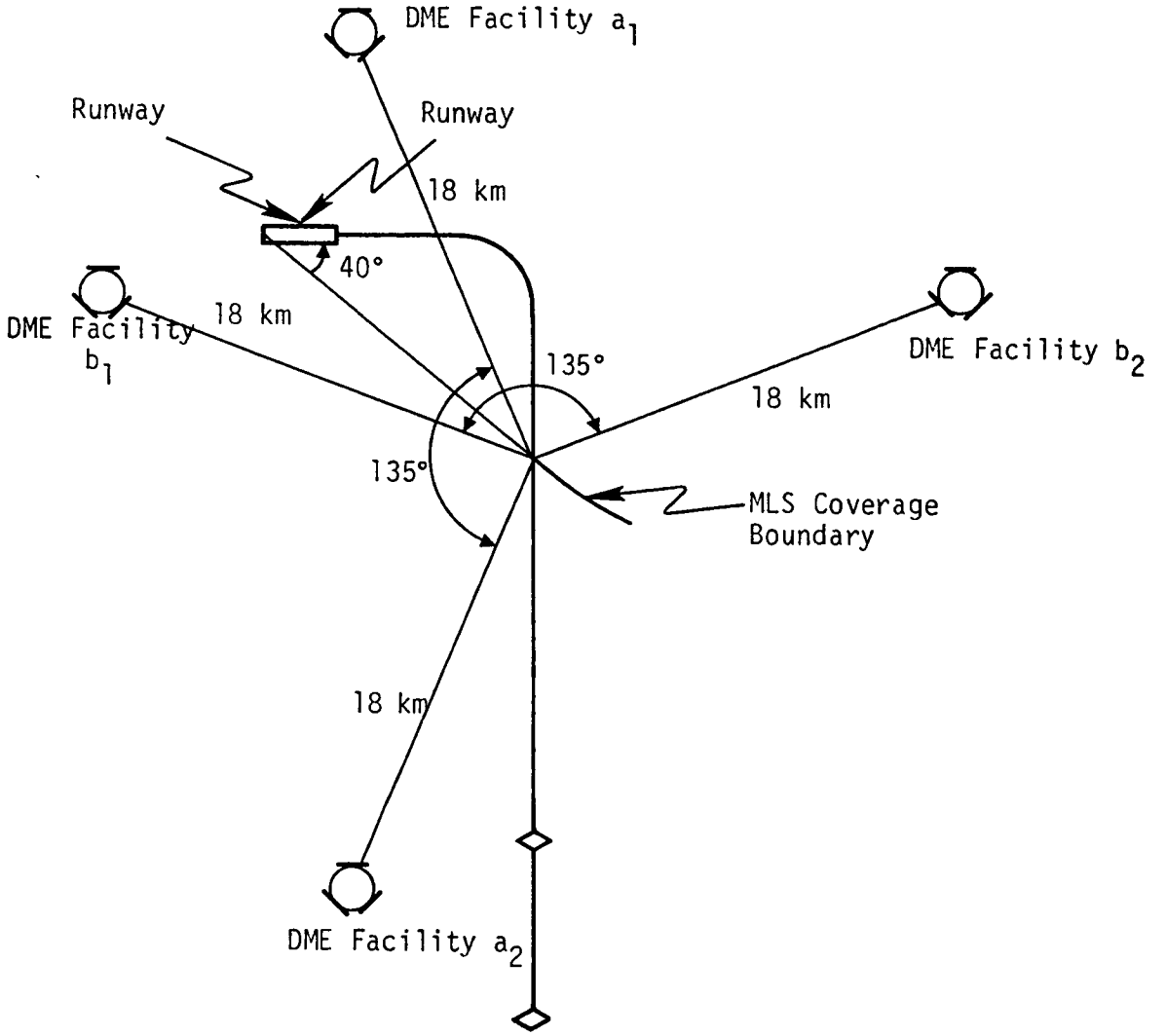

Figure 3.4 90° Turn to Final Approach for DME/DME Navigation Mode

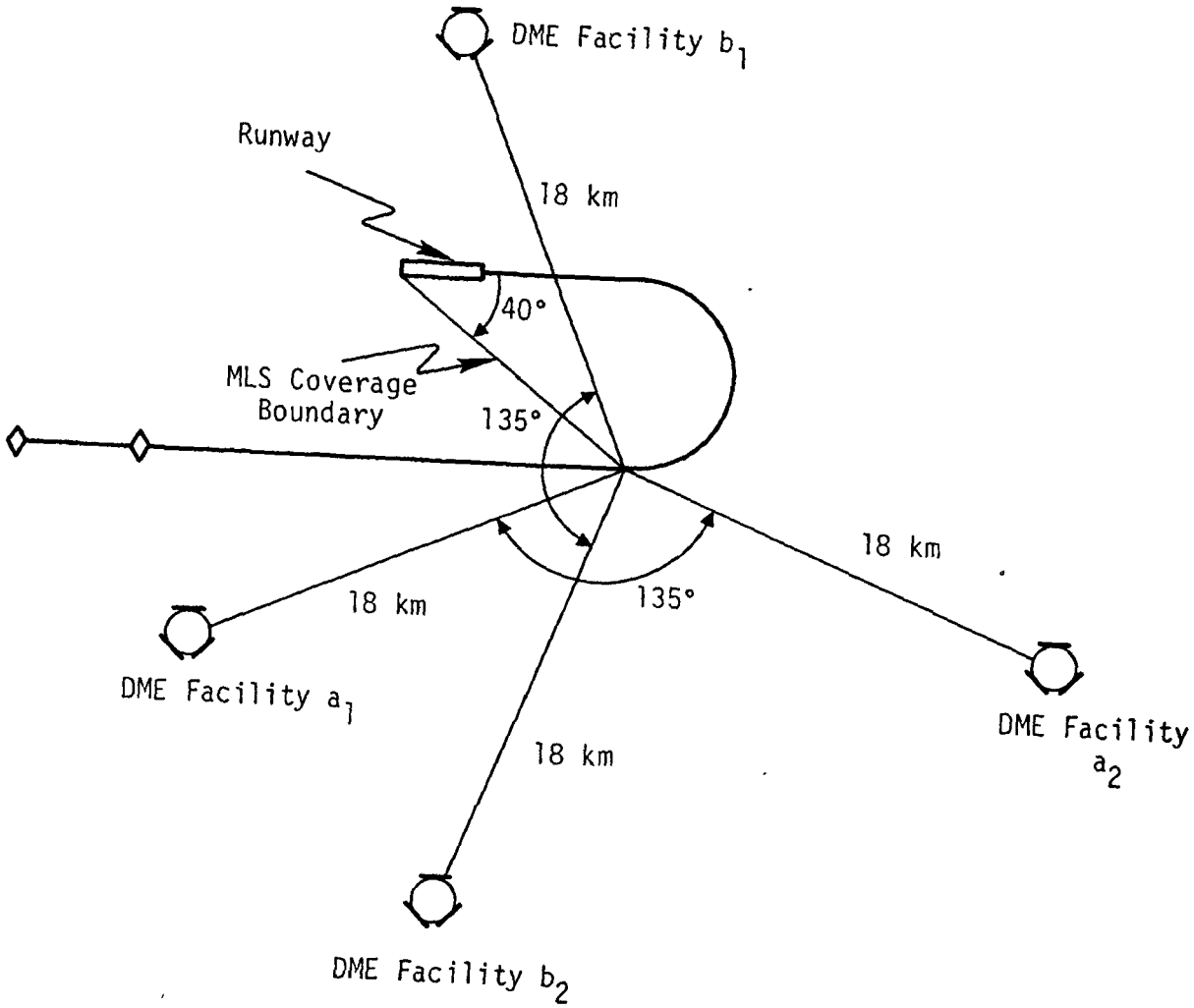

Figure 3.5 180° Turn to Final Approach for DME/DME Navigation Mode

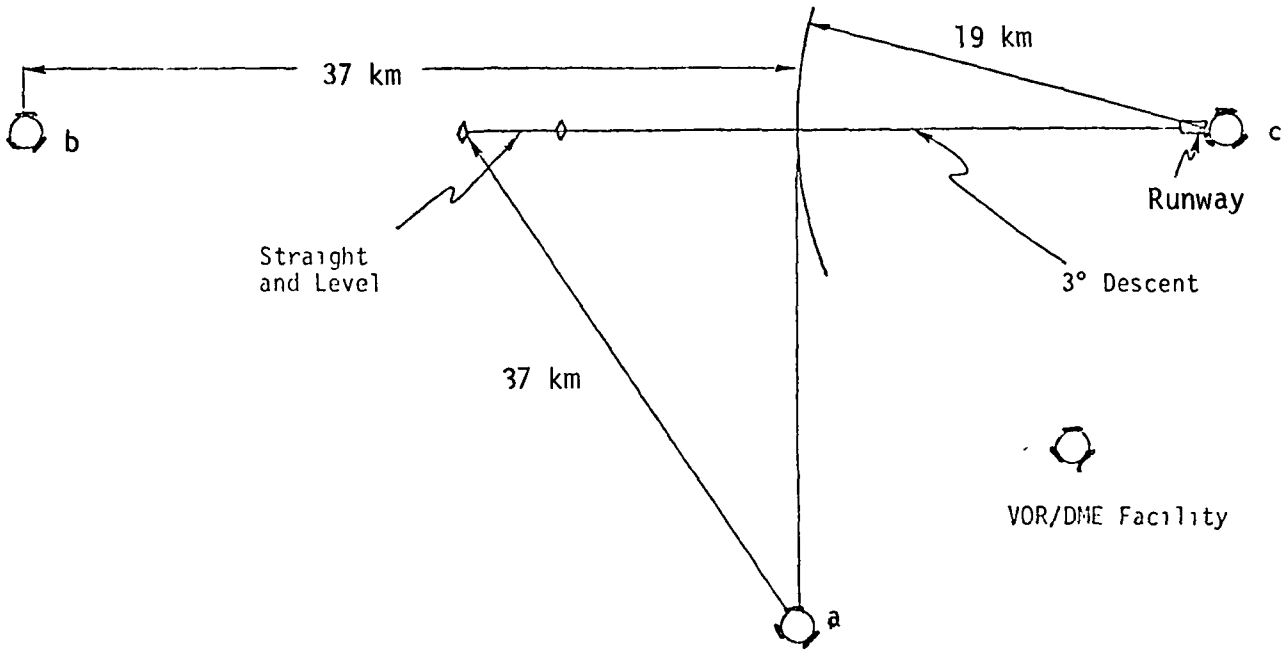

Figure 3.6 Straight-In Approach for VOR/DME Navigation Mode

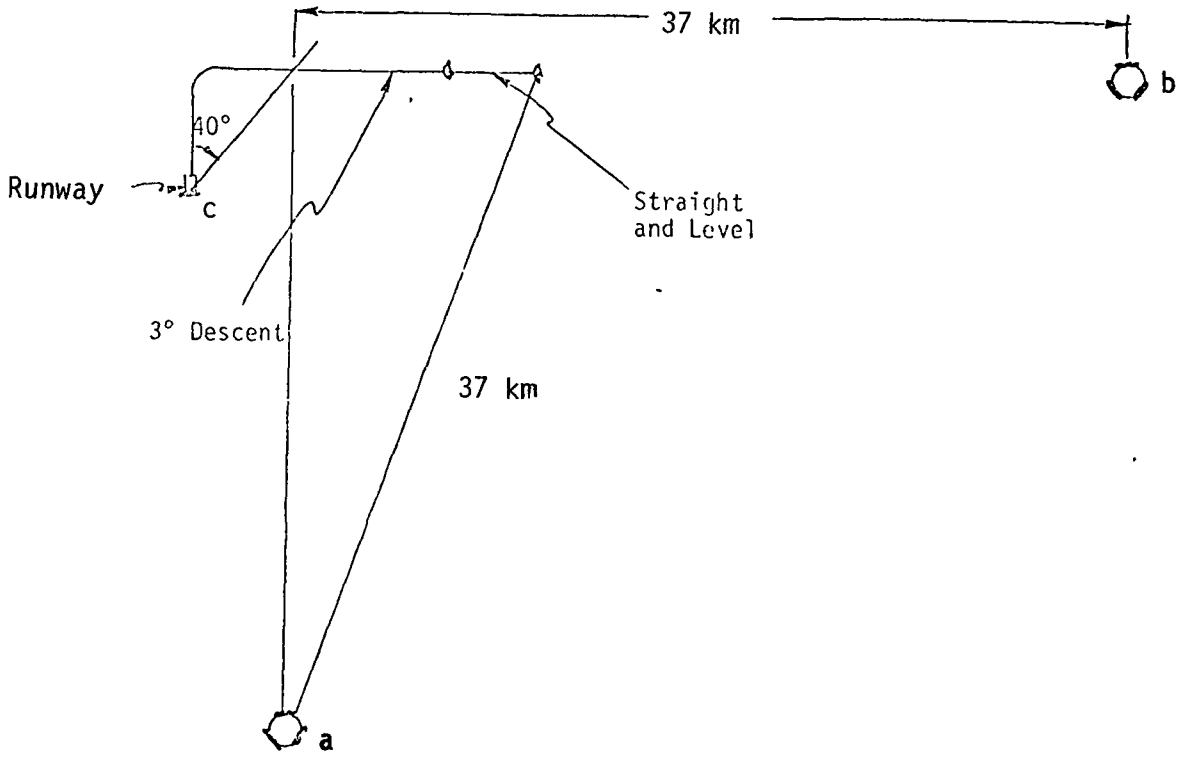

Figure 3.7 90° Turn to Final VOR/DME Navigation Mode

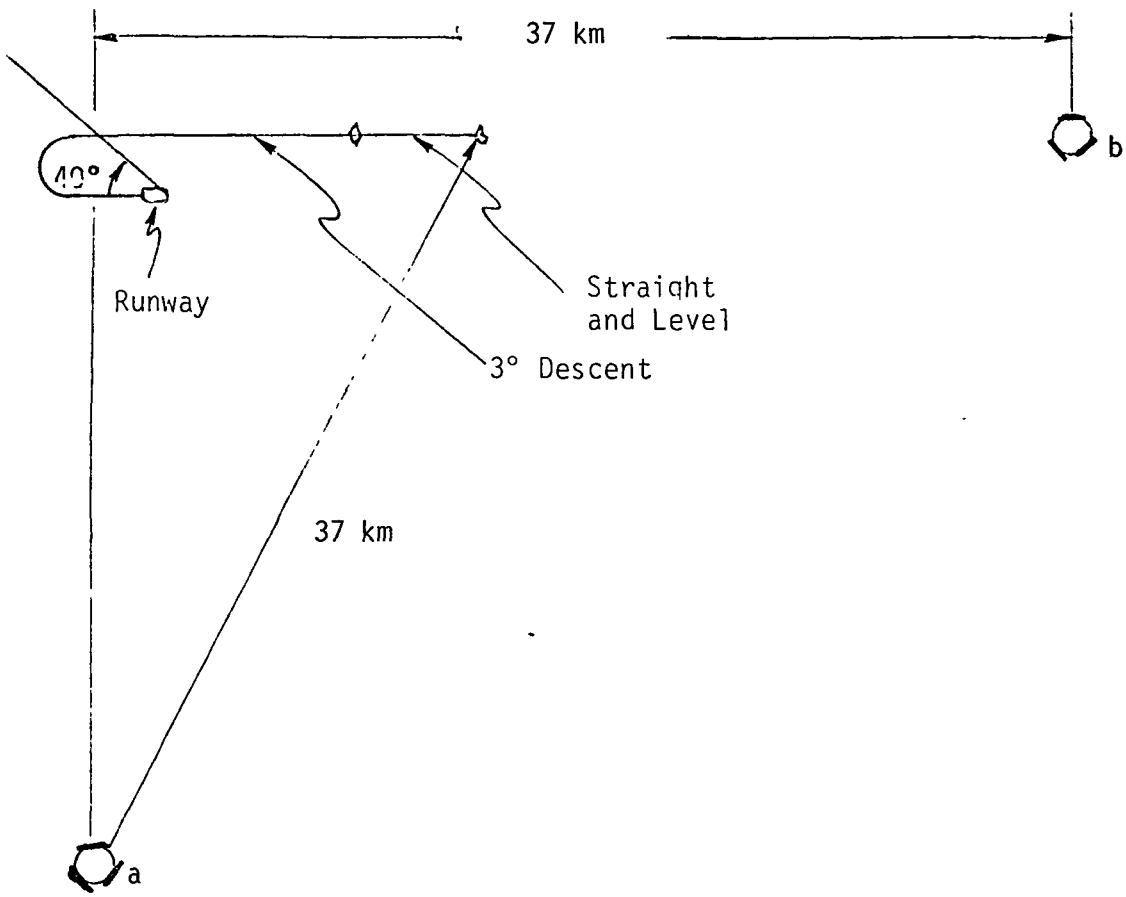

Figure 3.8 180° Turn to Final for VOR/DME Navigation Mode

Similarly, for the DME/DME mode the cases to be considered are:

(a) DME bias = 0.0 meters; DME noise = 945 meters

(b) DME bias = 660 meters; DME noise = 660 meters

(c) DME bias = 945 meters; DME noise = 0.0 nmi

The AC90-45A values are (for both ground and airborne)

VOR = 3.56°; DME = 945 meters

Page Intentionally Left Blank

page 38

IV. ANALYTICAL RESULTS

4.1 INTRODUCTION

As indicated previously, judicious selection of the experimental test parameters (VOR/DME location, DME/DME location, flight path geometry, runway orientation [MLS antenna orientation] and error source magnitudes) will provide the capability to generate an extensive data base. For each of these configurations, the avionics sensitivity to navigation errors for the 737-TCV aircraft were evaluated. The data base for this study consists of 36 cases, 18 DME/DME transitions to MLS and 18 VOR/DME transitions to MLS.

Meaningful presentation of the results becomes a difficult task in light of the scope of the data base. The primary quantities of interest are the cross-track and vertical deviation time histories through the RNAV/MLS transition as a function of the various study parameters. These time histories are presented in the form of plots. An attempt has also been made to tabulate several of the more important quantities, such as, the RNAV deviations at the MLS boundary as a function of the study parameters.

The results section outline is as follows. The simulation test conditions are presented in Section 4.2. These conditions essentially establish the ground rules for the subsequent experimentation program. Section 4.3 presents an explanation of the contents of each of the plots and on how each plot should be read. This explanation is performed via an example. The avionics sensitivity analysis results are presented in Section 4.4. This section contains the results of the entire sensitivity study. Demonstration results are shown in Section 4.5 which contains results for the ICAO demonstration flights. A brief summary of results is presented in Section 4.6 for quick reference.

4.2 SIMULATION TEST CONDITIONS

The purpose of this subsection is to identify those conditions established for the simulation experiments. These conditions relate primarily to the initialization of the covariance matrix. Specifically, the initialization of the covariance elements relating to the INS, altimeter and position estimates. Reinitialization of the covariance matrix at MLS transition is also discussed where it is assumed that the avionics switches directly from the RNAV mode to the MLS mode.

The INS initial position error estimates are dependent on the most recent radio navigation update. For example, an INS-equipped aircraft traversing the ocean without an update will experience a drift error of approximately 7413 meters assuming a drift rate of 1853 meters/hr and a flight time of 4 hours. This drift error is reduced, through external position fixes, to an amount equivalent to the measurement errors associated with the external source. For this study it is assumed, depending on the mode of operation, that the INS has been updated using VOR/DME or DME/DME. It is further assumed that the INS initial position errors are equivalent to the VOR/DME or DME/DME position errors at the initial position of the simulation test runs. Hypothetically, the INS could have been updated at more favorable geometries thereby decreasing the initial INS error estimate. However, for this study the motivation is to determine upper bounds, hence, it is more desirable to examine worst-case conditions. The magnitude of the initial INS errors is therefore determined using AC 90-45A [10] techniques to establish VOR and DME derived position errors for a given aircraft location relative to the facility.

For example, consider the initial geometry shown in Figure 4.1. An aircraft with a range of 20.7 km from the facility on a bearing of 154° will have VOR/DME-induced position errors, for an aircraft heading of 0°, of 730 meters along-track and 1170 meters cross-track (exclusive of flight technical and computer errors). Since the aircraft course for this example is due north the along-track error becomes the initial INS north position error and the cross-track error becomes the initial INS east position error.

The other elements of the INS are represented by the following quantities. The initial INS velocity error is considered to be 0.05 meters/sec. The gyro drifts, considered as biases because of the short flight times, are 0.01 deg/hr, the accelerometer errors, also assumed biases for this study, are $10^{-4}g$, where g is the gravitational constant. The bias assumptions are valid in light of the length of the correlation times of 5 hours for the gyro drift and 10 hours for the accelerometer relative to the flight times on the order of 5 to 10 minutes. The platform misalignment for this study is taken to be 0.005°.

The altimeter model for this study is assumed to consist of a bias of 30.5 meters and random noise of 7.6 meters. The altitude measurement is passed through a first order filter with a time constant of 2 seconds to simulate altimeter lag. The initial covariance for the altimeter is taken to be 30.5 meters, consistent with the altimeter bias.

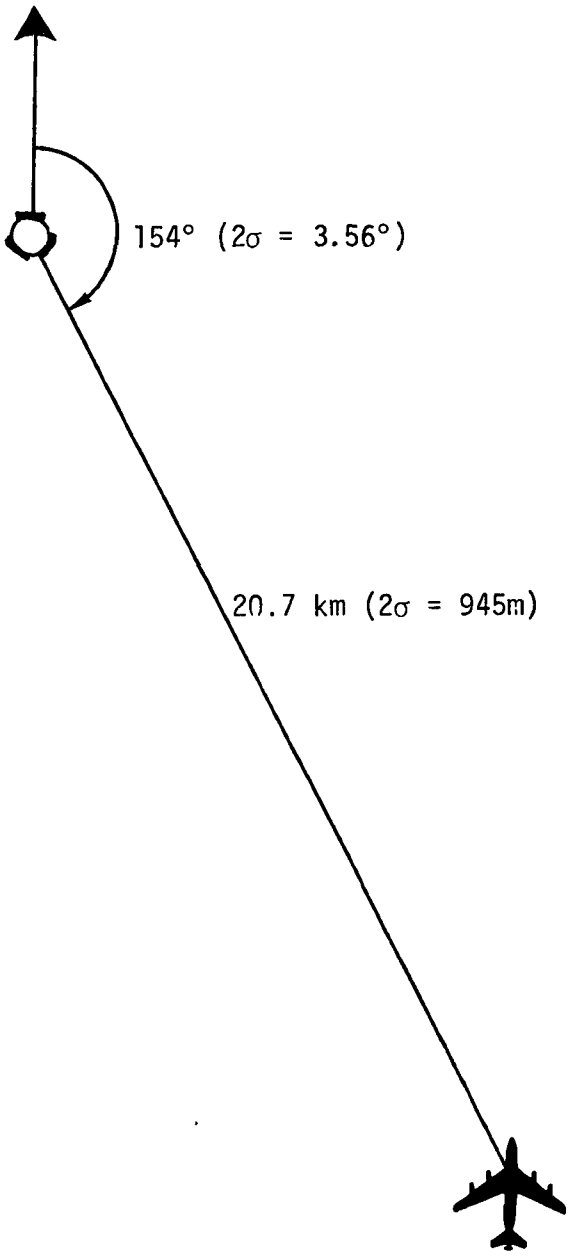

Figure 4.1 Along-Track and Cross-Track Errors Due to VOR/DME Errors Used for INS Initialization

The initial aircraft cross-track error is arbitrarily assumed to be 927 meters.

The covariance matrix is propagated through the RNAV region using the initial conditions specified above. At the MLS boundary the covariance is reinitialized to represent the fact that the RNAV measurements and filters are replaced by the appropriate MLS measurements and filters. The elements of the covariance matrix common to both the RNAV and MLS simulations remain unaltered through transition. These include the aircraft dynamics, autopilots and vertical complementary filter. The diagonal terms of the MLS complementary filter are set at the diagonal values of the RNAV complementary filter. The MLS accelerometer and platform alignment inputs (from the AHRU) are assumed to be the same as the INS. The MLS measurement biases are set in accordance with Table 3.1.

To conserve computer time in order to examine as many test cases as possible, the length of the simulation tests was shortened. More specifically, the simulation was terminated after the covariance reached a steady state (except for geometry variations) after transition into the MLS. This still provided the most useful information for the current study on RNAV/MLS transition behavior.

4.3 PRESENTATION OF RESULTS

The results of the sensitivity analysis will be displayed using 20 plots. Ten plots will contain the cross-track deviation time history and the other 10 plots will contain the vertical deviation time histories. Each corresponding cross-track and vertical deviation time history plot is associated with a particular geometry. The geometric configurations consist of three flight profiles (straight-in approach, 90° turn-to-final, and 180° turn-to-final) and two ground facility locations for both VOR/DME and DME/DME.

Figure 4.2 shows an example cross-track deviation time history plot. Each of the other plots presented generally have the same information content. Three curves are presented on each plot depicting the avionics sensitivity to navigation sensor errors. For this particular example the curves correspond to: (1) a VOR bias of 3.56° and no noise component (bias), (2) a VOR bias and noise component of 2.51° (bias/noise), and (3) a VOR noise component of 3.56° without bias (noise). The DME errors for all three cases is DME bias and noise components of 660 meters. On the time axis are indicated the two points defining the straight and level portion to allow initial condition transients to dissipate (between waypoints WP_1 and WP_2) and the point of MLS transition.

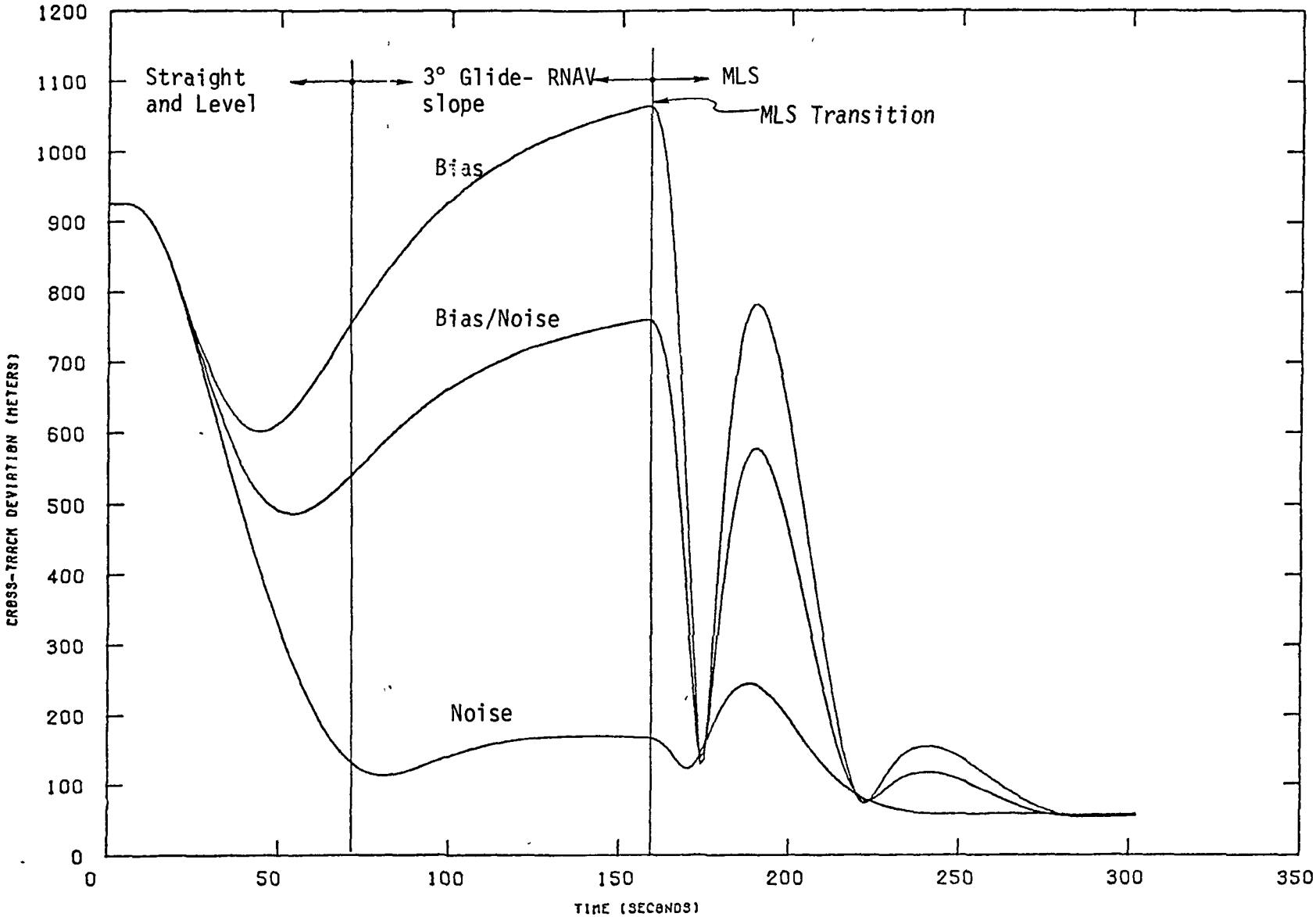

Figure 4.2 Example Result Plot for Illustration

Hence, each plot will reveal sensitivities to error parameter variations.

Geometric sensitivities can be determined by comparing various plots. To facilitate this comparison, Table 4.1 has been established as a cross-reference guide. The "figure numbers" in column one correspond to a particular figure in the results. The geometry and its corresponding figure number are shown in the third and fourth columns. The final two columns indicate the mode of operation, VOR/DME or DME/DME, and the facilities being used to provide navigation support (the letters correspond to the letters in the appropriate geometric figure).

4.4 SENSITIVITY ANALYSIS

The presentation of the sensitivity results is broken down into two subsections for clarity. The first subsection presents the VOR/DME results and the second the DME/DME results. The motivation stems from the fact that most of the DME/DME cases can be represented by a VOR/DME case. For example, the DME/DME delivery errors, for facilities B_1 and B_2 (worst-case cross-track) and DME bias and noise of 465 meters, are 355 meters in cross-track and 38 meters in vertical deviation. The comparable VOR/DME case is facility A (worst-case along-track) with a VOR bias of 0° and noise of 3.56°. The RNAV delivery errors associated with this case are 394 meters in cross-track and 33 meters in vertical deviation. To conserve computer time it is assumed that these two cases would have the same transient response in the MLS region since they represent almost identical initial conditions at the MLS boundary. Table 4.2 indicates the RNAV delivery errors for each geometry tested and indicates which of the DME/DME case was selected to be represented by which VOR/DME case. For example, the cross-track transient response of DME/DME case h is represented by the cross-track transient response of VOR/DME case g.

4.4.1 VOR/DME

The cross-track and vertical deviation time histories for the VOR/DME RNAV test cases are shown in Figures 4.3 through 4.14. Figures 4.3 and 4.4 show the straight-in approach for VOR/DME facility A (worst-case along-track). During the RNAV mode the observation can be made that the initial condition transients have decayed during the straight and level portion of the flight path. For the vertical deviation pitch over is easily recognized by the vertical channel response to the along-track feeding in (Figure 4.4) which is typical of 3D RNAV systems. Also of special interest is the sensitivity of the RNAV filter to sensor error content.

Table 4.1

Sensitivity Analysis Results Plots Cross-Reference Table

RESULTS FIGURE NUMBER	TIME HISTORY	GEOMETRY	GEOMETRY FIGURE NUMBER	NAVIGATION MODE	FACILITY(IES)*
4.3	CTD	Straight-In	3.6	VOR/DME	A
4.4	VD	Straight-In	3.6	VOR/DME	A
4.5	CTD	90° Turn	3.7	VOR/DME	A
4.6	VD	90° Turn	3.7	VOR/DME	A
4.7	CTD	180° Turn	3.8	VOR/DME	A
4.8	VD	180° Turn	3.8	VOR/DME	A
4.9	CTD	Straight-In	3.6	VOR/DME	B
4.10	VD	Straight-In	3.6	VOR/DME	B
4.11	CTD	90° Turn	3.7	VOR/DME	B
4.12	VD	90° Turn	3.7	VOR/DME	B
4.13	CTD	180° Turn	3.8	VOR/DME	B
4.14	VD	180° Turn	3.8	VOR/DME	B
4.15	CTD	Straight-In	3.3	DME/DME	A_1, A_2
4.16	VD	Straight-In	3.3	DME/DME	A_1, A_2
4.17	CTD	90° Turn	3.4	DME/DME	A_1, A_2
4.18	VD	90° Turn	3.4	DME/DME	A_1, A_2
4.19	CTD	180° Turn	3.5	DME/DME	A_1, A_2
4.20	VD	180° Turn	3.5	DME/DME	A_1, A_2
4.21	CTD	---	3.3	DME/DME	B_1, B_2
4.22	VD	---	3.3	DME/DME	B_1, B_2

* Facility A: Worst-Case Along-Track

Facility B: Worst-Case Cross-Track

Table 4.2

MLS Transition Cases Executed to Complete Simulation Test Plan

CASE	MODE	FACILITY	ERROR	RNAV DELIVERY ERROR		CORRESPONDING CASE	
				CROSS-TRACK (METERS)	VERTICAL (METERS)	CROSS-TRACK	VERTICAL
a	VOR/DME	A (Along-Track)	Bias	407	64.3	*	*
b			Bias/Noise	400	50.9	*	*
c			Noise	394	32.6	*	*
d		B (Cross-Track)	Bias	1057	37.2	*	*
e			Bias/Noise	755	37.2	*	*
f			Noise	169	37.2	*	*
g	DME/DME	A_1,A_2 (Along-Track)	Bias	323	46.3	*	*
h			Bias/Noise	245	39.6	g	d
i			Noise	126	31.7	f	c
j		B_1,B_2 (Cross-Track)	Bias	486	43.0	a	d
k			Bias/Noise	355	37.8	c	d
l			Noise	131	31.7	f	c

* MLS transitions were executed for these cases.

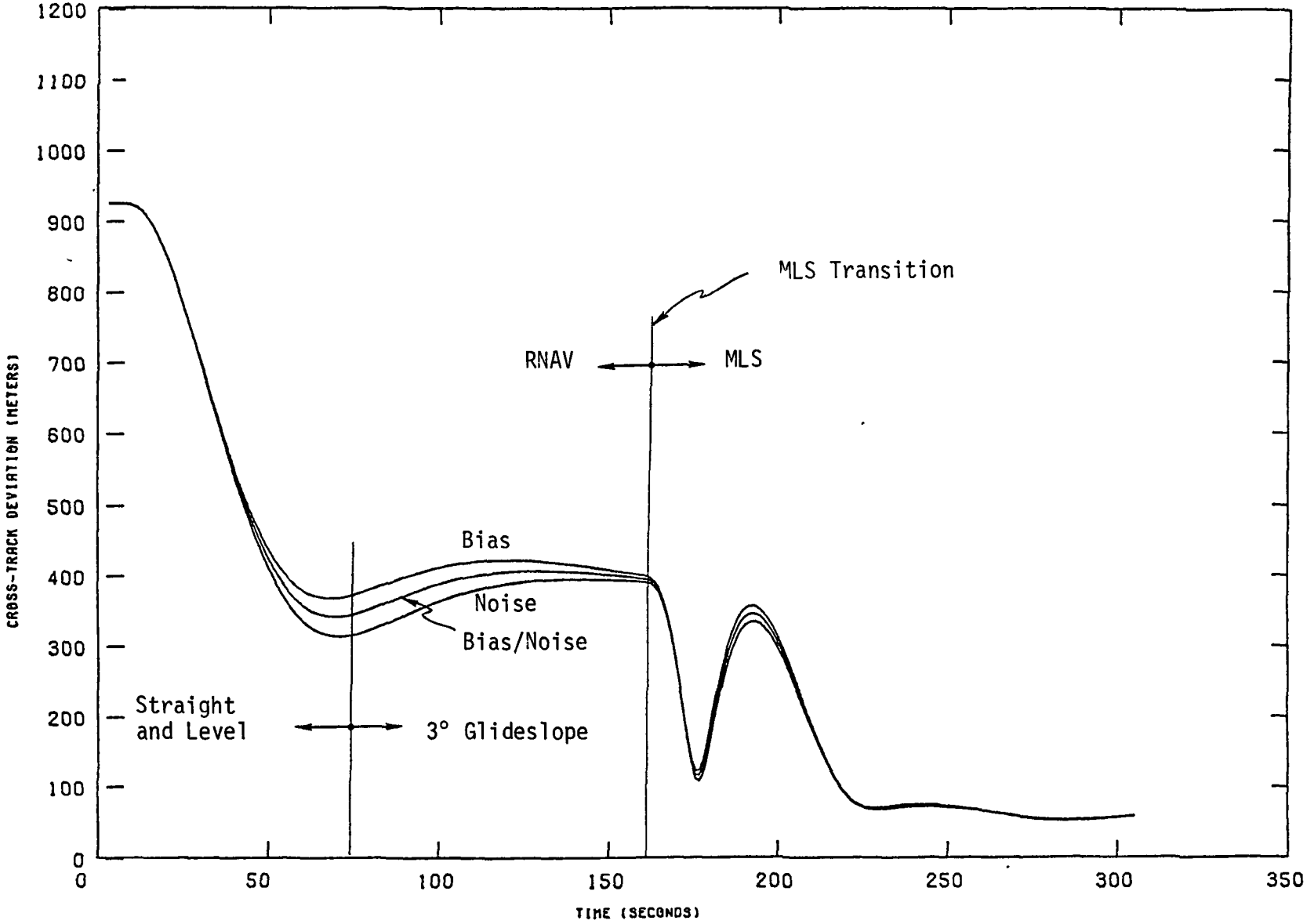

Figure 4.3 Cross-Track Deviation for Straight-In, VOR/DME, Facility A

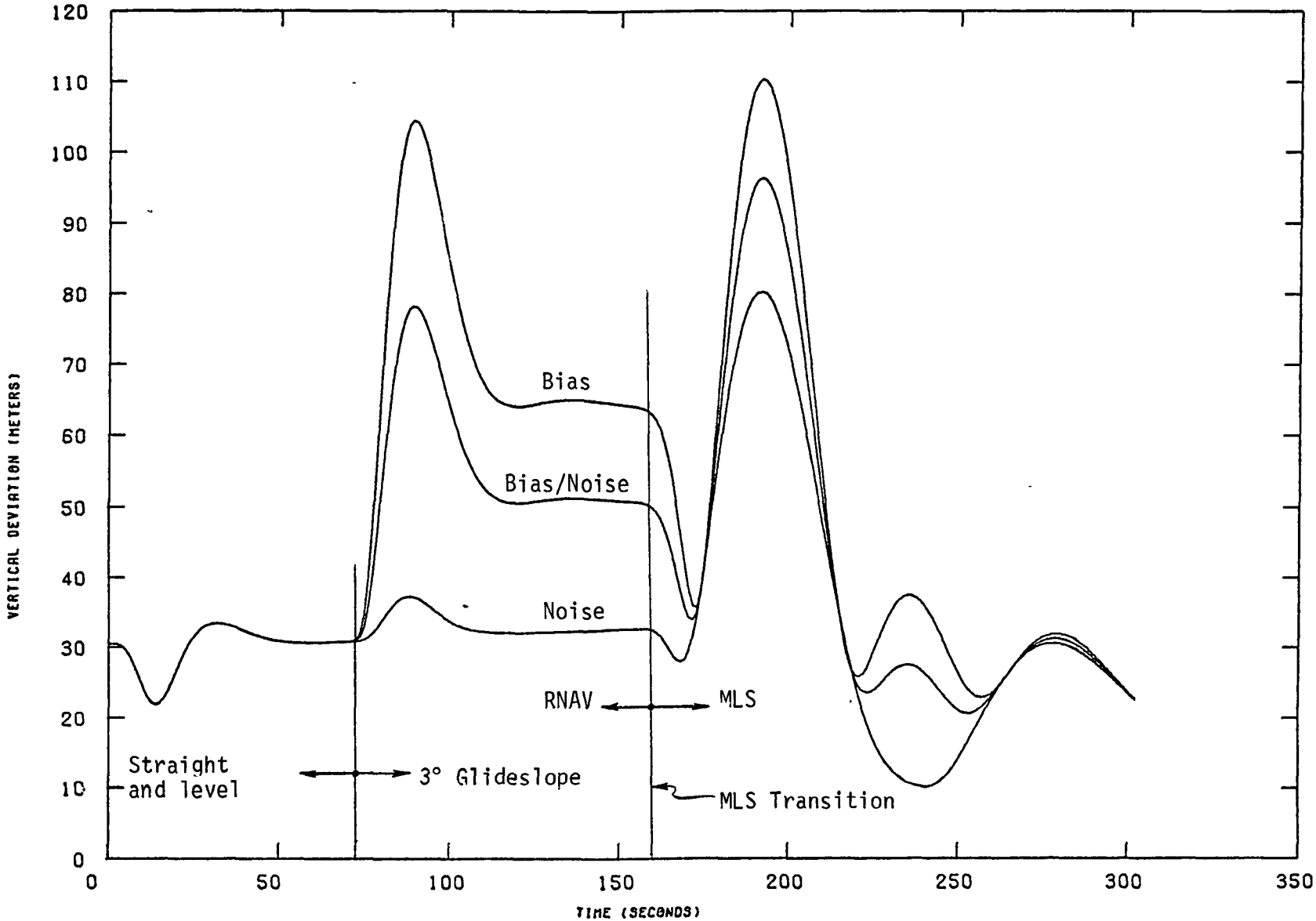

Figure 4.4 Vertical Deviation for Straight-In, VOR/DME, Facility A

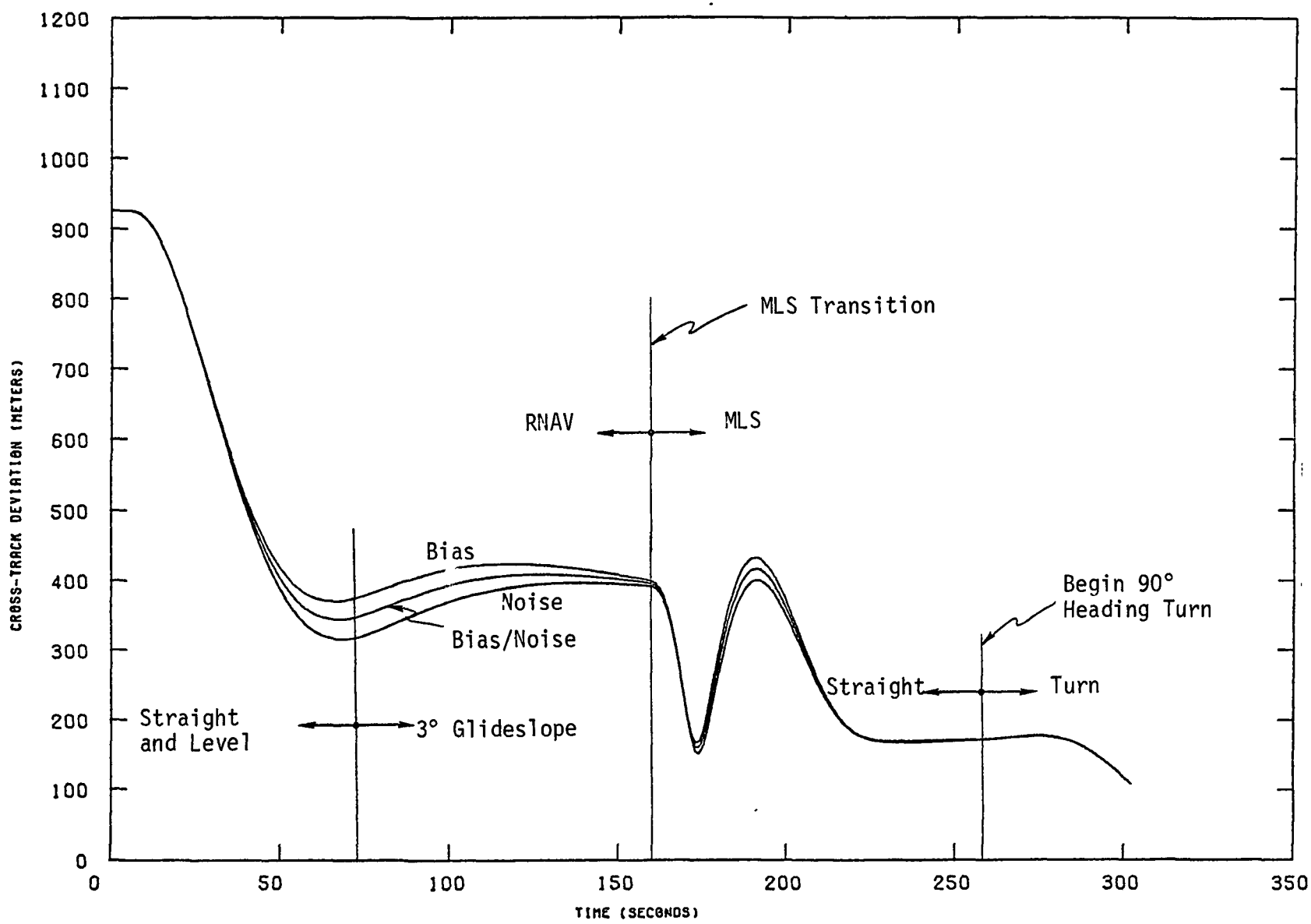

Figure 4.5 Cross-Track Deviation for 90° Turn to Final, VOR/DME, Facility A

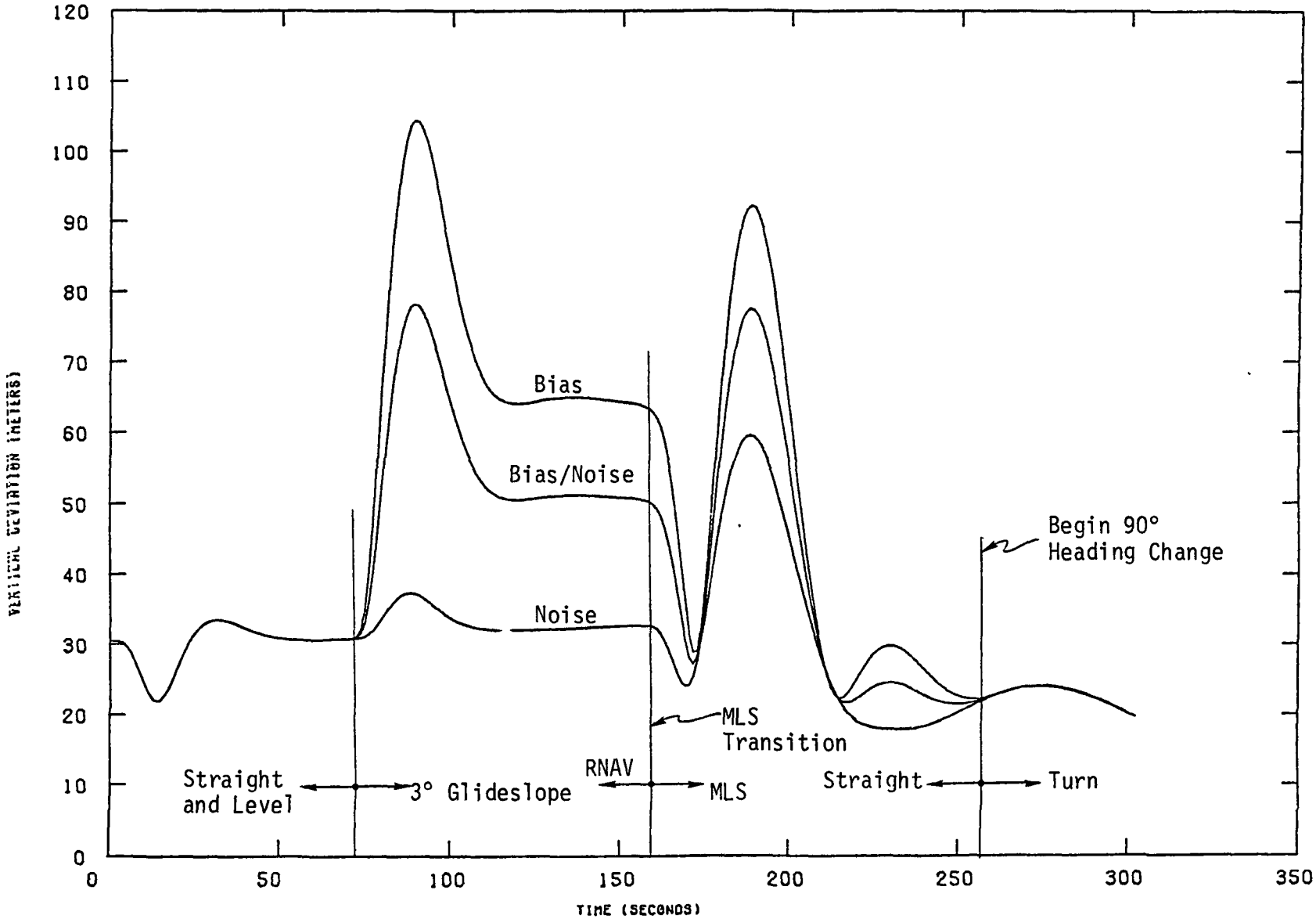

Figure 4.6 Vertical Deviation for 90° Turn to Final, VOR/DME, Facility A

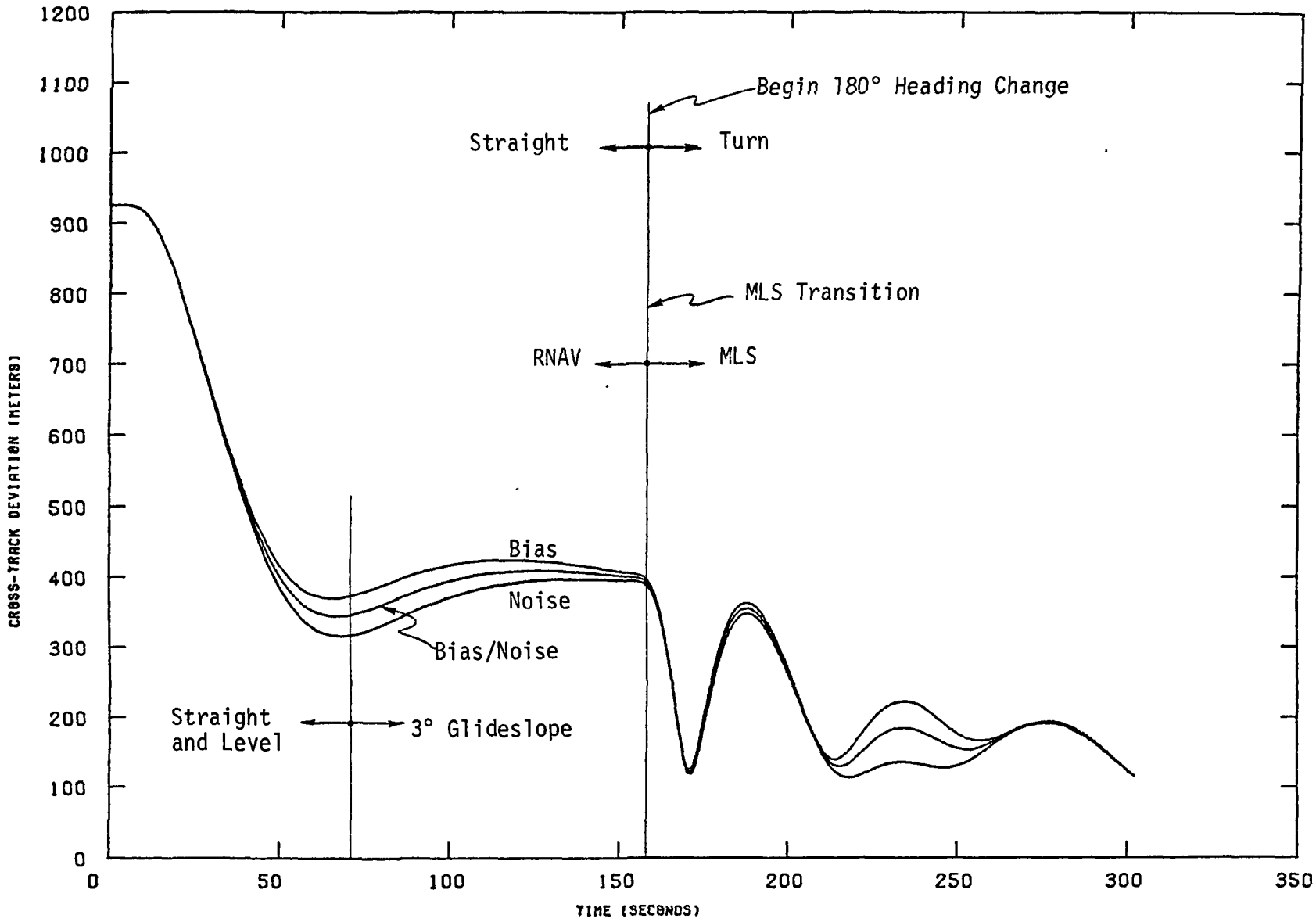

Figure 4.7 Cross-Track Deviation for 180° Turn to Final, VOR/DME, Facility A

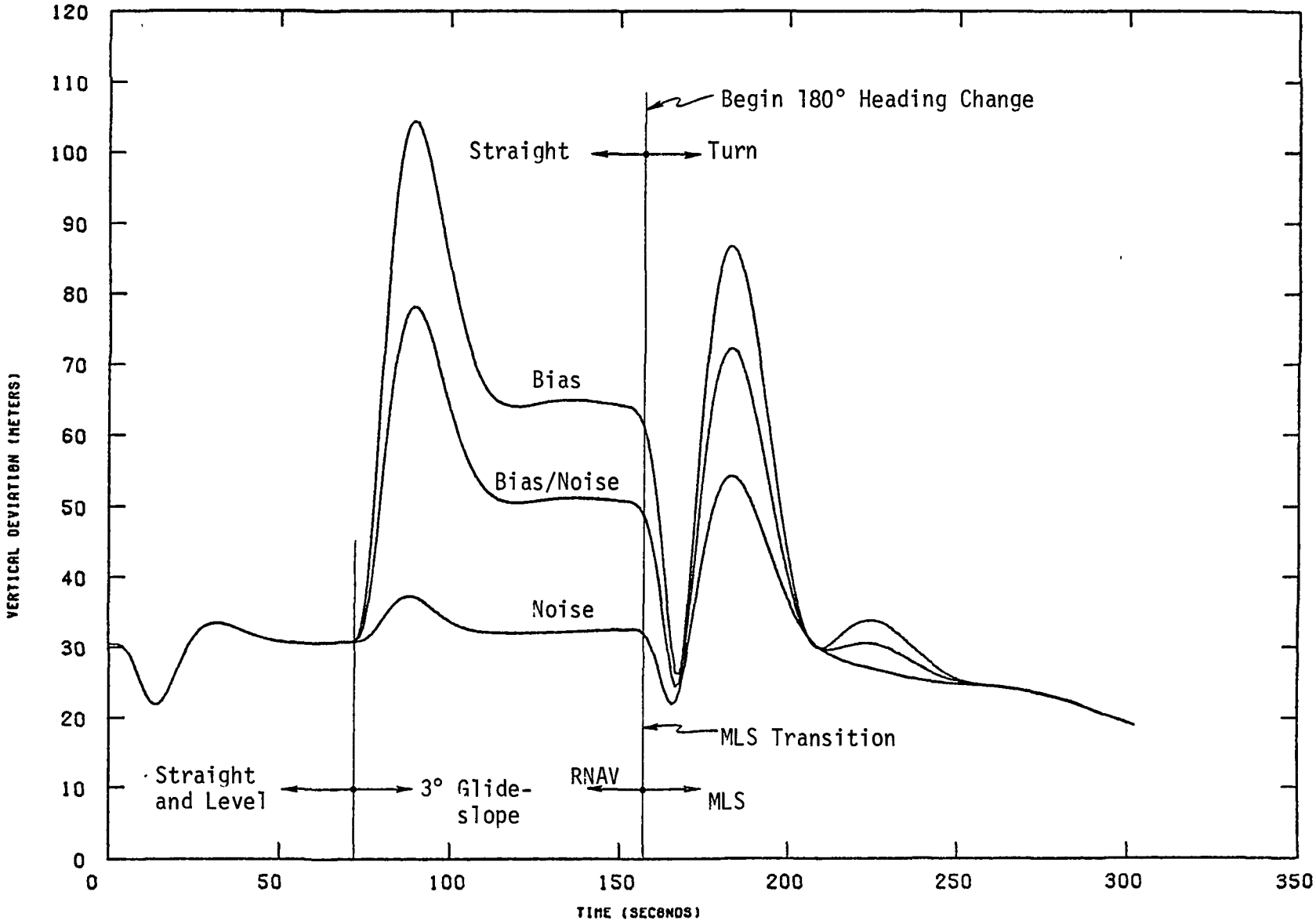

Figure 4.8 Vertical Deviation for 180° Turn to Final, VOR/DME, Facility A

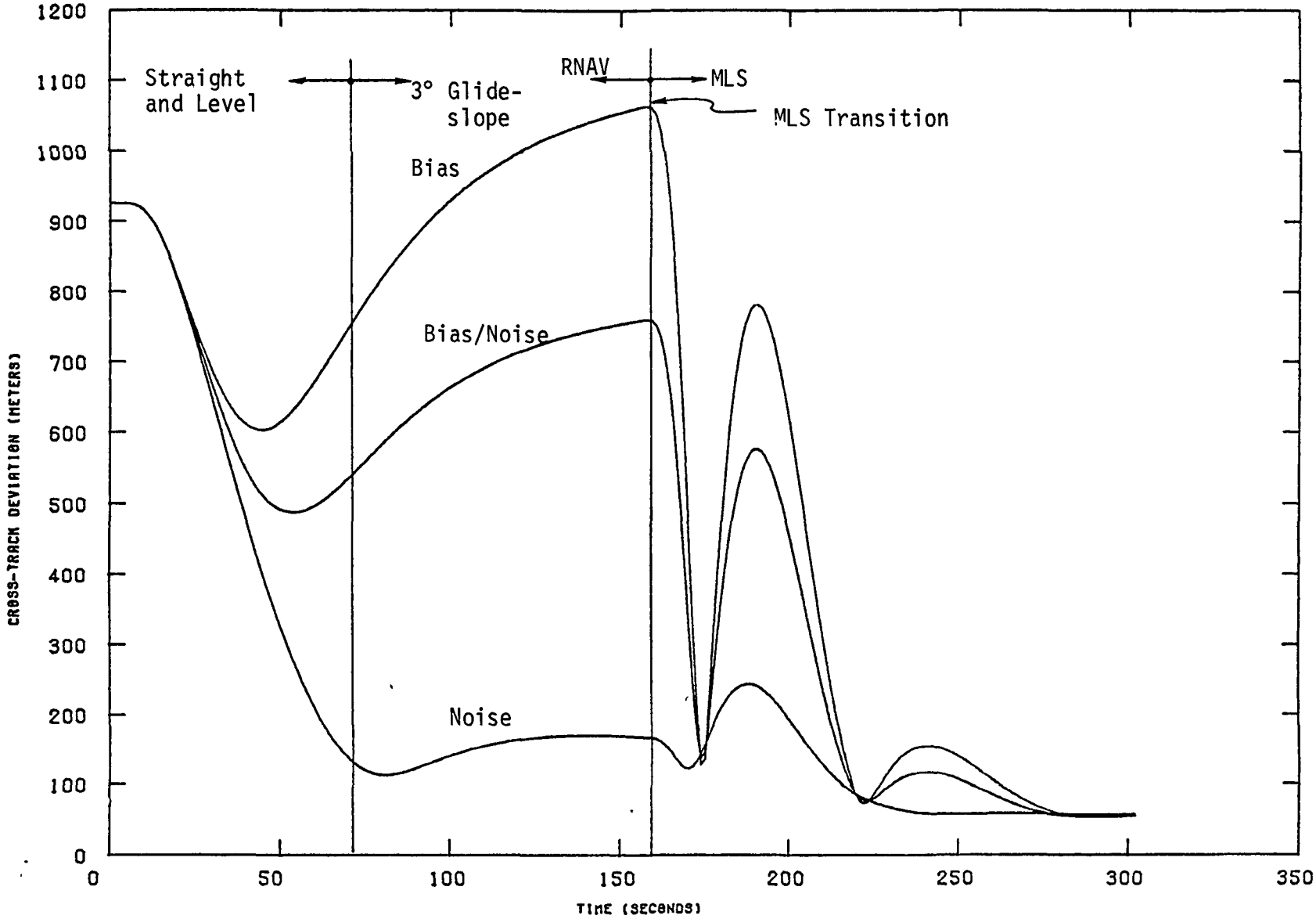

Figure 4.9 Cross-Track Deviation for Straight-In, VOR/DME, Facility B

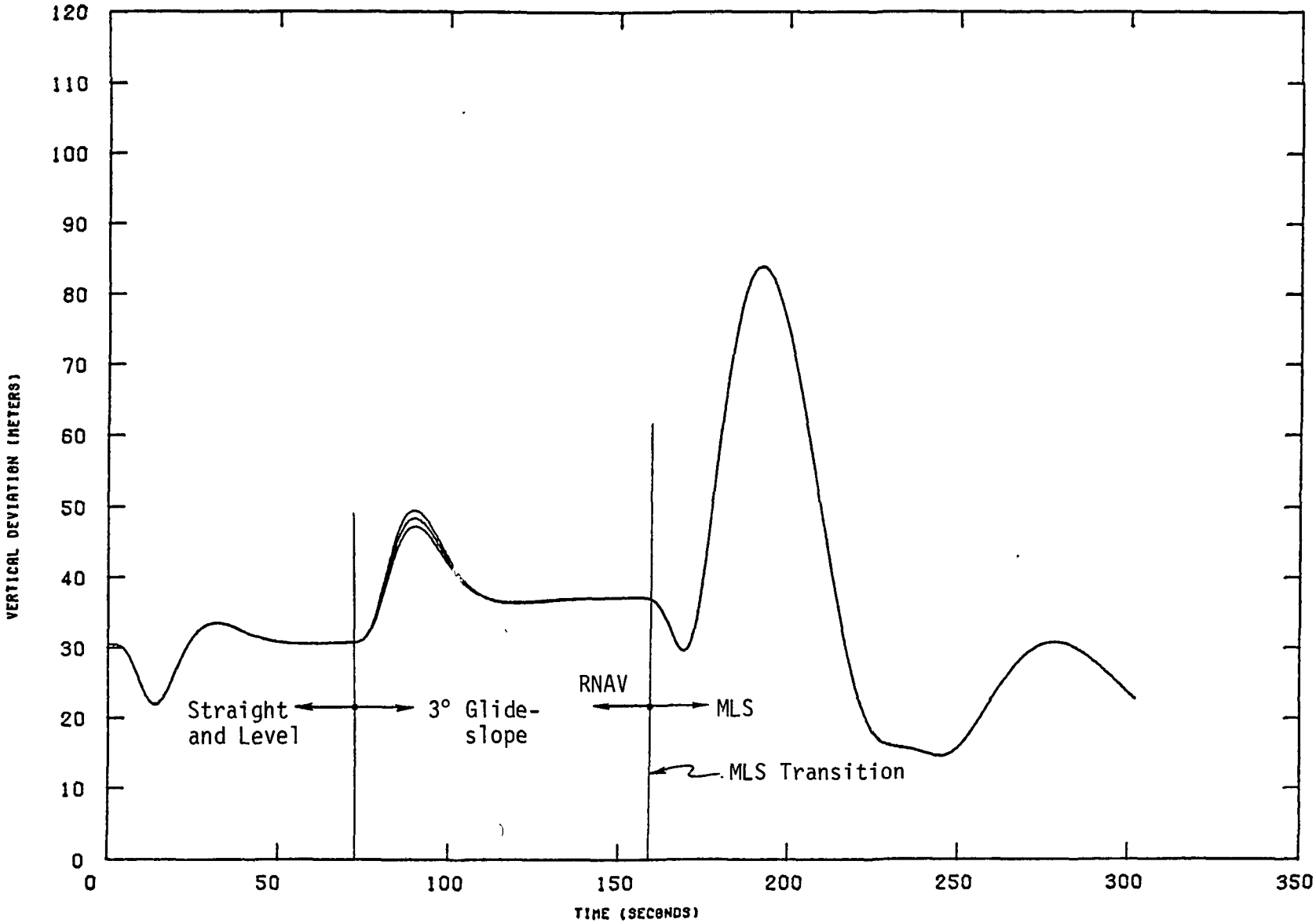

Figure 4.10 Vertical Deviation for Straight-In, VOR/DME, Facility B

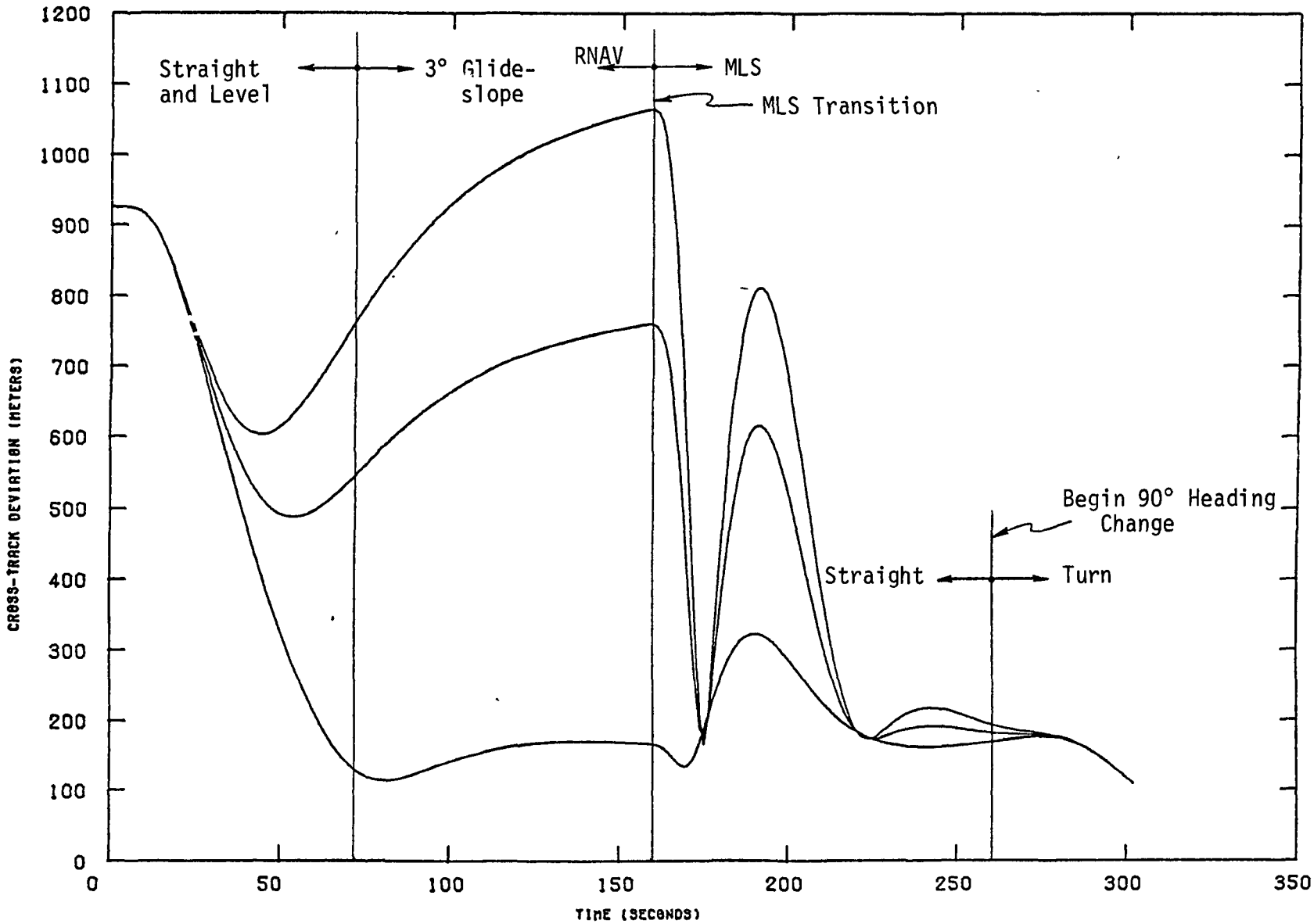

Figure 4.11 Cross-Track Deviation for 90° Turn to Final, VOR/DME, Facility B

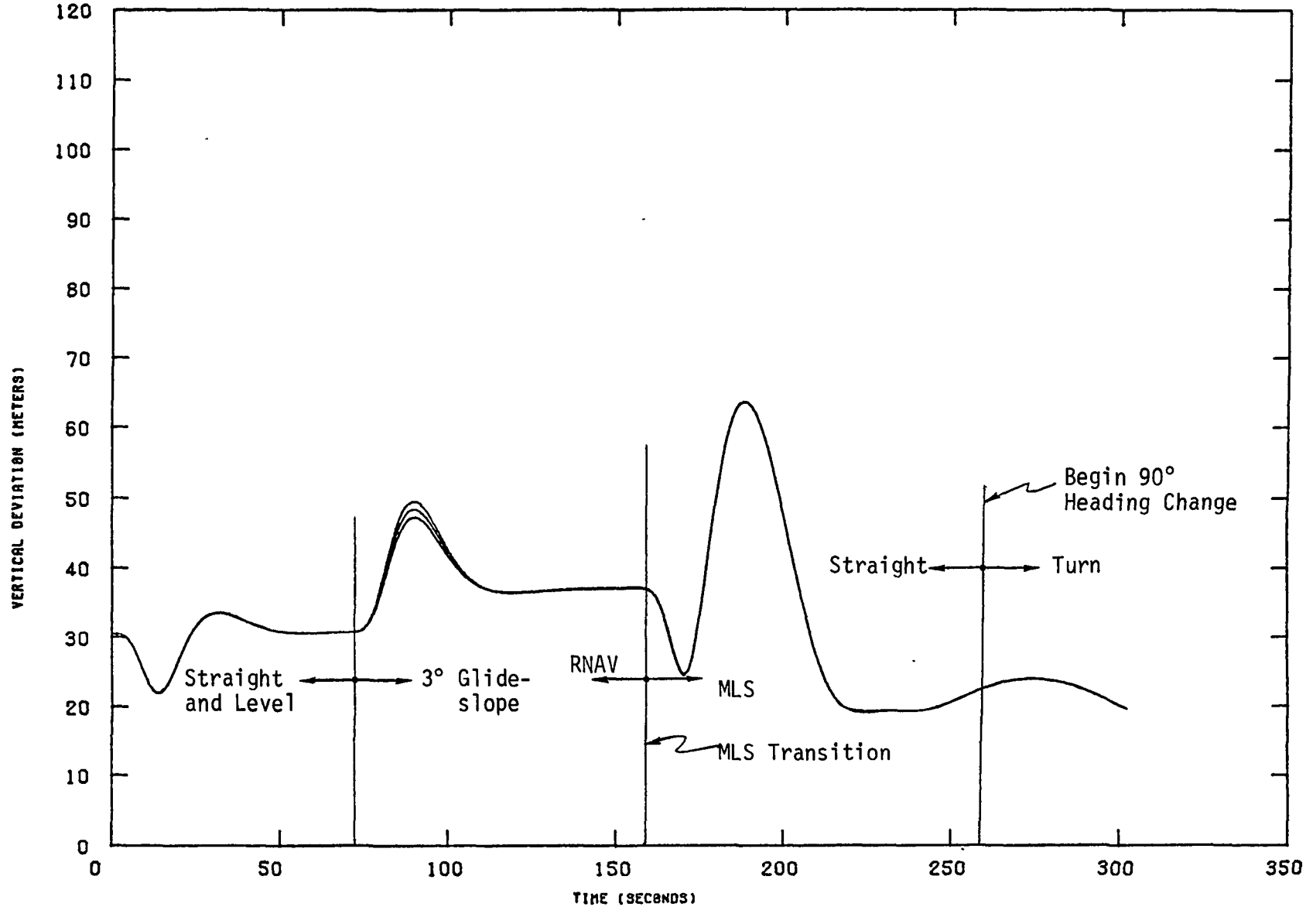

Figure 4.12 Vertical Deviation for 90° Turn to Final, VOR/DME, Facility B

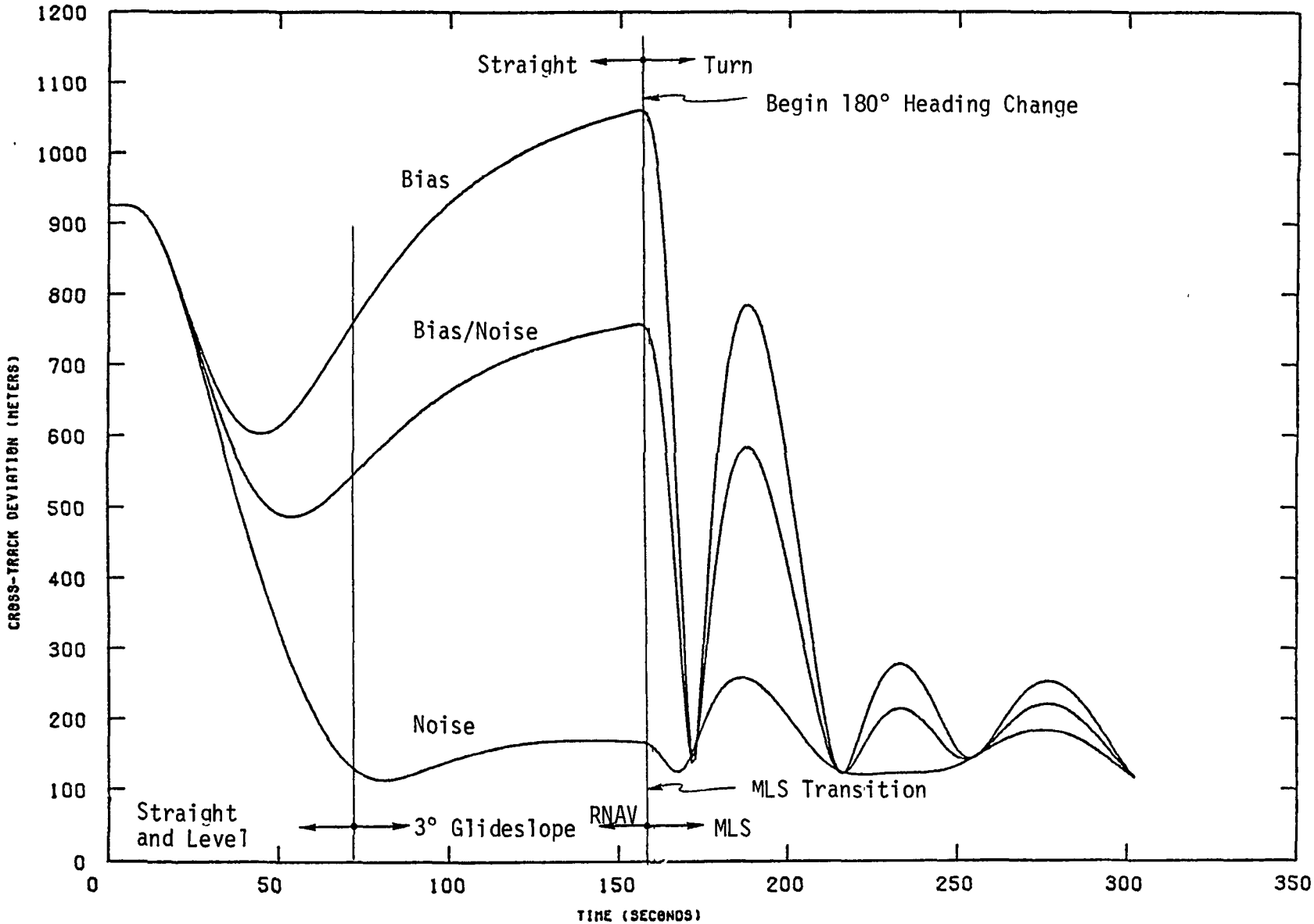

Figure 4.13 Cross-Track Deviation for 180° Turn to Final, VOR/DME, Facility B

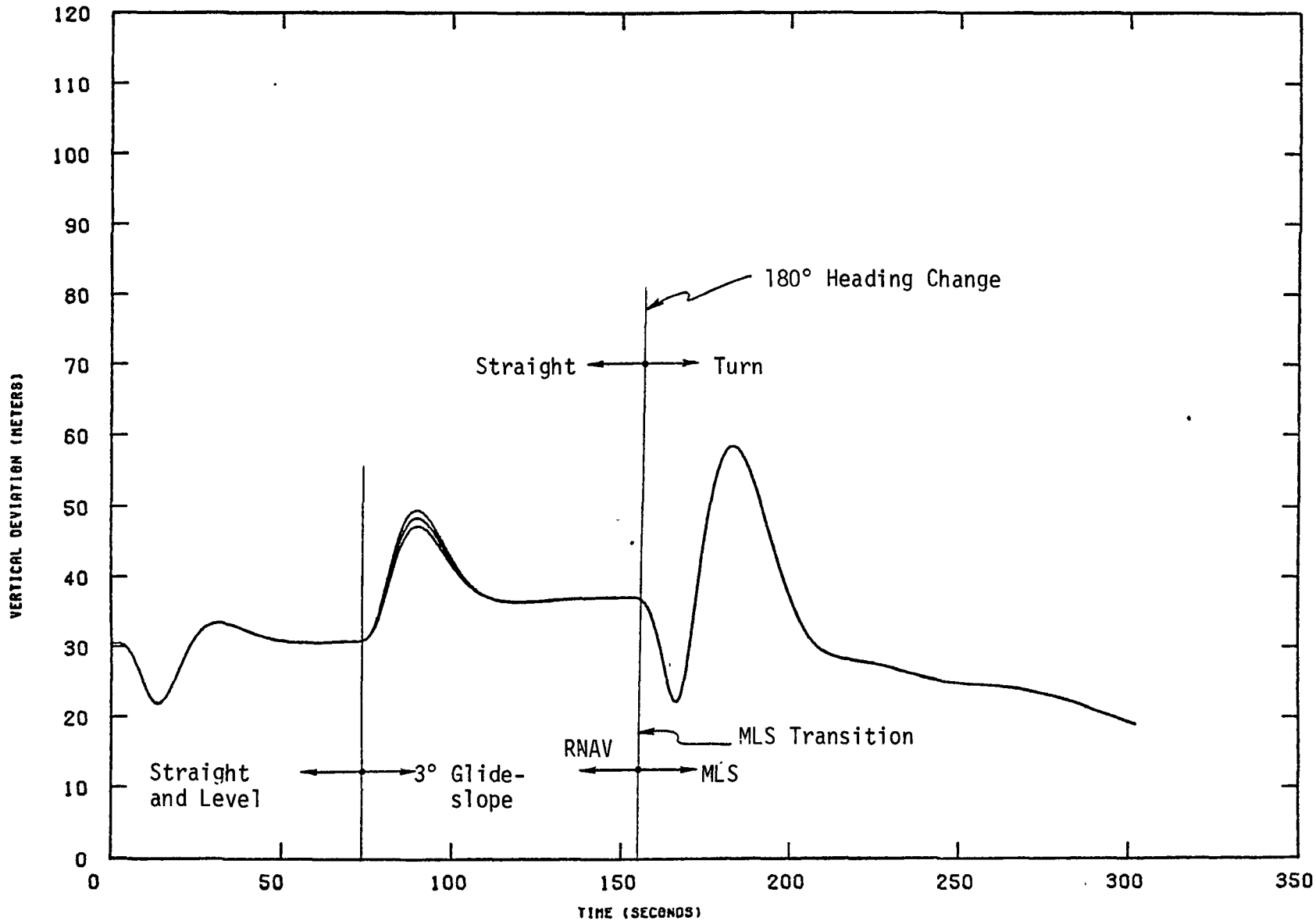

Figure 4.14 Vertical Deviation for 180° Turn to Final, VOR/DME, Facility B

With pure random noise (high frequency) the filter displays excelelnt performance. Addition of bias into the signal content significantly degrades filter performance.

During MLS transition it can be observed that the initial transients are significant. This is particularly true of the vertical channel (note also that the vertical channel has a significant transient at pitch over initiation). Several offline studies indicated that the magnitude of the response was sensitive to filter initialization at the onset of MLS transition. However, initialization did not impact the settling time.

At MLS transition the filters are subjected to a step input (bias) which can be significant. The filter and autopilot coupling during transition was found to be the primary cause for the subsequent transient responses to this input bias. One factor not included in the ensemble simulation because of the linear characteristics of this technique, is the control bound normally imposed on a control system. This will reduce the magnitude of the transient and will probably lengthen the settling time. However, this needs to be verified through nonlinear simulation techniques or through describing function techniques in the ensemble simulation.

Figures 4.5 and 4.6 show the cross-track and vertical deviation time histories respectively for the 90° turn-to-final approach. Similarly, Figures 4.7 and 4.8 show the results for the 180° turn-to-final approach. Note that the variation of the magnitude of the errors and the settling times of the position errors in the MLS region vary as a function of geometry. This is primarily due to the range dependence of the azimuth and elevation-induced position errors. Hence, the MLS geometry effects impacts both the magnitude and the settling times. This implies that the route design and MLS coverage region must provide sufficient airspace to null the RNAV delivery errors such that aircraft stabilization is achieved prior to final approach and landing.

Figures 4.9 through 4.14 display the cross-track and vertical deviation time histories for the VOR/DME RNAV cases with the worst-case cross-track delivery errors. Note that the vertical time histories are the same for all error parameter values. This is due to the fact that the along-track error is driven by the DME errors only which, for the VOR/DME cases, are not varied. Similar transient behavior is noted with these cases as with the worst-case along-track error cases discussed previously.

An additional peculiarity of interest is the transient response due to increased delivery errors as observed in Figures 4.9, 4.11 and 4.13. For larger cross-track errors

the MLS transients display additional oscillations. Particularly in the 180° turn-to-final (Figure 4.13), several additional oscillations are observed (these are probably geometry-induced since the aircraft/runway orientation is continually changing throughout the turn). For these cases the settling time is assumed to occur after the second oscillation since the response appears to be approaching steady state at this point.

In Figures 4.10, 4.12, and 4.14 the vertical channel transients are observed to be significant. Again it is partially attributable to initial condition transients and to filter/autopilot coupling.

4.4.2 DME/DME

Figures 4.15 through 4.22 indicate the results for the DME/DME updated INS RNAV simulation. Only Figures 4.15 through 4.20 show transition into MLS for the reasons stated previously. Generally, the DME/DME-induced RNAV delivery errors are less than the VOR/DME-induced delivery errors. For this reason the transients tend to be more well behaved during transition. The improved navigation performance characteristics of the DME/DME system (relative to the VOR/DME system) is also observed in the RNAV portion.

Figures 4.21 and 4.22 indicate the worst-case cross-track tests for DME/DME. To determine the MLS transient response the corresponding VOR/DME transient is consulted as indicated in Table 4.2.

4.5 ICAO DEMONSTRATION FLIGHTS

For illustrative purposes the 130° turn-to-final and "S-turn" approach utilized during the ICAO demonstration flights were simulated. The DME/DME facilities selected for each case were Sea Isle and Millville. These were chosen since it was difficult to determine a facility pair, using the Atlantic City VORTAC as primary, that provided a favorable geometry. The error associated with these facilities was assumed to be a DME bias of 350 meters and DME noise of 650 meters. The waypoints associated with the ICAO demonstration flight profiles are indicated on the plots shown in Figures 4.23 through 4.26. These correspond to the profiles shown in Figures 3.1 and 3.2.

4.6 SUMMARY OF RESULTS

The significant results of the sensitivity analysis are presented here as a quick-look summary. The summary is given in Table 4.3. The table includes the RNAV delivery

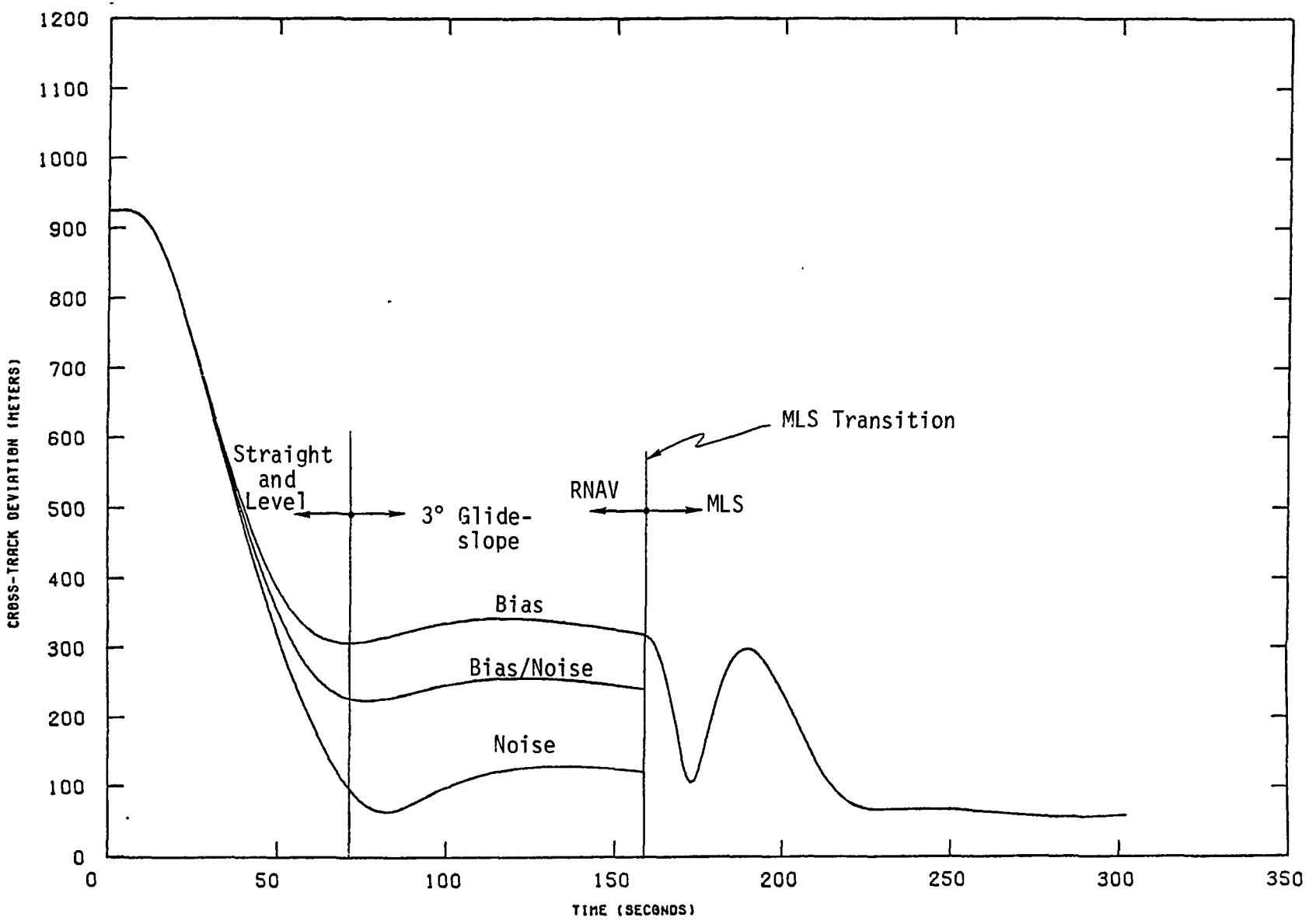

Figure 4.15 Cross-Track Deviation for Straight-In, DME/DME, Facilities A

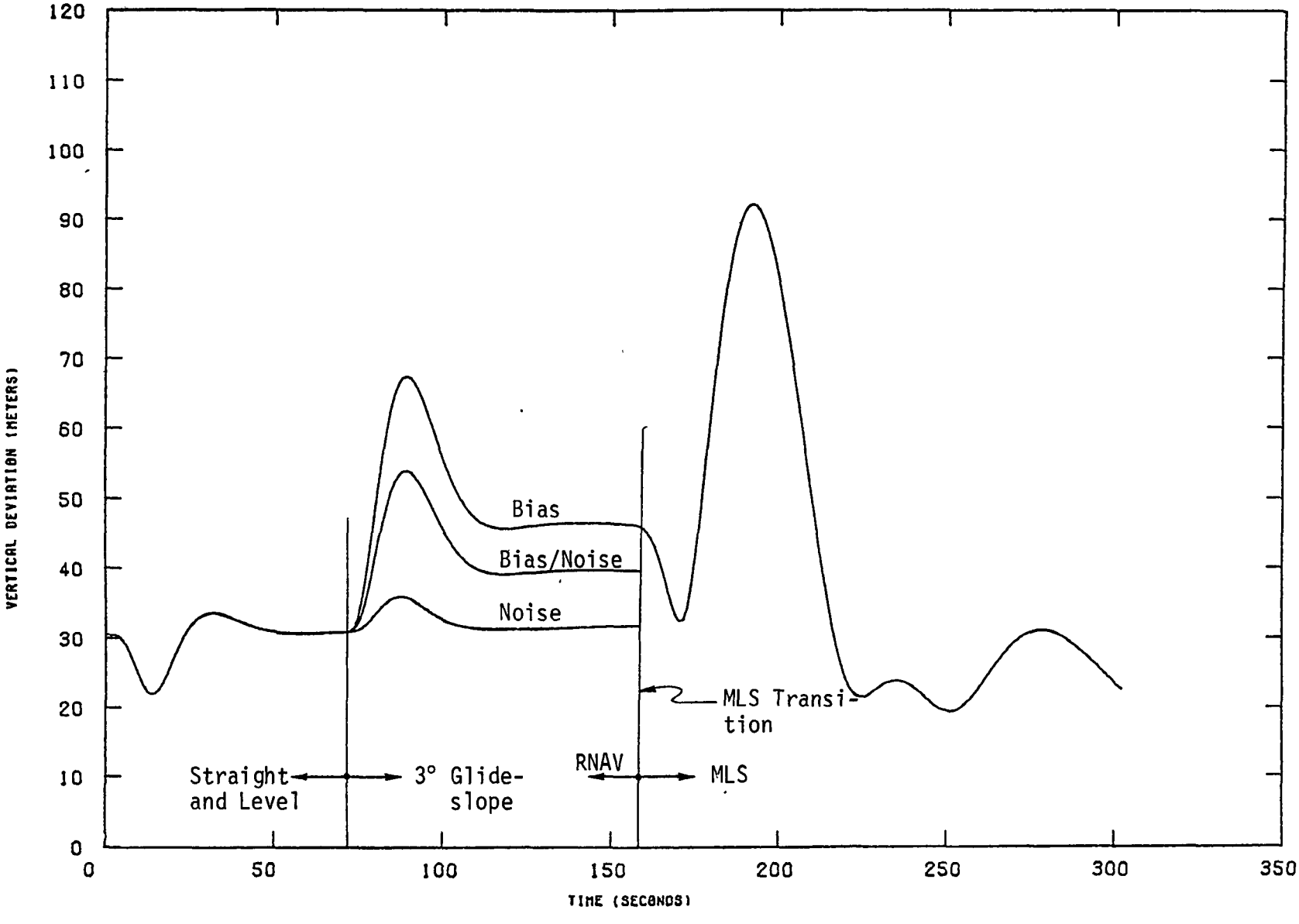

Figure 4.16 Vertical Deviation for Straight-In, DME/DME, Facilities A

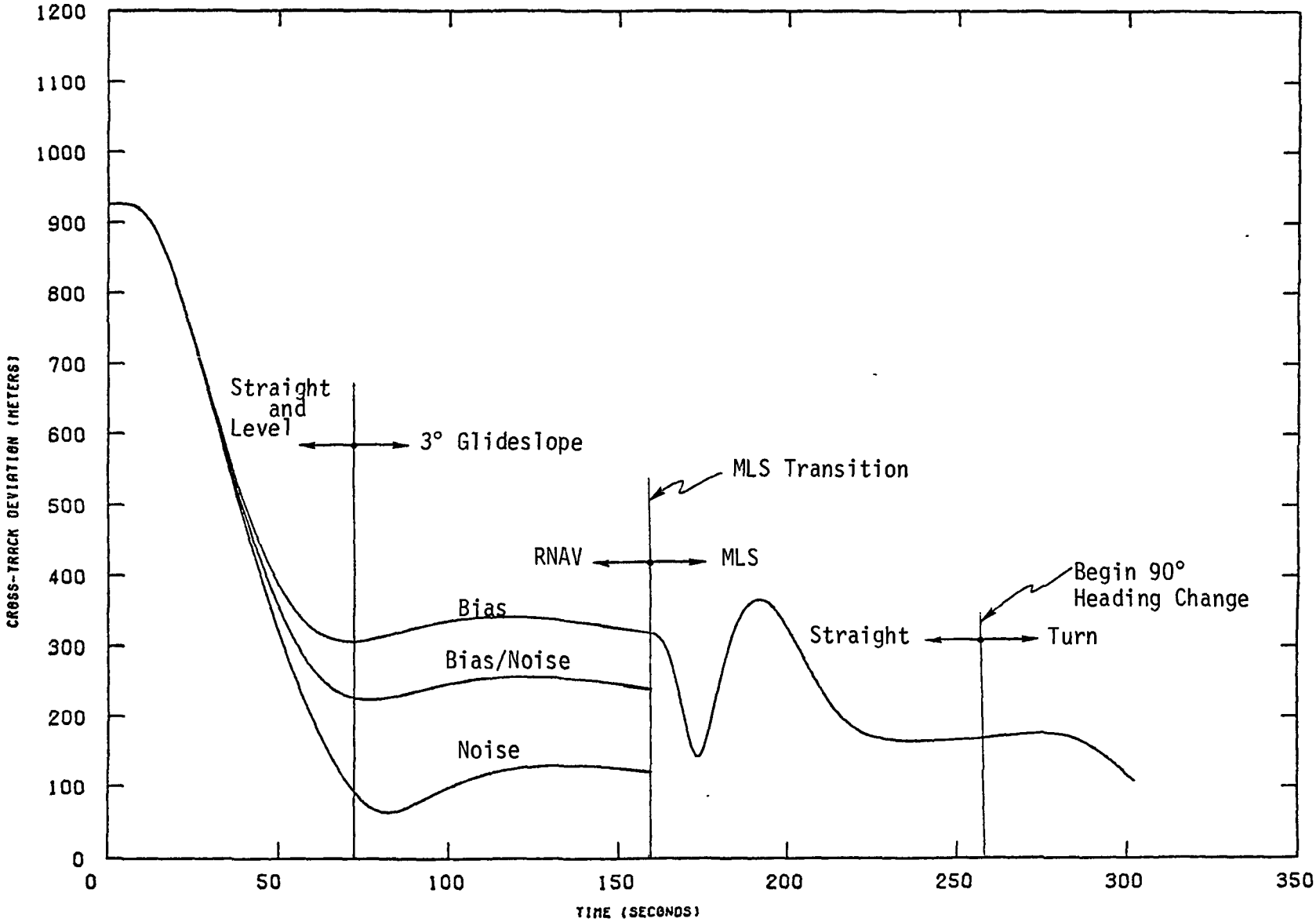

Figure 4.17 Cross-Track Deviation for 90° Turn to Final, DME/DME, Facilities A

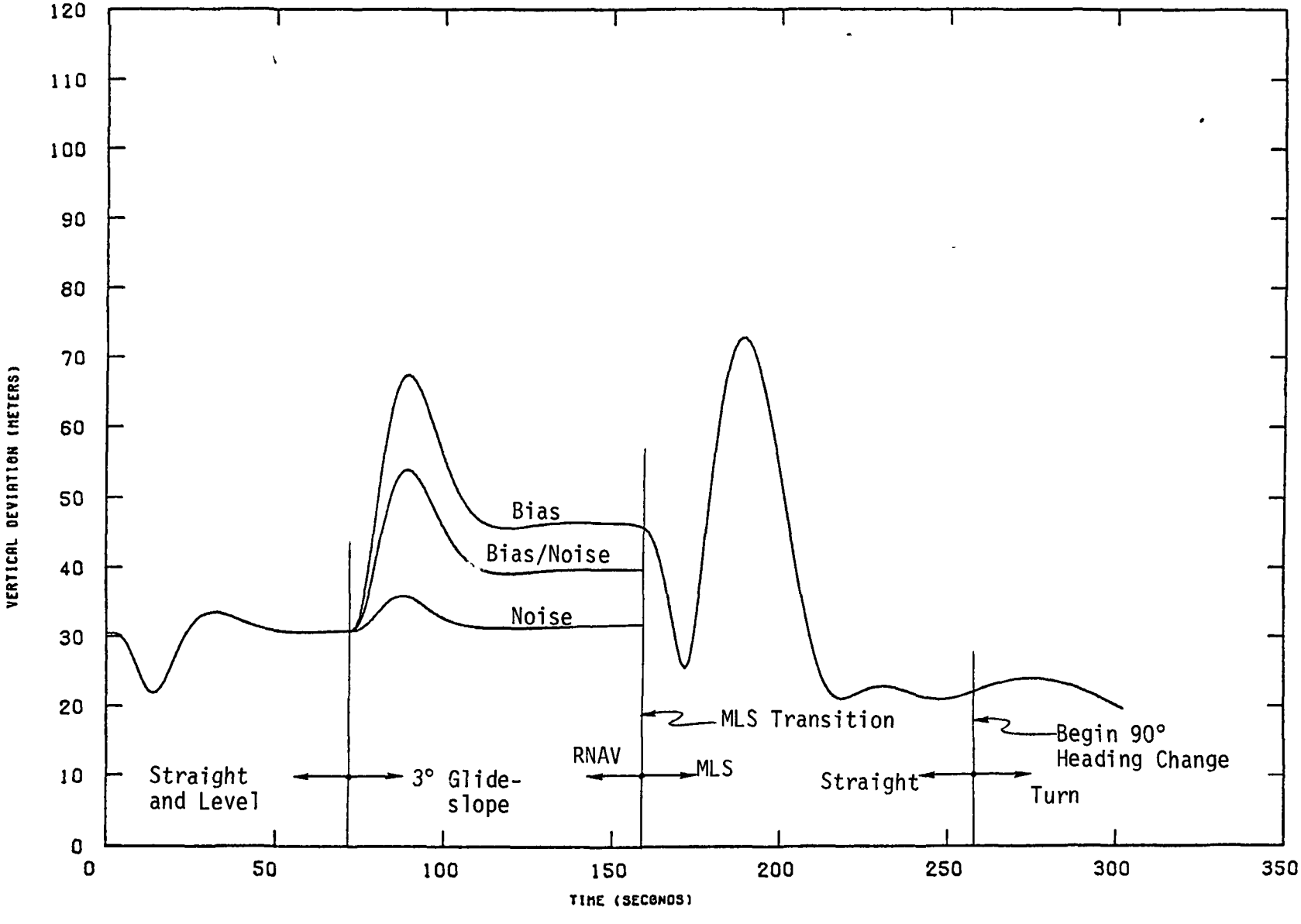

Figure 4.18 Vertical Deviation for 90° Turn to Final, DME/DME, Facilities A

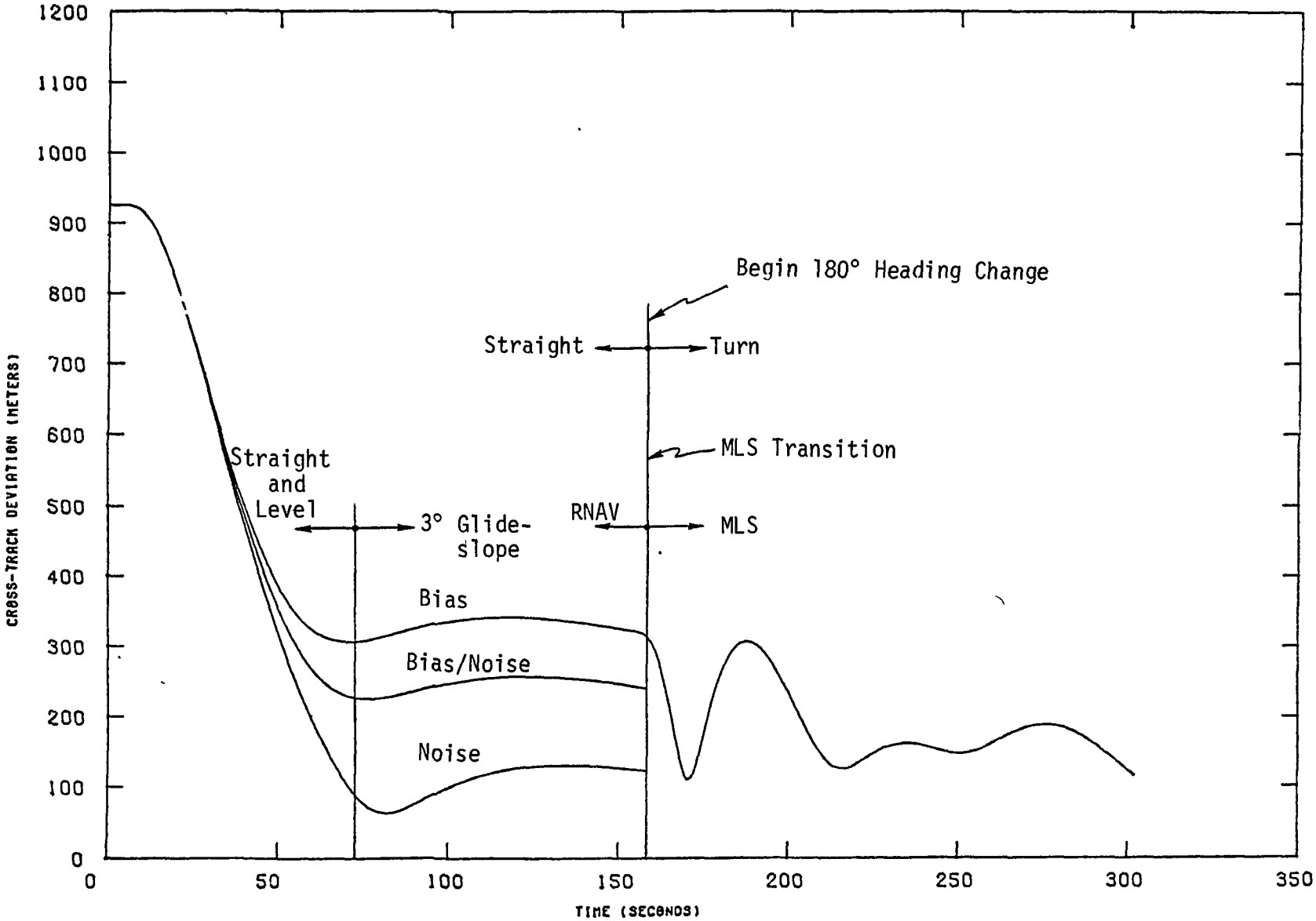

Figure 4.19 Cross-Track Deviation for 180° Turn to Final, DME/DME, Facilities A

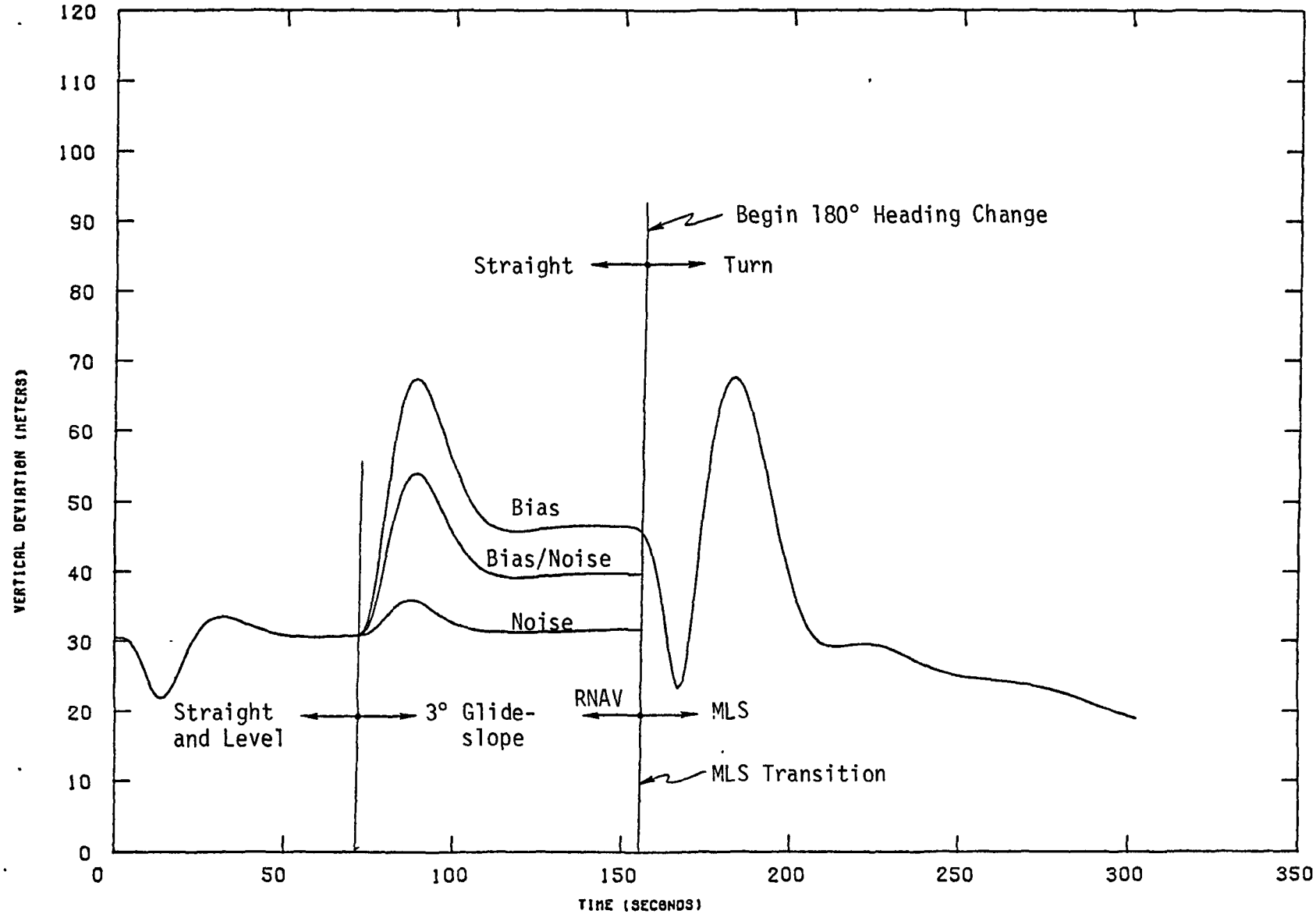

Figure 4.20 Vertical Deviation for 180° Turn to Final, DME/DME, Facilities A

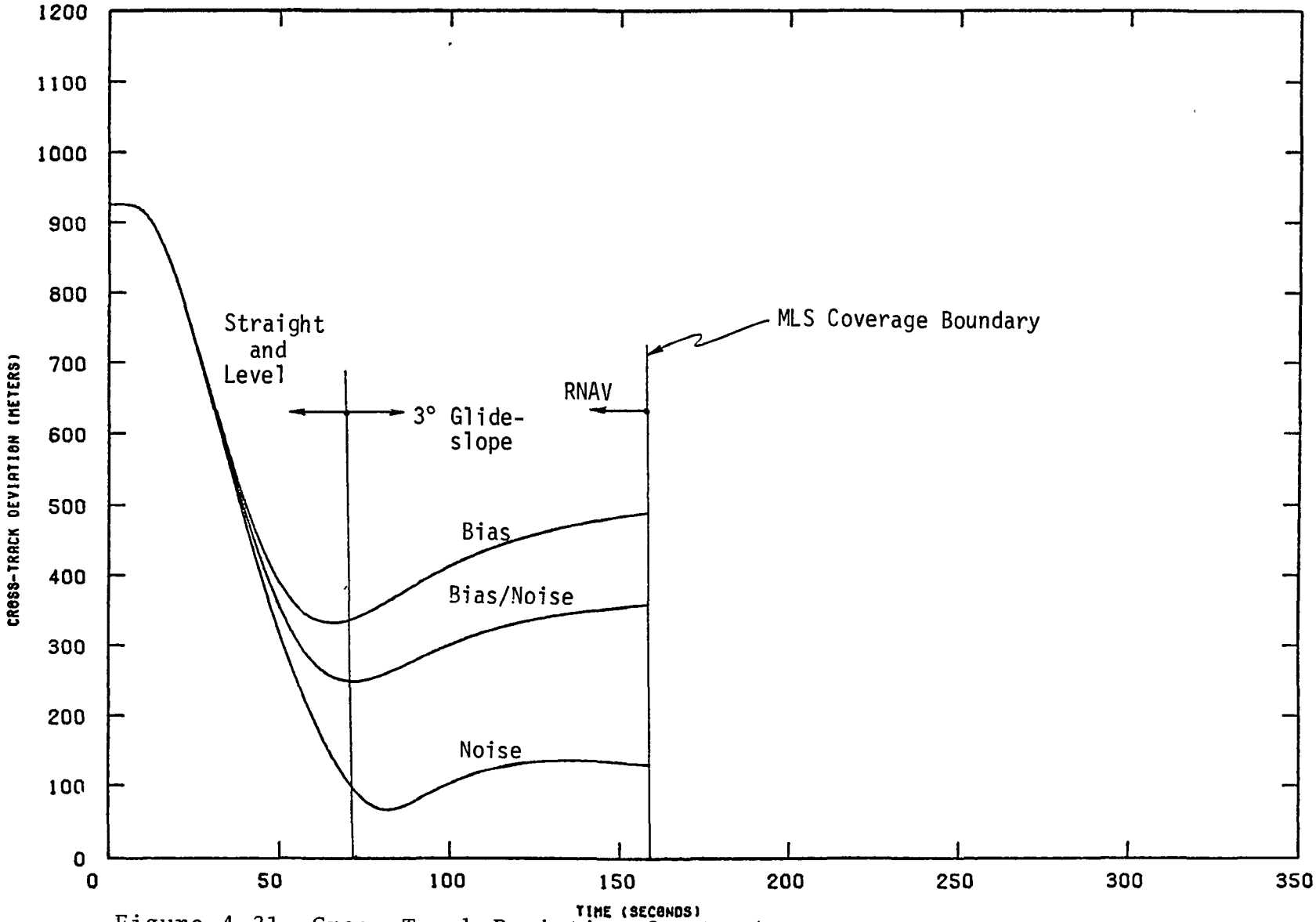

Figure 4.21 Cross-Track Deviation for DME/DME, Facilities B

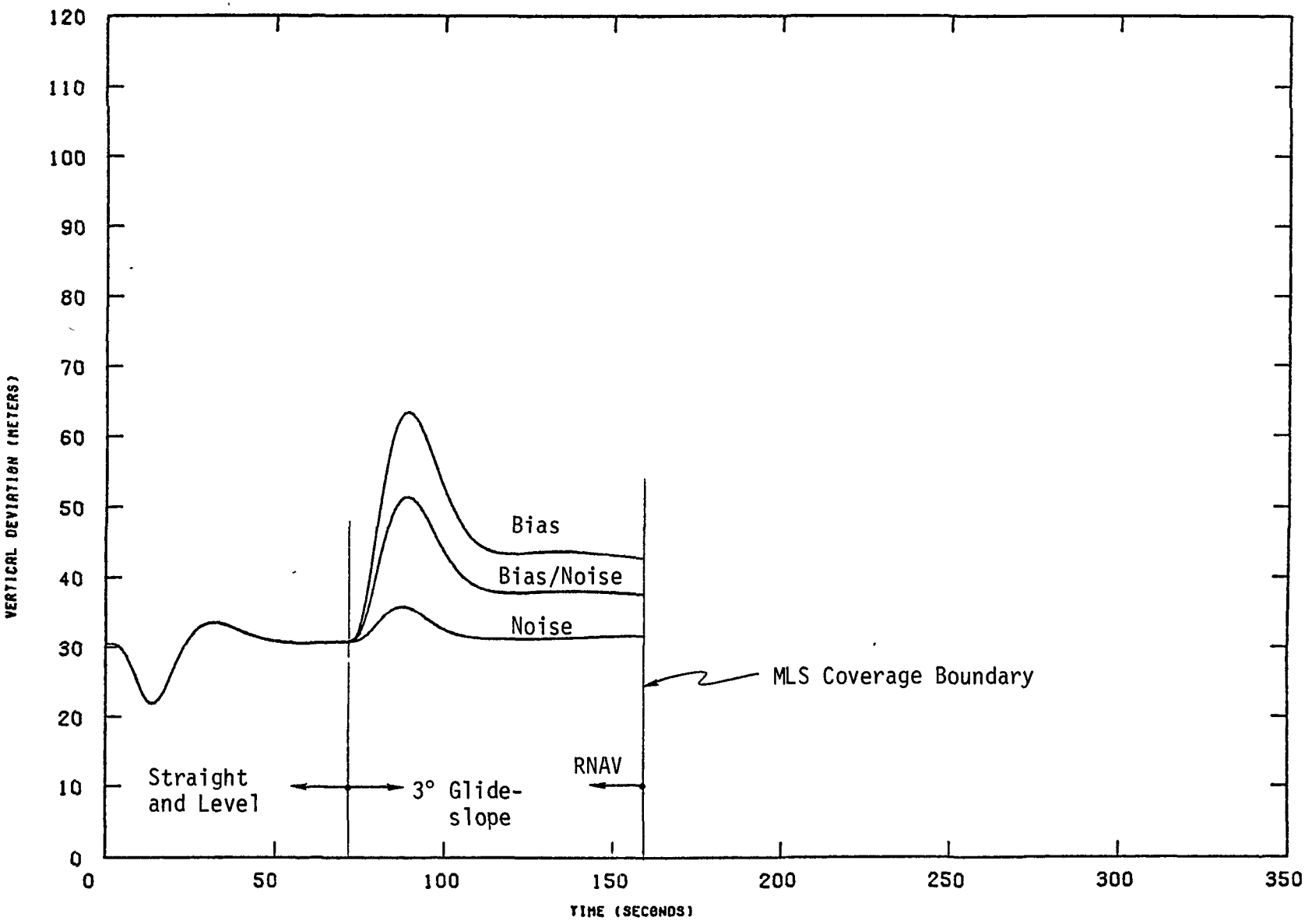

Figure 4.22 Vertical Deviation for DME/DME, Facilities B

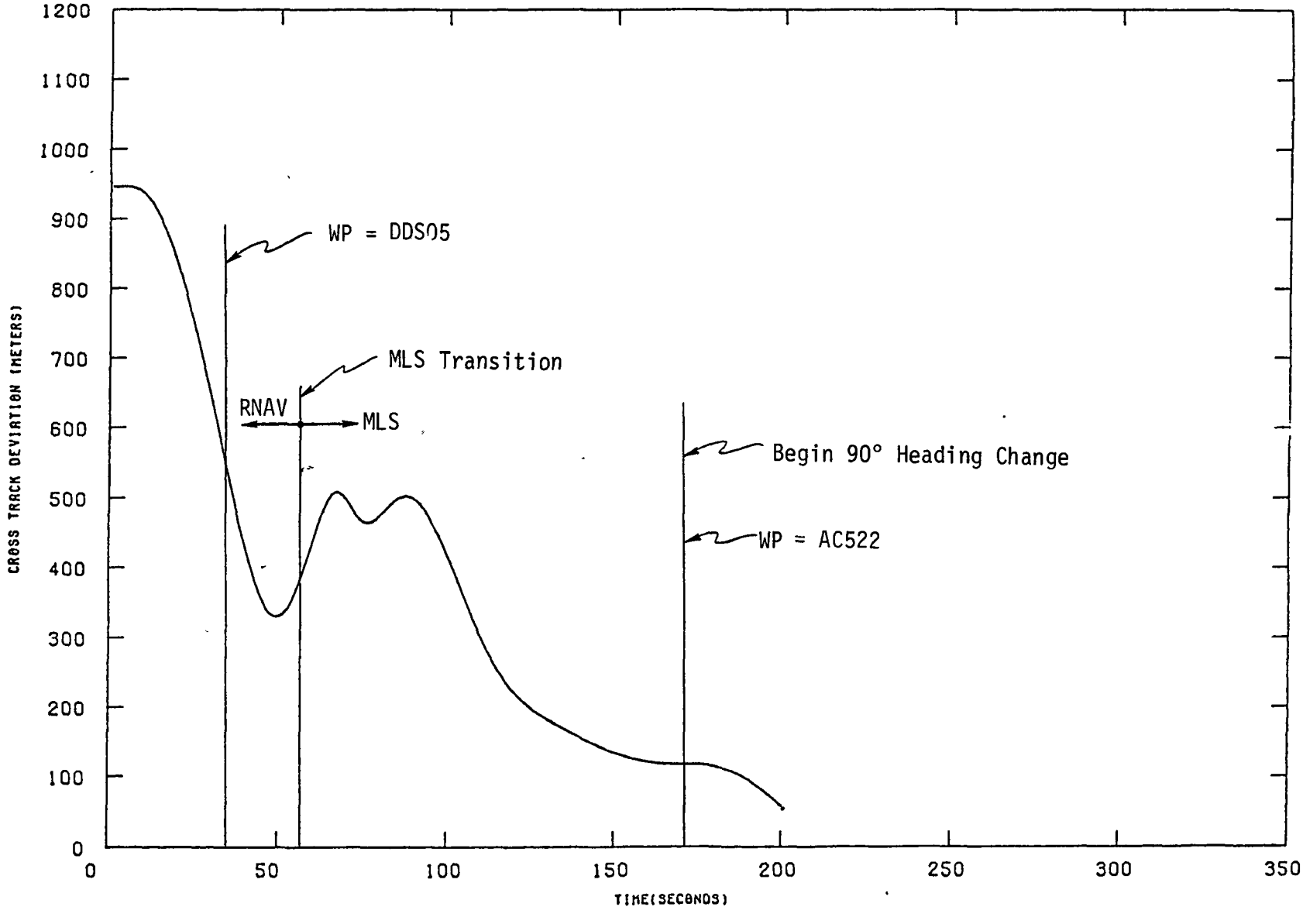

Figure 4.23 Cross-Track Deviation Time History for S-Turn ICAO Profile

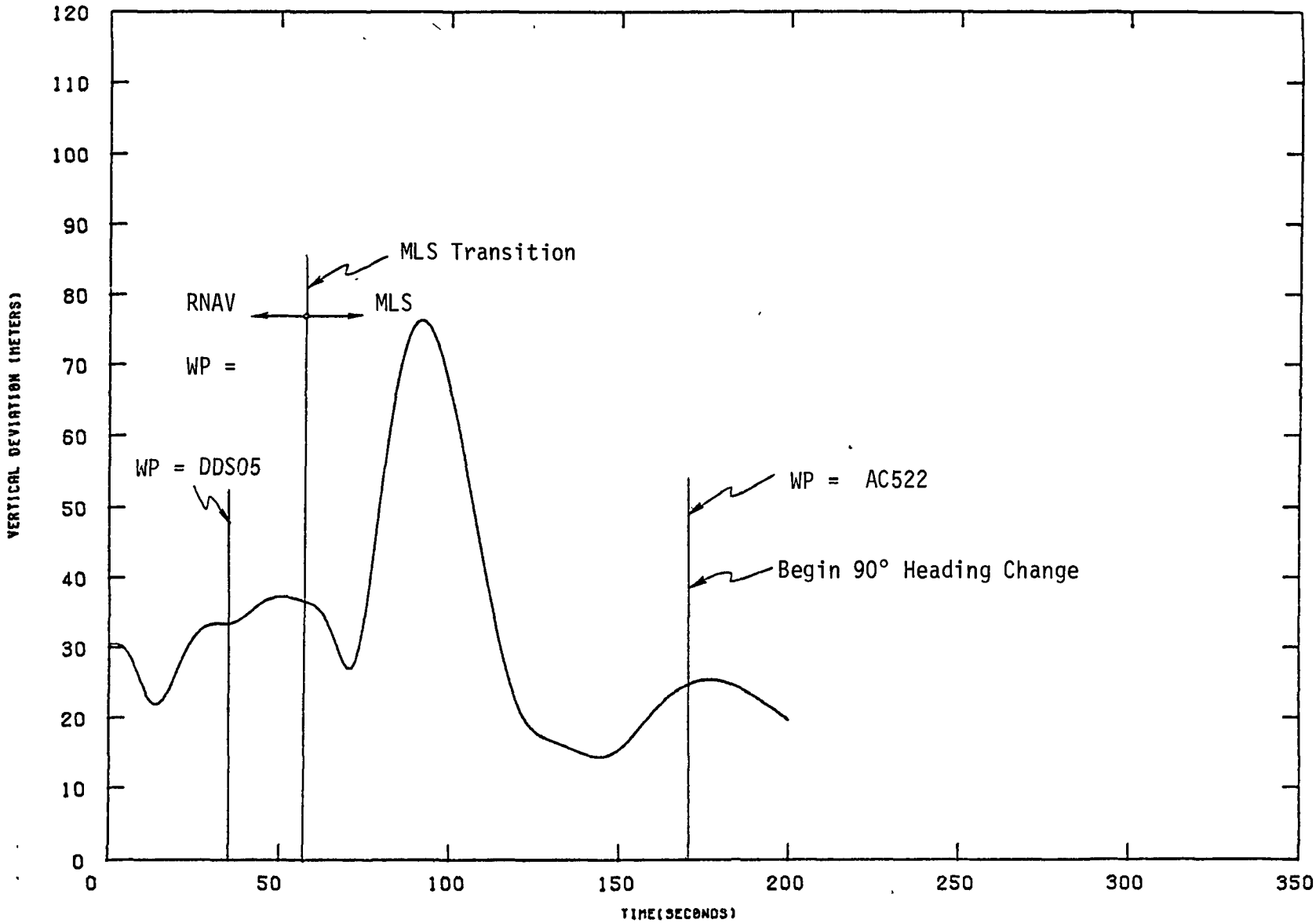

Figure 4.24 Vertical Deviation Time History for S-Turn ICAO Profile

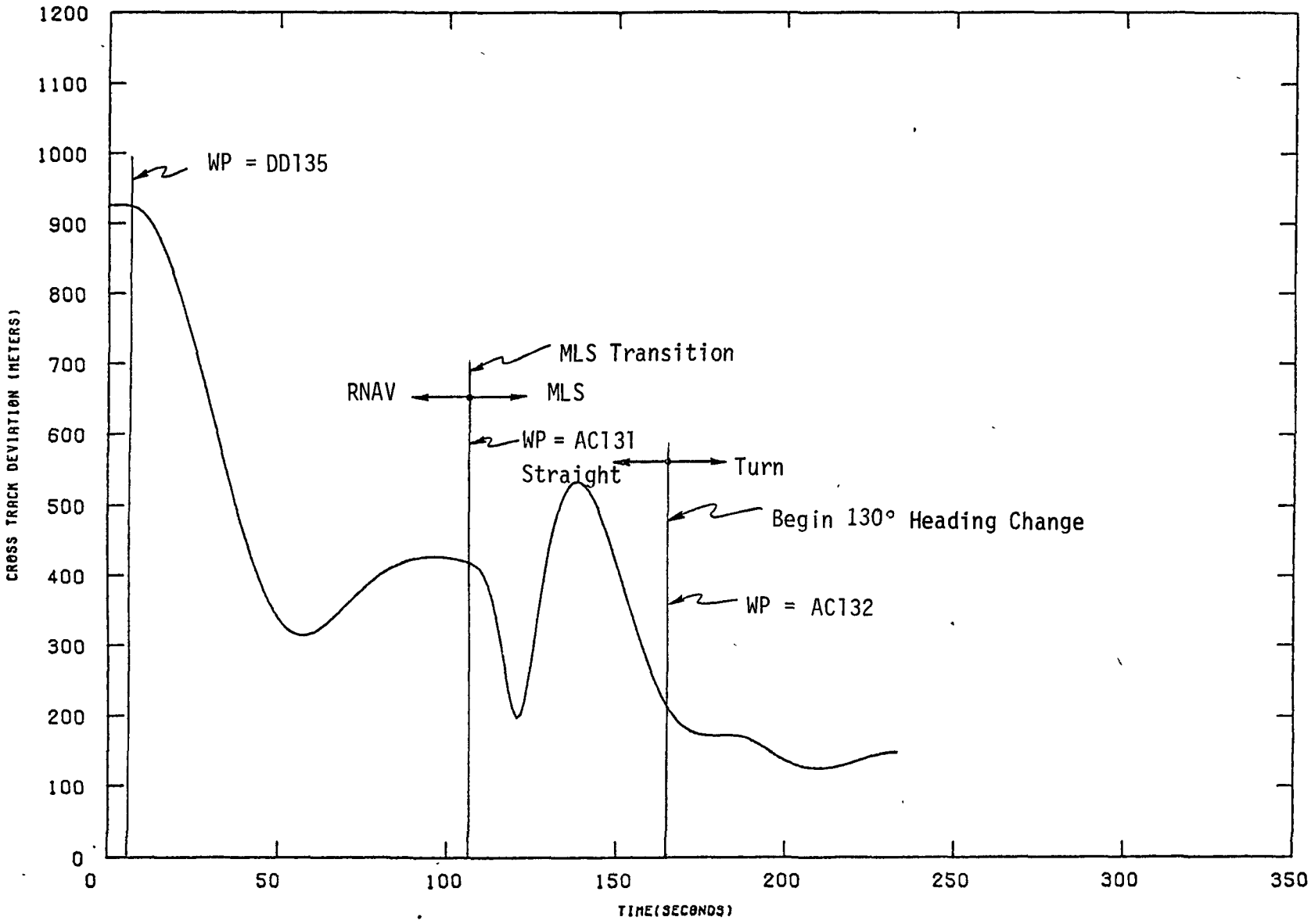

Figure 4.25 Cross-Track Deviation Time History for 130° Turn ICAO Profile

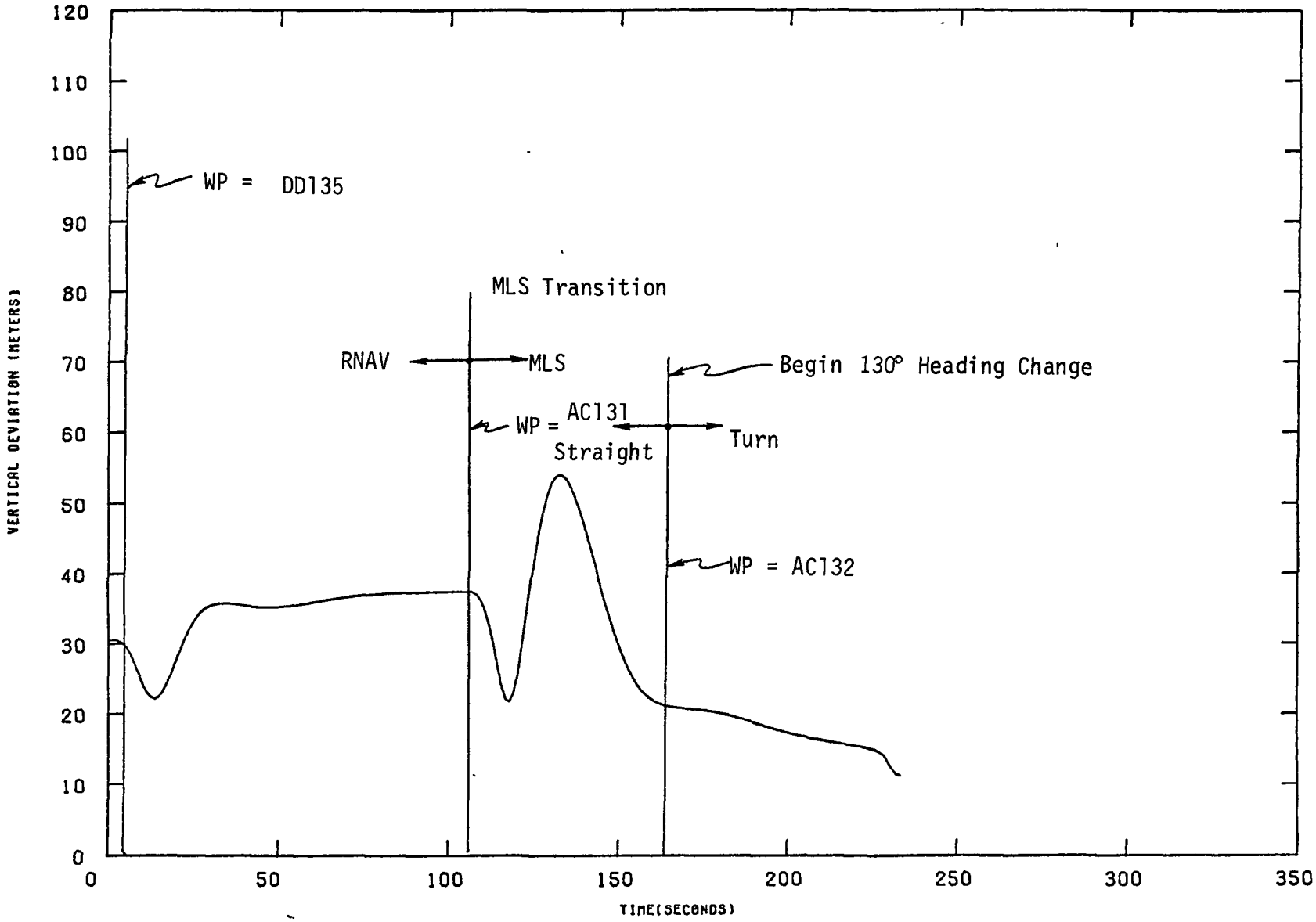

Figure 4.26 Vertical Deviation Time History for 130° Turn ICAO Profile

Table 4.3

Summary Results

MODE	FACILITY	ERROR	RNAV DELIVERY ERRORS(METERS)		MLS SETTLING TIMES (MINUTES)					
					STRAIGHT-IN		90° TURN		180° TURN	
			CROSS-TRACK	VERTI-CAL	CROSS-TRACK	VERTI-CAL	CROSS-TRACK	VERTI-CAL	CROSS-TRACK	VERTI-CAL
VOR/DME	Worst-Case Along-Track	Bias	407	64.3	0.95	2.33	0.95	1.63	0.95	1.54
		Bias/Noise	400	50.9	0.95	2.33	0.95	1.63	0.95	1.54
		Noise	394	32.6	0.95	2.33	0.95	1.63	0.95	0.83
	Worst-Case Cross-Track	Bias	1057	37.2	1.77	0.95	1.48	0.95	*	0.85
		Bias/Noise	755	37.2	1.67	0.95	1.35	0.95	*	0.85
		Noise	169	37.2	0.95	0.95	0.95	0.95	0.90	0.85
DME/DME	Worst-Case Along-Track	Bias	323	46.3	0.95	*	0.95	0.95	0.95	0.95
		Bias/Noise	245	39.6	0.95	0.95	0.95	0.95	0.95	0.95
		Noise	126	31.7	0.95	0.95	0.95	0.95	0.95	0.95
	Worst-Case Cross-Track	Bias	486	43.0	0.95	*	0.95	0.95	0.95	0.95
		Bias/Noise	355	37.8	0.95	0.95	0.95	0.95	0.95	0.95
		Noise	131	31.7	0.95	0.95	0.95	0.95	0.95	0.95

* Oscillations remain at end of simulation run (2.5 minutes after MLS transition)

errors at the MLS boundary for each geometry and error magnitude considered in the study. The associated settling time was estimated from the plots for each of the MLS geometries (flight profile/runway configuration).

The settling times reflect the impact of two contributing factors. The first is the magnitude of the RNAV delivery errors and the second is the magnitude of the range-dependent MLS errors (azimuth and elevation). The latter factor implies the need for range-dependent filter gains to minimize this effect.

V. CONCLUSIONS

The primary objective of this study was to generate a data base of position errors for the TCV aircraft in the RNAV/MLS transition region. From the data base an analysis is performed to evaluate TCV avionics sensitivity to flight profile, sensor errors, ground facility location and runway orientation (MLS antenna orientation). The avionics sensitivity analysis provides insight into such issues as RNAV/MLS transition feasibility (for various geometries and flight profiles), transition guidance requirements and MLS airspace and operational procedure requirements. The data base is also useful for subsequent flight test planning.

Generally, the data base consists of cross-track and vertical deviation time histories from the RNAV region through MLS transition. The RNAV system performance is best assessed by examination of the delivery errors at the MLS boundary. For the DME/DME updated inertial RNAV system the cross-track delivery error varies from 126 meters to 486 meters. The vertical delivery error ranges from 31.7 meters to 46.3 meters. For the VOR/DME updated system the cross-track delivery error ranges from 169 meters to 1057 meters and the vertical delivery error ranges from 32.6 meters to 64.3 meters. The improved navigation system performance in the DME/DME mode as opposed to the VOR/DME mode is obvious from these ranges.

The error source magnitudes for this study were assumed to be consistent with the quantities specified in AC 90-45A [10]. This document, however, does not specify the relative content of random bias and noise value for each navigation source. The amount of bias and noise was varied parametrically to assess avionics sensitivity to signal noise content. It was found that the complementary filter performance is sensitive to signal content in that delivery error magnitude increased significantly with bias content increase. For example, for the VOR/DME RNAV system the cross-track delivery error increased from 169 meters for all noise and no bias to 1057 meters for all bias and no noise. Similarly, the vertical delivery error ranges from 32.6 meters for all noise and no bias to 64.3 meters for the all-bias case. The corresponding DME/DME delivery increases were from 131 meters to 486 meters in cross-track error and from 31.7 meters to 46.3 meters in vertical error.

An area of concern in RNAV/MLS transition is the requirement for additional guidance during transition. This requirement stems from the need to null out RNAV delivery errors upon transition to MLS in an expeditious and smooth manner. The

requirement will depend on the magnitude of the delivery errors. For the DME/DME updated inertial system the delivery errors were considered sufficiently small not to warrant additional guidance transition. The magnitude of the delivery errors for the VOR/DME updated inertial system were considered to be sufficiently significant to require additional transition guidance.

The MLS complementary filters were observed to display significant transients immediately upon transition. This behavior was attributed to two factors. First of all, an extensive amount of cross-coupling exists between the filters and the autopilot/aircraft dynamics. Secondly, the magnitude of the transients was found to be sensitive to filter initialization. The transient settling time was found to be primarily a function of the system time constants and input magnitudes (RNAV delivery errors and range dependent MLS errors). To minimize initialization transients the filters were initialized with the RNAV filter estimates at transition. The transient response magnitude was thereby reduced.

As indicated, however, the magnitude of the RNAV delivery errors and the magnitude of the MLS sensor errors (especially the range-dependent azimuth and elevation errors) have a significant impact on the settling time. For certain flight profiles and delivery errors, additional oscillations are induced thereby increasing the settling time. The settling times for the cases examined during this study varied from 0.85 minutes to 2.33 minutes (although several cases had not settled at the end of the simulation run).

These settling times have a significant impact on airspace requirements and operational procedures in the MLS environment. This is particularly true for approach speeds of 260 km/hr typical of TCV-737 type aircraft. Hence, the route design and the alloted airspace must be adequate to provide sufficient space for aircraft stabilization prior to final approach and landing.

The feasibility of a particular flight profile and runway/flight path configuration to support RNAV/MLS transition is dependent on the transient response associated with that particular configuration. The transient response has potential improvements available through appropriate filter initialization. Other modifications are possible filter design changes effective immediately after transition. This may include some sort of blending of navigation signals or implementing range-dependent gains.

VI. RECOMMENDATIONS

While meeting the objectives of this study, several issues were uncovered which require further analysis and evaluation. The issues stem primarily from the behavior of the transient response during MLS transition. The current study addressed rather highly sophisticated RNAV systems, INS updated with DME/DME or VOR/DME. It was observed that the MLS transition transient was dependent on RNAV delivery errors. Of interest would be to evaluate less sophisticated RNAV systems which would yield larger delivery errors. Such systems would include air data, updated with VOR/DME and DME/DME and course-line RNAV computers.

The current study examined only a limited data base scope. The scope should be expanded to include additional geometries and flight profiles and additional error source variations such as MLS sensor errors. The broadened data base would provide greater insight into the evaluation of MLS airspace requirements and operational procedures. This, in turn, impacts the route design and the requirement for expanded MLS coverage (for example, an assessment of whether MLS azimuth coverage should be 20°, 40° or 60°).

The transient behavior has indicated additional research in the area of MLS filter design. The dependence of the transient (magnitude and settling time) on the magnitude of delivery errors and subsequent flight path/runway geometry indicates a potential need for time or range dependent gain filter or filter blending techniques at MLS transition. Evaluation of potential filter modifications at transition can be accomplished through the simulation techniques described in this report.

Of current interest in the navigation community is the evaluation of proposed navigation systems such as LORAN-C, Omega, and GPS. These are future systems in the same sense as the MLS. It would be of interest to evaluate the transition from these systems to MLS in a similar manner as performed during this study.

The final recommendation is that maximum use be made of the covariance propagation simulation for subsequent flight test design. It is possible, through implementation of this technique, to evaluate candidate flight test profiles and identify additional profiles of interest in a cost effective manner.

Page Intentionally Left Blank

APPENDIX A

RNAV/MLS ENSEMBLE SIMULATION

A.1 INTRODUCTION

The purpose of this appendix is to present the analytical models of the RNAV and MLS simulations utilized in the avionics sensitivity analysis. The models are derived from information gathered from the NASA Langley Research Center. Unfortunately, the necessary information did not exist in a concise form and it became necessary to compile the required analytical expressions from various documents and computer listings. Since it is difficult to ascertain which documents the various models were extracted from it is impossible to furnish a list of references. Hopefully, the data gathered in this appendix will be useful as a future reference source.

For the sake of convenience the models are presented in conjunction with the block diagrams shown in Figures 2.1 and 2.2. These figures are repeated in the appendix for easy reference.

A.2 RNAV SIMULATION

The VOR/DME RNAV simulation block diagram is shown in Figure A.1. Due to the input and output requirements of the various models making up the entire TCV system, several coordinate transformations will be presented to provide completeness to this discussion.

The basic measurements of the TCV RNAV system are the range, ρ , bearing, θ , the altitude, h_m , and the inertial navigation system (INS) horizontal velocity components, V_N and V_E , and vertical acceleration, α_z. The VOR/DME measurements are assumed to consist of a random noise and bias component (this assumption is for the current study only, correlated noise is readily included requiring, however, an additional state). Hence, these measurements are expressed as

$$\rho_m = \rho_a + b_\rho + n_\rho \text{ , and} \qquad \text{(A.1)}$$

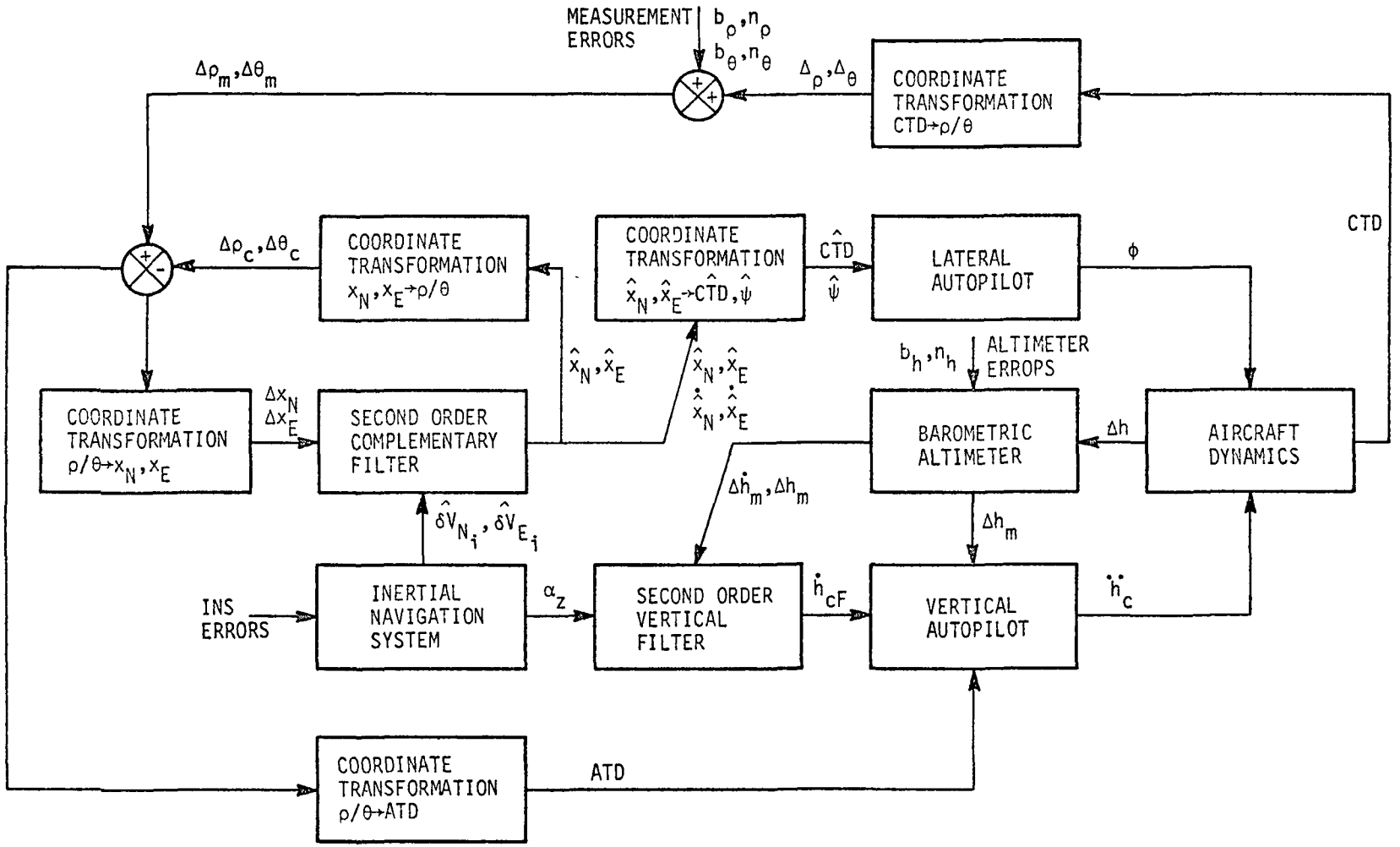

Figure A.1 VOR/DME RNAV Simulation Block Diagram

$$\theta_m = \theta_a + b_\theta + n_\theta \qquad (A.2)$$

where

$$\dot{b}_\rho = \dot{b}_\theta = 0.$$

These expressions must be linearized for the ensemble simulation. In the above expressions ρ_a and θ_a are the actual values and (b_ρ, b_θ) are the bias components and (n_ρ, n_θ) the noise components. Linearizing about a nominal (ρ_N, θ_N) the measured and actual values become

$$\rho_m = \rho_N + \Delta\rho_m \ , \qquad (A.3)$$

$$\theta_m = \theta_N + \Delta\theta_m \ , \qquad (A.4)$$

$$\rho_a = \rho_N + \Delta\rho \ , \quad \text{and} \qquad (A.5)$$

$$\theta_a = \theta_N + \Delta\theta \ . \qquad (A.6)$$

Substitution of Equations (A.3) through (A.5) into Equations (A.1) and (A.2) yields

$$\Delta\rho_m = \Delta\rho + b_\rho + n_\rho \qquad (A.7)$$

$$\Delta\rho_m = \Delta\theta + b_\theta + n_\theta \qquad (A.8)$$

$\Delta\rho$ and $\Delta\theta$, the deviations of the actual values from the nominal (due to aircraft displacement from the nominal) are based on the cross-track deviation, CTD, of the aircraft. The along-track is not included since for 3D RNAV systems only an indicated and not an actual along-track deviation is defined. The coordinate transformation from CTD to $\Delta\rho$ and $\Delta\theta$ is given as

$$\Delta\rho = \text{CTD} \sin(\psi - \theta_N), \text{ and} \qquad (A.9)$$

$$\Delta\theta = \frac{\text{CTD}}{\rho_N} \cos(\psi - \theta_N) \qquad (A.10)$$

where ρ_N and θ_N are the nominal measurement values and ψ is the nominal aircraft heading.

The altimeter model is assumed to have noise and bias corrupting the actual altitude. This corrupted altitude is

then passed through a first order filter to simulate altimeter delay in recording the altitude. The analytical expressions defining the altimeter model are

$$\dot{h}_m = \frac{1}{\tau_h} h_m + \frac{1}{\tau_h} (z + b_h + n_h), \text{ and} \quad \text{(A.11)}$$

$$\dot{b}_h = 0 \quad \text{(A.12)}$$

where

τ_h - altimeter lag,

h_m - measured altitude,

z - actual altitude,

b_h - altimeter bias, and

n_h - altimeter noise

Because of the large number of states required to fully represent the TCV RNAV system, the INS models are kept as simplistic as potentially possible. For this presentation only the final linearized form used in the simulation is given. Normally, the platform drift errors and accelerometer errors are assumed to be correlated with a correlation time of 5 hours and 10 hours respectively. Since the flight times in question for this study are much less these errors are assumed to be biases. The INS model is therefore

$$\delta\dot{x}_N = -\rho_z \delta x_E + \delta V_N \quad \text{(A.13)}$$

$$\delta\dot{x}_E = \rho_z \delta x_N + \delta V_E \quad \text{(A.14)}$$

$$\delta\dot{V}_N = -\omega_s^2 \delta x_N - (2\Omega_z + \rho_z) \delta V_E + a_z \psi_x - a_x \psi_z \quad \text{(A.15)}$$

$$\delta\dot{V}_E = \omega_s^2 \delta x_E + (2\Omega_z + \rho_z) \delta V_N - a_z \psi_y + a_y \psi_z \quad \text{(A.16)}$$

$$\dot{\psi}_x = \omega_z \psi_y - \omega_y \psi_z + \varepsilon_x \quad \text{(A.17)}$$

$$\dot{\psi}_y = -\omega_z \psi_x + \omega_x \psi_z + \varepsilon_y \quad \text{(A.18)}$$

$$\dot{\psi}_z = \omega_y \psi_x - \omega_x \psi_y + \varepsilon_z \quad \text{(A.19)}$$

$$\dot{\varepsilon}_x = \dot{\varepsilon}_y = \dot{\varepsilon}_z = \dot{\alpha}_x = \dot{\alpha}_y = \dot{\alpha}_z = 0 \quad \text{(A.20)}$$

(time constants = 5 hrs & 10 hrs)

"Page missing from available version"

where $\Delta\rho_c$ and $\Delta\theta_c$ are outputs of the second order filter. The equations representing the second order filter are

$$\dot{\hat{x}}_N = - K_1 \hat{x}_N + x_{2N} + \delta V_N + K_1 x_{mN}, \quad (A.25)$$

$$\dot{x}_{2N} = - K_2 \hat{x}_N + K_2 x_{mN}, \quad (A.26)$$

$$\dot{\hat{x}}_E = - K_1 \hat{x}_E + x_{2E} + \delta V_E + K_2 x_{mE}, \text{ and} \quad (A.27)$$

$$\dot{x}_{2E} = - K_2 \hat{x}_E + K_2 x_{mE}. \quad (A.28)$$

where

$\hat{x}_N, \hat{x}_E$ - filtered north and east position errors,

x_{2N}, x_{2E} - filter states (north and east),

$\delta V_N, \delta V_E$ - INS velocities (north and east), and

x_{mN}, x_{mE} - measured north and east positions.

Integration of Equations (A.25) and (A.27) and an appropriate coordinate transformation provide the computed range, $\Delta\rho_c$, and bearing, $\Delta\theta_c$, as

$$\Delta\rho_c = \hat{x}_N \cos\theta_N + \hat{x}_E \sin\theta_N, \text{ and} \quad (A.29)$$

$$\Delta\theta_c = - \frac{\hat{x}_N}{\rho_N} \sin\theta_N + \frac{\hat{x}_E}{\rho_N} \cos\theta_N. \quad (A.30)$$

The inputs to the vertical complementary filter are the measured altitude h_m and the vertical acceleration, α_z, from the INS. The analytical equations of the second order vertical complementary filter are given by

$$\dot{z}_1 = \frac{1}{\tau_1} z_1 + \frac{K^*}{\tau_1} \alpha_z - \frac{1}{\tau_1 \tau_h} h_m + \frac{1}{\tau_1 \tau_h} (z + b_h + n_h) + \frac{K_1}{\tau_1} h_{mc} \quad (A.31)$$

and

$$\dot{h}_{mc} = -\frac{1}{\tau_h} h_m + \frac{1}{\tau_h}(z + b_h + n_h) - z_1 \qquad (A.32)$$

where

z_1 - commanded altitude rate,

α_z - vertical acceleration from INS,

b_h - altitude bias (altimeter),

h_m - measured altitude (baro),

n_h - altimeter noise,

h_{mc} - integral feedback term

τ_l, τ_h - filter time constants, and

K^*, K_1 - filter gains.

The outputs of the vertical complementary filter are fed directly into the vertical autopilot. The horizontal filter outputs, however, are converted into an estimated cross track deviation, $\hat{CTD}$, and estimated aircraft heading, $\hat{\psi}$, as

$$\hat{CTD} = -\hat{x}_N \sin\psi + \hat{x}_E \cos\psi \text{ , and} \qquad (A.33)$$

$$\hat{\psi} = -\dot{\hat{x}}_N \frac{\sin\psi}{V} + \dot{\hat{x}}_E \frac{\cos\psi}{V} \qquad (A.34)$$

where $\hat{x}_N$, $\hat{x}_E$, $\dot{\hat{x}}_N$ and $\dot{\hat{x}}_E$ are filter outputs, ψ is the nominal aircraft heading and V is the nominal aircraft speed. The quantities given by these two equations are input into the lateral autopilot according to

$$\dot{\phi} = \phi_1 \qquad (A.35)$$

and

$$\dot{\phi}_1 = -\frac{1}{\tau_p}\phi_1 - \frac{K_p}{\tau_p}\phi - \frac{K_y K_p}{\tau_p}\hat{x} - \frac{K_p V_{gs} K_{\dot{y}}}{57.3 g \tau_p}\hat{\psi} \quad (A.36)$$

where

ϕ - roll angle (input to dynamics),

ϕ_1 - roll rate,

τ_p - time constant,

K_p, K_y, $K_{\dot{y}}$ - autopilot gains,

V_{gs} - ground speed,

$\hat{x}$ - computed cross-track error , and

$\hat{\psi}$ - computed heading error.

For 3D RNAV systems the along-track deviation, ATD, propagates into the vertical channel. As indicated in Figure 2.3 in the main text, an indicated along-track deviation will shift the vertical profile so as to produce a vertical deviation. The indicated along-track is computed from the measured and filter computed range and bearing according to

$$ATD = (\Delta\rho_m - \Delta\rho_c)\cos(\theta_N - \psi) + (\Delta\theta_m - \Delta\theta_c)\rho_N \sin(\theta_N - \psi) \quad (A.37)$$

where $\Delta\rho_m$ and $\Delta\theta_m$ are given by Equations (A.7) and (A.8), $\Delta\rho_c$ and $\Delta\theta_c$ are given by Equations (A.29) and (A.30), ρ_N and θ_N are the nominal range and bearing, and ψ is the nominal aircraft heading. With this along-track deviation and the outputs of the second order vertical complementary filter, the vertical autopilot equations are

$$\dot{h}_z = z_1 \quad (A.38)$$

and

$$\dot{h}_2 = \frac{1}{\tau} h_2 + \frac{1}{\tau}\left[.6 \frac{\partial \dot{h}}{\partial(ATD)} ATD - z_1 + .09 (h_d - h_z)\right] \quad (A.39)$$

where z is obtained from Equation (A.39), h_d is the desired altitude, and τ is the autopilot time constant.

The aircraft dynamics are expressed as second order in the lateral degree of freedom and second order in the vertical degree of freedom. The four equations, therefore, expressing the dynamics are

$$\dot{CTD} = V, \quad (A.40)$$

$$\dot{\psi} = \frac{g}{V} \phi, \quad (A.41)$$

$$\dot{z} = h_1, \text{ and} \quad (A.42)$$

$$\dot{h}_1 = h_2 \quad (A.43)$$

where ϕ is given by Equation (A.35) and h_2 is given by Equation (A.39). The remaining variables are

CTD - cross track deviation,

V - nominal aircraft speed,

ψ - nominal aircraft heading

g - gravitational constant, and

z - altitude.

The DME/DME RNAV simulation block diagram is given in Figure A.2. The primary difference between this simulation and the VOR/DME simulation depicted in Figure A.1 are several coordinate transformations between various analytical models. The coordinate transformations are different for DME/DME since these measurements are in a different frame of reference.

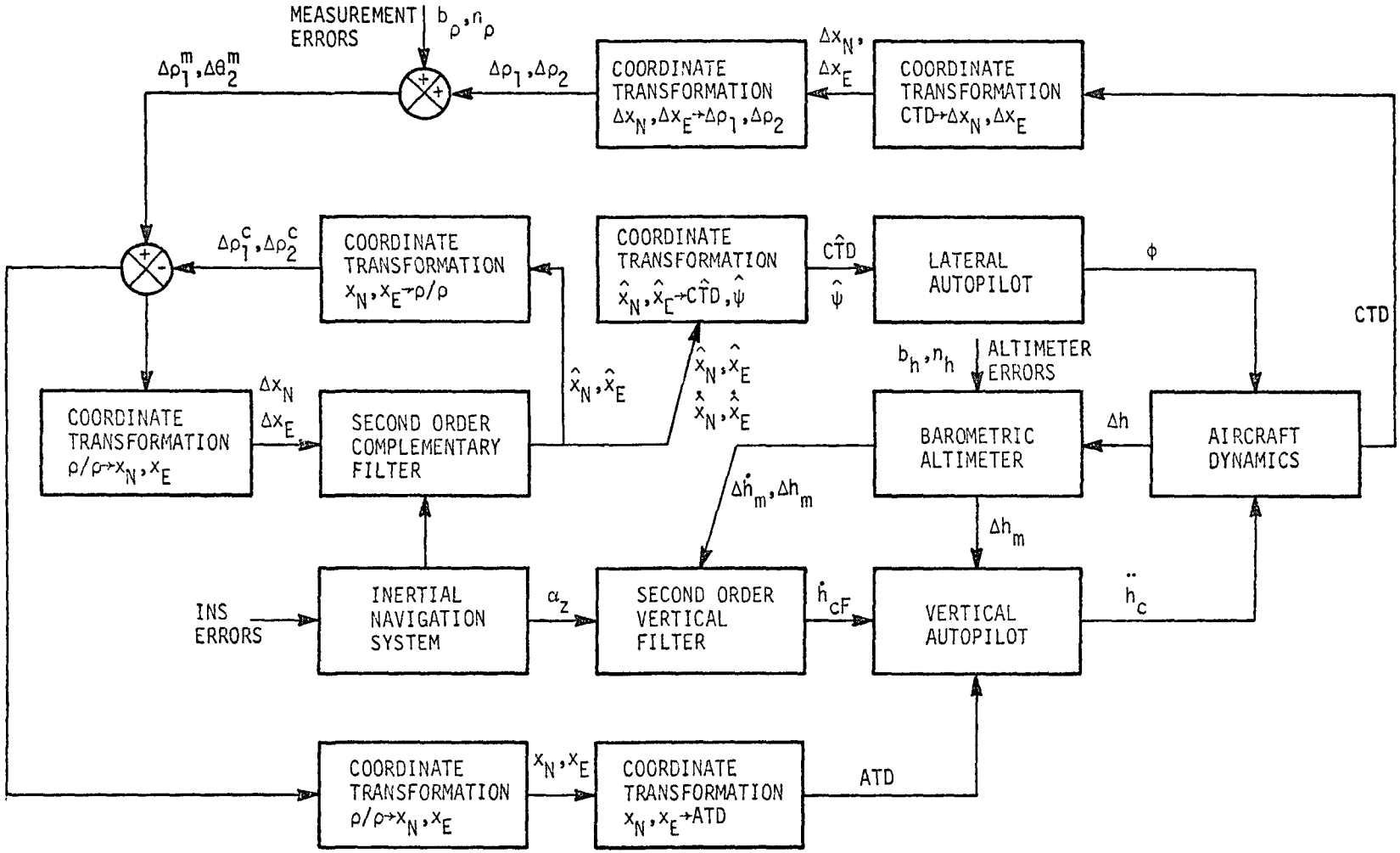

Figure A.2 DME/DME RNAV Simulation Block Diagram

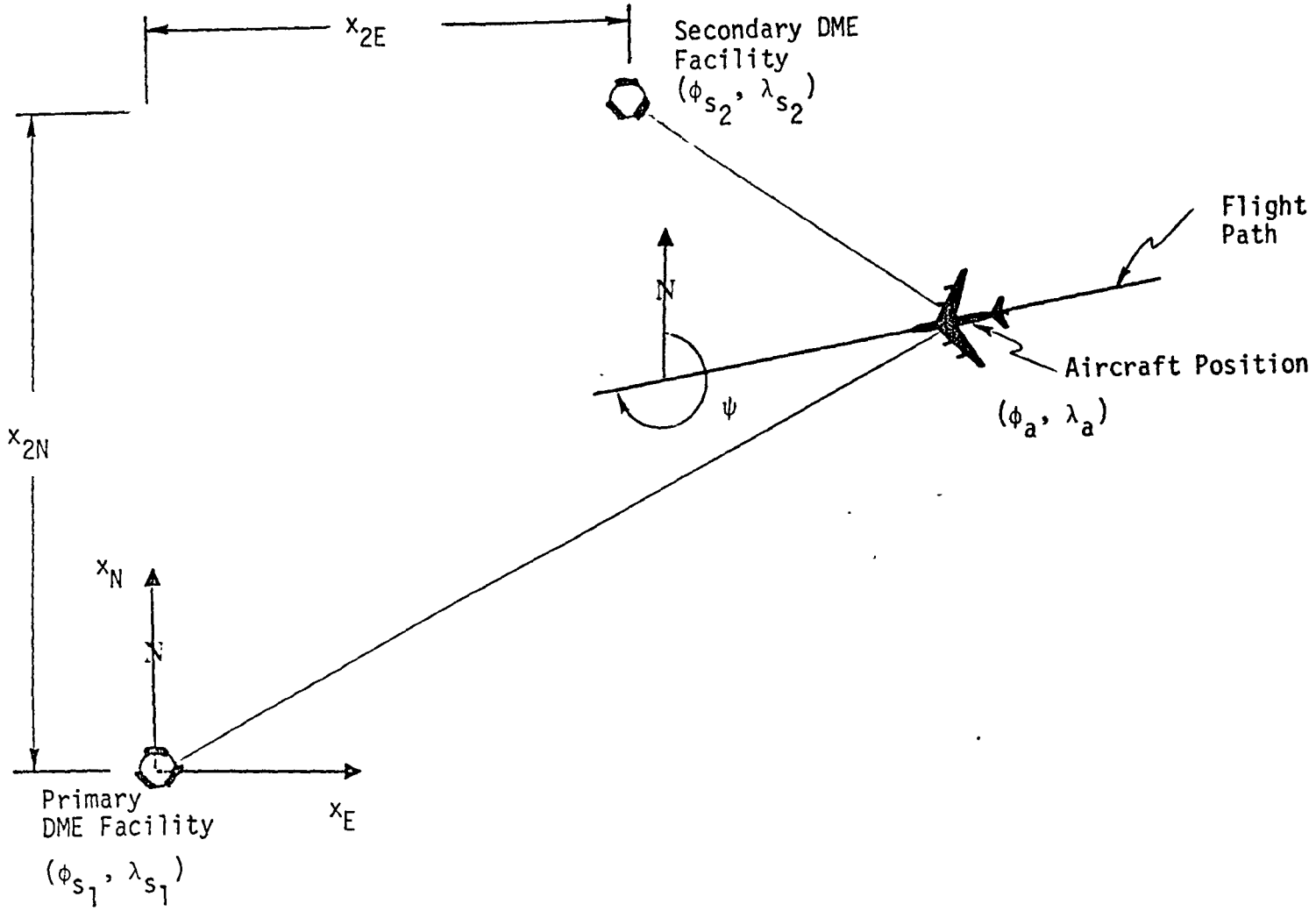

Figure A.3 DME/DME Facility Geometry

First of all, the transformation from the actual aircraft CTD to the measurement errors requires a transformation to north and east error components. Then error components, along with a vertical error, are transformed into two DME errors. The first transformation is given by

$$\Delta x_N = - \text{CTD} \sin\psi, \text{ and} \tag{A.44}$$

$$\Delta x_E = \text{CTD} \cos\psi \tag{A.45}$$

where

Δx_N - north position error,

Δx_E - east position error,

CTD - actual cross track deviation, and

ψ - nominal aircraft heading

The transformation from north and east errors to the measurement errors, $\Delta\rho_1$, and $\Delta\rho_2$, is given by

$$\Delta\rho_1 = \frac{x_N}{\rho_1} \Delta x_N + \frac{x_E}{\rho_1} \Delta x_E + \frac{h_1}{\rho_1} \Delta h_1 \tag{A.46}$$

$$\Delta\rho_2 = \frac{(x_N - x_{2N})}{\rho_2} \Delta x_N + \frac{(x_E - x_{2E})}{\rho_2} \Delta x_E +$$

$$+ \frac{(h_2 - h_1)}{\rho_2} \Delta h_2 \tag{A.47}$$

where

ρ_1 - nominal slant range from reference facility to aircraft,

x_N - nominal aircraft position north of reference facility,

x_E - nominal aircraft position east of reference facility,

x_{2N} - displacement of secondary facility north of reference facility,

x_{2E} - displacement of secondary facility east of reference facility,

h_1 - nominal aircraft altitude with respect to reference facility,

h_2 - altitude of secondary facility with respect to reference facility, and

ρ_2 - nominal slant range from secondary facility to aircraft given by

$$\rho_2 = \{(x_N - x_{2N})^2 + (x_E - x_{2E})^2 + (h_1 - h_2)^2\}^{1/2} \quad (A.48)$$

These quantities are shown schematically in Figure A.3.

The two DME measurements are given as

$$\Delta\rho_1{}^m = \Delta\rho_1 + b_\rho + n_\rho, \text{ and} \quad (A.49)$$

$$\Delta\rho_2{}^m = \Delta\rho_2 + b_\rho + n_\rho \quad (A.50)$$

where

b_ρ - DME bias

n_ρ - DME noise

$\Delta\rho_1$ - given in Equation (A.46)

$\Delta\rho_2$ - given in Equation (A.47), and

$\Delta\rho_1{}^m$, $\Delta\rho_2{}^m$ - DME/DME measurement errors

The differential equation governing b_ρ is

$$\dot{b}_\rho = 0 \quad (A.51)$$

Two coordinate transformations remain the first transforming the DME/DME measurements into north and east components to be compatible with the complementary filter inputs and the second deriving the indicated along-track deviation from the north and east error components. The first

transformation is

$$\Delta x_N = \frac{1}{D}\left\{ \left(\frac{x_E - x_{2E}}{\rho_2}\right)\Delta\rho_1' - \frac{x_E}{\rho_1}\Delta\rho_2' \right\} \text{ , and} \qquad (A.52)$$

$$\Delta x_E = \frac{1}{D}\left\{ - \left(\frac{x_N - x_{2N}}{\rho_2}\right)\Delta\rho_1' + \frac{x_N}{\rho_1}\Delta\rho_2' \right. \qquad (A.53)$$

where

$$D = \frac{x_E\, x_{2N} - x_N\, x_{2E}}{\rho_1 \rho_2} \text{ .} \qquad (A.54)$$

It is of interest to note that the quantity D approaches zero as the angle between the slant ranges approach 0° or 180°, a peculiarity of the DME/DME mode of navigation. In these expressions $\Delta\rho_1'$ and $\Delta\rho_2'$ are given by

$$\Delta\rho_1' = \Delta\rho_1^{\,m} - \Delta\rho_1^{\,c} \text{ , and} \qquad (A.55)$$

$$\Delta\rho_2' = \Delta\rho_2^{\,m} - \Delta\rho_2^{\,c} \qquad (A.56)$$

where

$\Delta\rho_1^{\,m}$, $\Delta\rho_2^{\,m}$ - measurement errors, and

$\Delta\rho_1^{\,c}$, $\Delta\rho_2^{\,c}$ - filter outputs.

The indicated along-track is computed from the position error components given in Equations (A.52) and (A.53) as

$$ATD = \Delta x_N \cos\psi + \Delta x_E \sin\psi \qquad (A.57)$$

where ψ is the nominal aircraft heading.

For completeness it is desirable to represent the north and east displacements of Equations (A.46) and (A.47) in terms of various latitudes and longitudes. Using the primary facility as the origin of the coordinate system the various displacements are represented by

$$x_N = R_e(\phi_a - \phi_{s_1}), \tag{A.58}$$

$$x_E = R_e \cos\phi_{s_1}(\lambda_a - \lambda_{s_1}), \tag{A.59}$$

$$x_{2N} = R_e(\phi_{s_2} - \phi_{s_1}), \text{ and} \tag{A.60}$$

$$x_{2E} = R_e \cos\phi_{s_1} (\lambda_{s_2} - \lambda_{s_1}) \tag{A.61}$$

where

(ϕ_a, λ_a) - aircraft latitude and longitude,

$(\phi_{s_1}, \lambda_{s_1})$ - primary facility latitude and longitude, and

$(\phi_{s_2}, \lambda_{s_2})$ - secondary facility latitude and longitude.

A.3 MLS SIMULATION

Figure A.4 depicts the MLS simulation. For the current study it is assumed that on entering the MLS region that the navigation mode changes from RNAV to MLS without any blending. This implies that at the MLS boundary the navigation mode is switched directly and that the non-navigation elements of the covariance matrix are retained and the navigation elements are reinitialized as appropriate. The non-navigation states are those relating to the autopilots and aircraft dynamics. Hence, this subsection will not deal with the autopilot or aircraft dynamics as these have already been discussed in the previous section.

The primary measurements for the MLS consist of range, bearing and elevation angle. These measurements are referenced with respect to a coordinate system fixed at the runway. Figure A.5 indicates a schematic of the MLS measurements. Note that the bearing is with respect to the runway centerline rather than with respect to magnetic north as is the case for the VOR system.

As with the RNAV system the MLS measurements are assumed to consist of a random noise and bias component. Again, for purposes of this study no correlated noise components are induced but can be easily added for subsequent studies. The measurement equations are given by

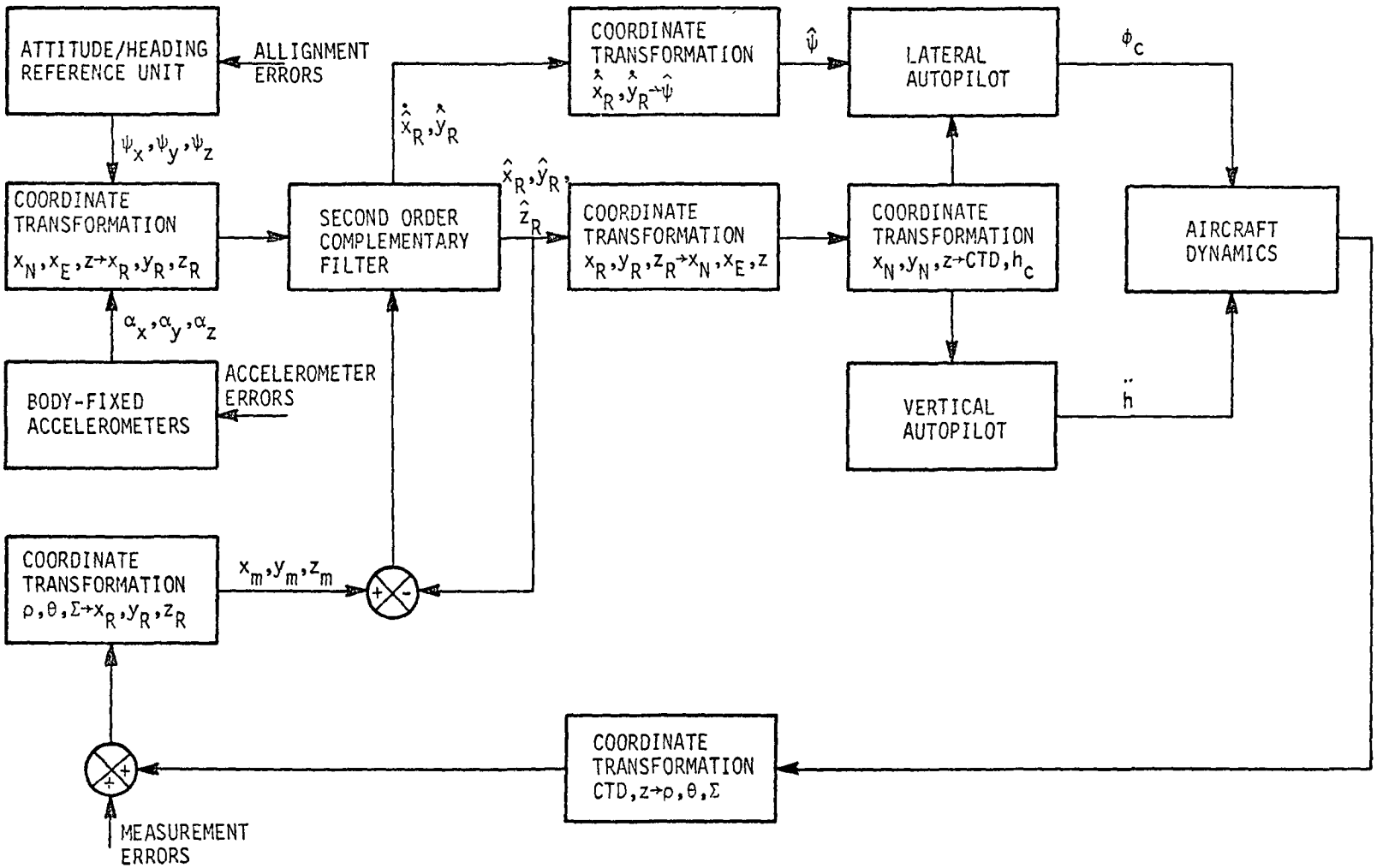

Figure A.4 MLS Simulation Block Diagram

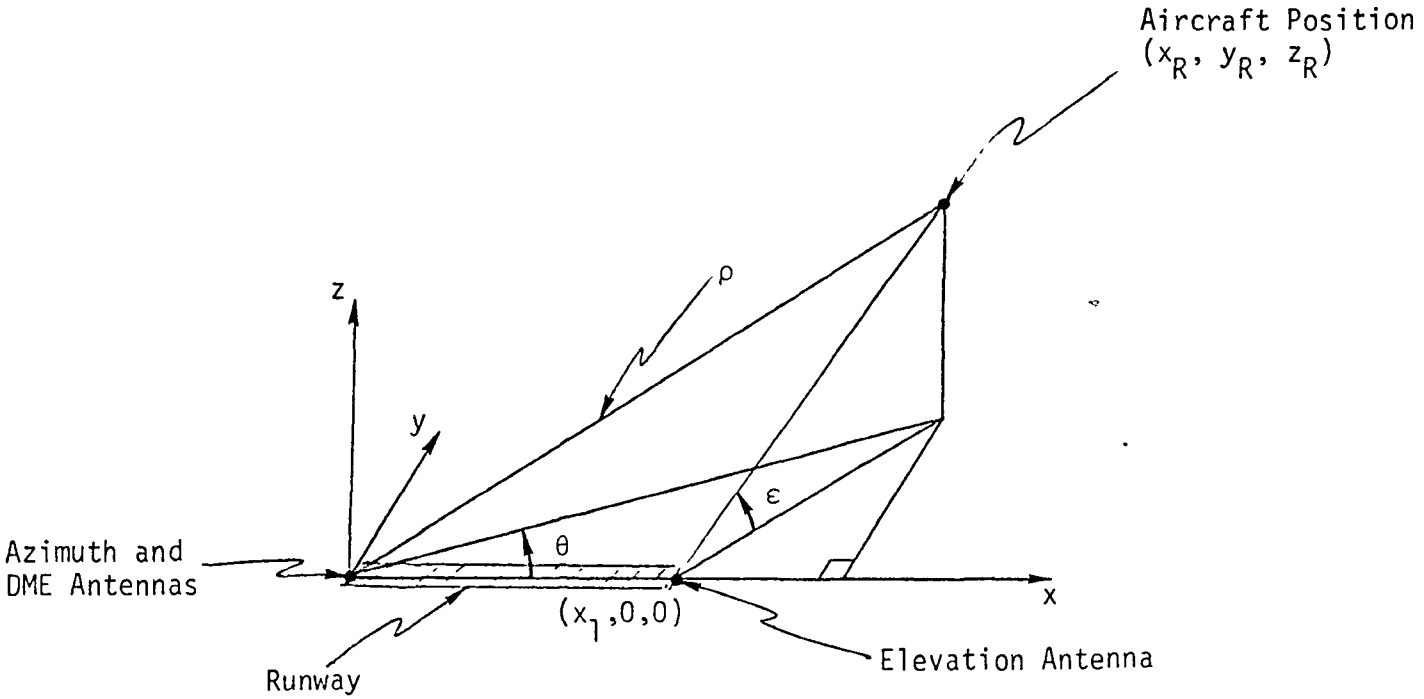

Figure A.5 MLS Antenna Coordinate System

$$\rho_m = \rho_a + b_\rho + n_\rho, \quad (A.62)$$

$$\theta_m = \theta_a + b_\theta + n_\theta, \text{ and} \quad (A.63)$$

$$\varepsilon_m = \varepsilon_a + b_\varepsilon + n_\varepsilon, \quad (A.64)$$

where $(\rho_a, \theta_a, \varepsilon_a)$ are the actual range, azimuth and elevation angles, $(b_\rho, b_\theta, b_\varepsilon)$ are the bias components with their dynamic behavior governed by

$$\dot{b}_\rho = \dot{b}_\theta = \dot{b}_\varepsilon = 0 \quad (A.65)$$

and $(n_\rho, n_\theta, n_\varepsilon)$ are the noise components. Linearization about the nominal yields

$$\rho_m = \rho_N + \Delta\rho_m, \quad (A.66)$$

$$\theta_m = \theta_N + \Delta\theta_m, \text{ and} \quad (A.67)$$

$$\varepsilon_m = \varepsilon_N + \Delta\varepsilon_m, \quad (A.68)$$

$$\rho_a = \rho_N + \Delta\rho \ , \quad (A.69)$$

$$\theta_a = \theta_N + \Delta\theta \ , \text{ and} \quad (A.70)$$

$$\varepsilon_a = \varepsilon_N + \Delta\varepsilon \quad (A.71)$$

Substitution of these six equations into Equations (A.62) through (A.64) yields

$$\Delta\rho_m = \Delta\rho + b_\rho + n_\rho, \quad (A.72)$$

$$\Delta\theta_m = \Delta\theta + b_\theta + n_\theta, \text{ and} \quad (A.73)$$

$$\Delta\varepsilon_m = \Delta\varepsilon + b_\varepsilon + n_\varepsilon, \quad . \quad (A.74)$$

The variation in the actual range, bearing and elevation with respect to the nominal, $\Delta\rho$, $\Delta\theta$, and $\Delta\varepsilon$ respectively are based on the actual aircraft cross-track and vertical deviations, CTD and Δz. As with the RNAV simulation, the actual aircraft along-track deviation is not defined as 4D is considered beyond the scope of this study. The appropriate transformation from the actual aircraft deviations to the MLS measurement coordinate systems results in the following relationships.

$$\Delta\rho = CTD \left\{ \frac{x_R}{\rho_N} \sin(\Theta_R - \psi) - \frac{y_R}{\rho_N} \cos(\Theta_R - \psi) \right\} + \frac{z}{\rho_N} \Delta z \qquad (A.75)$$

$$\Delta\Theta = - \frac{CTD}{\sqrt{x_R^2 + y_R^2}} \cos(\Theta_R - \psi - \Theta_N), \text{ and} \qquad (A.76)$$

$$\Delta\varepsilon = - \frac{CTD}{[(x_N - x_{el})^2 - x_N^2 + z^2] \sqrt{(x - x_{el})^2 + y^2}} \left\{ (x_R - x_{el}) \sin(\Theta_R - \psi) + \right.$$

$$\left. + y_R \cos(\Theta_R - \psi) \right\} + \frac{\cos\varepsilon_N}{\sqrt{(x_N - x_{el})^2 + x_N^2 + z^2}} \Delta z . \qquad (A.77)$$

Here, x_R, y_R are the nominal aircraft lateral coordinates relative to the runway based MLS, z is the nominal aircraft altitude relative to the runway, θ_R is the orientation of the runway centerline with respect to magnetic north, ψ is the nominal aircraft heading, ρ_N, θ_N and ε_N are the nominal MLS measurements and x_{el} is the displacement of the elevation antenna from the DME and azimuth antennas which are assumed to be located at the origin of the coordinate system. Note that the aircraft altitude is derived from the MLS measurements thereby eliminating the need for an altimeter model.

To utilize the MLS measurements in the second order complementary filter requires a coordinate transformation from the polar ρ, θ and ε coordinate system to a rectangular runway referenced coordinate system. The transformation equations are given by

$$\Delta x_R = \left\{ \frac{C}{2\sqrt{B - AC}} - \frac{x_R}{A} \right\} \Delta A - \frac{x_R}{\sqrt{B^2 - AC}} \Delta B + \frac{1}{2\sqrt{B^2 - AC}} \Delta C, \quad (A.78)$$

$$\Delta y_R = \tan\Theta \, \Delta x_R \, \frac{x_R}{\cos^2\Theta_N} \Delta\Theta , \quad (A.79)$$

$$\Delta z_R = \frac{(x_R - x_{el})\tan\varepsilon_N}{\sqrt{(x_R - x_{el})^2 + y_R^2}} \Delta x_R + \frac{y_R \tan\varepsilon_N}{\sqrt{(x_R - x_{el})^2 + y_R}} \Delta y_R$$

$$\frac{\sqrt{(x_R - x_{el})^2 + y_R^2}}{\cos^2} \Delta\varepsilon, \quad (A.80)$$

where

$$A = 1 + \tan^2\Theta_N + \tan^2\varepsilon_N + \tan^2\Theta_N \tan^2\varepsilon_N , \quad (A.81)$$

$$B = x_{el} \tan^2\varepsilon_N \quad (A.82)$$

$$C = x_{el}^2 \tan^2\varepsilon_N - \rho_N^2 , \quad (A.83)$$

$$\Delta A = \frac{2 \tan\varepsilon_N}{\cos^2\theta_N \cos^2\varepsilon_N} \Delta\theta + \frac{2 \tan\varepsilon_N}{\cos^2\theta_N \cos^2\varepsilon_N} \Delta\varepsilon \quad (A.84)$$

$$\Delta B = \frac{2 x_{el}^2 \tan\varepsilon_N}{\cos^2\varepsilon_N} \Delta\varepsilon, \quad \text{and} \quad (A.85)$$

$$\Delta C = \frac{2 x_{el}^2 \tan\varepsilon_N}{\cos^2\varepsilon_N} \Delta\varepsilon - 2\rho_N \Delta\rho \quad (A.86)$$

For the MLS the second order complementary filter requires additional acceleration inputs. The accelerometers are assumed to be body-mounted hence a suitable attitude reference system is required for the appropriate coordinate transformation for suitable filter input. The linearized accelerometer error quantities are given by

$$\ddot{x}_N = \alpha_x + a_y \psi_z - a_z \psi_y \tag{A.87}$$

$$\ddot{x}_E = \alpha_y + a_z \psi_x - a_x \psi_z \tag{A.88}$$

$$\ddot{z} = \alpha_z + a_x \psi_y - a_y \psi_x \tag{A.89}$$

$$\dot{\psi}_x = \dot{\psi}_y = \dot{\psi}_z = \dot{\alpha}_x = \dot{\alpha}_y = \dot{\alpha}_z = 0 \tag{A.90}$$

where

$\alpha_x, \alpha_y, \alpha_z$ - accelerometer errors

ψ_x, ψ_y, ψ_z - misalignment errors, and

a_x, a_y, a_z - accelerometer outputs.

The flight times of concern for this particular study are short compared to accelerometer and alignment drifts. Hence, these error quantities are assumed to be biases governed by the differential equations given by Equation. (A.90).

The MLS second order complementary filter operates in the coordinate system referenced at the runway. Hence, the accelerometer outputs must be rotated from the east/north system to the runway fixed system. The runway system is fixed hence the accelerations can be written as

$$\ddot{x}_R = \ddot{x}_N \cos\theta_R + \ddot{x}_E \sin\theta_R, \tag{A.91}$$

$$\ddot{y}_R = \ddot{x}_N \sin\theta_R - \ddot{x}_E \cos\theta_R, \text{ and} \tag{A.92}$$

$$\ddot{z}_R = \ddot{z}$$

where θ_R is the runway orientation relative to magnetic north.

Having resolved the accelerations into the runway coordinate system, the MLS second order complementary filter equations can be written as

$$\dot{x}_1 = x_2 + K_3 (x_m - x_1), \tag{A.94}$$

$$\dot{x}_2 = x_3 + K_2 (x_m - x_1) + \ddot{x}_R , \tag{A.95}$$

$$\dot{x}_3 = K_5 (x_m - x_1), \tag{A.96}$$

$$\dot{x}_4 = x_5 + K_3 (y_m - x_4), \tag{A.97}$$

$$\dot{x}_5 = x_6 + K_2 (y_m - x_4) + \ddot{y}_R , \tag{A.98}$$

$$\dot{x}_6 = K_5 (y_m - x_4) , \tag{A.99}$$

$$\dot{x}_7 = x_8 + K_3 (z_m - x_7) , \tag{A.100}$$

$$\dot{x}_8 = x_9 + K_2 (z_m - x_7) + \ddot{z}_R , \text{ and} \tag{A.101}$$

$$\dot{x}_9 = K_5 (z_m - x_7) , \tag{A.102}$$

where

$\hat{x} = x_1$, $\hat{y} = x_4$, $\hat{z} = x_7$, $\dot{\hat{x}} = x_2$, $\dot{\hat{y}} = x_5$,

K_2, K_3, K_5- filter constants,

x_m, y_m, z_m- MLS measurements, and

$\ddot{x}_R$, $\ddot{y}_R$, $\ddot{z}_R$- given by Equations (A.91) through (A.93).

Several coordinate transformations are required to resolve the runway referenced filter outputs into values appropriate for input into the steering command computations. The first coordinate transformation resolves the estimated velocity into a heading error estimate given by

$$\hat{\psi} = - \frac{\sin\psi}{V_N} \dot{\hat{x}}_N + \frac{\cos\psi}{V_N} \dot{\hat{x}}_E \tag{A.103}$$

where V_N is the nominal aircraft velocity and the north and east velocity error estimates are given in terms of the runway reference velocity error estimates as

$$\dot{\hat{x}}_N = \dot{\hat{x}}_R \cos\theta_R + \dot{\hat{y}}_R \sin\theta_R \ , \quad \text{and} \tag{A.104}$$

$$\dot{\hat{x}}_E = \dot{\hat{x}}_R \sin\theta_R - \dot{\hat{y}}_R \cos\theta_R \ . \tag{A.105}$$

where θ_R is the orientation of the runway relative to magnetic north. The indicated cross-track deviation $\hat{CTD}$ is given by

$$\hat{CTD} = - \hat{x}_N \sin\psi + \hat{x}_E \cos\psi \tag{A.106}$$

where ψ is the nominal aircraft heading and the north and east position error estimates are given in terms of the filter output as

$$\hat{x}_N = \hat{x}_R \cos\theta_R = \hat{y}_R \sin\theta_R, \text{ and} \tag{A.107}$$

$$\hat{x}_E = \hat{x}_R \sin\theta_R - \hat{y}_R \cos\theta_R \ . \tag{A.108}$$

The indicated altitude error is simply given by

$$\hat{h}_c = \hat{z}_R \tag{A.109}$$

where $\hat{z}_R$ is the filter estimate of the altitude error.

A.4 SIMULATION STATES

The states of the VOR/DME RNAV system simulation are

$$x^T_{RNAV} = \{CTD, \psi, z, h_1, \phi, \phi_1, h_z, h_2, z_1, h_{mc}, \hat{x}_N, x_{2N}, \hat{x}_E, x_{2E}, \delta x_N, \delta x_E, \delta V_N, \delta V_E, \psi_x, \psi_y, \psi_z, \varepsilon_x, \varepsilon_y, \varepsilon_z, \alpha_x, \alpha_y, \alpha_z, b_h, h_m, b_\rho, b_\theta\} \tag{A.110}$$

With the differential equations expressed in the form

$$\dot{x}_{RNAV} = F_{RNAV} x + n \tag{A.111}$$

it can be observed that the F matrix elements are made up of the equations presented in Section A.2. For the DME/DME RNAV simulation the states are identical as the VOR/DME with the exception that b_θ is replaced by b_ρ .

For this study it is assumed that the state transition matrix can be expressed by the following approximation

$$\phi = I + F_{RNAV}\,\Delta t \tag{A.112}$$

where I is the identity matrix, F is the matrix describing the dynamics of the system and Δt is the integration step size.

The formulation for the MLS simulation is the same with the exception that the MLS states are given by

$$x_{MLS}^T = \{CTD,\ \psi,\ z,\ h_1,\ \phi,\ \phi_1,\ h_z,\ h_2,\ x_1,\ x_2,\ x_3,$$

$$x_4,\ x_5,\ x_6,\ x_7,\ x_8,\ x_9,\ \psi_x,\ \psi_y,\ \psi_z,\ \alpha_x,\ \alpha_y,$$

$$\alpha_z,\ b_\rho,\ b_\theta,\ b_\varepsilon \tag{A.113}$$

The F_{MLS} matrix associated with the MLS is given by the equations presented in Section A.3.

The measurement noise matrix for the VOR/DME RNAV system is

$$Q_1 = \begin{bmatrix} \sigma_\theta^2 & 0 & 0 \\ 0 & \sigma_{\dot\rho}^2 & \sigma_2 \\ 0 & 0 & \sigma_h^2 \end{bmatrix} \tag{A.114}$$

and for the DME/DME RNAV system as

$$Q_2 = \begin{bmatrix} \sigma_\rho^2 & 0 & 0 \\ 0 & \sigma_\rho^2 & 0 \\ 0 & 0 & \sigma_h^2 \end{bmatrix} \tag{A.115}$$

where

σ_θ - VOR bearing error variance,

σ_ρ - DME range error variance, and

σ_n - altimeter error variance.

Similarly, the MLS measurement matrix is

$$Q_3 = \begin{bmatrix} \sigma^2_{\rho'} & 0 & 0 \\ 0 & \sigma^2_{\theta'} & 0 \\ 0 & 0 & \sigma^2_{\varepsilon} \end{bmatrix} \qquad \text{(A.116)}$$

where

$\sigma_{\rho'}$ - MLS range error variance,

$\sigma_{\theta'}$ - MLS azimuth error variance, and

σ_ε - MLS elevation angle error variance.

APPENDIX B

RNAV/MLS SIMULATION GEOMETRIES

The purpose of this appendix is to present the details of the geometries for the simulation experiments. The geometries are shown in Figures B.1, B.2 and B.3 for the DME/DME analysis and Figures B.4, B.5 and B.6 for the VOR/DME analysis. Tables B.1, B.2, and B.3 contain the waypoint and station data for DME/DME and Tables B.4, B.5 and B.6 contain the waypoint and station data for VOR/DME. The figures are duplicates of those presented in Section III of the report and are merely included here for reference. IN all cases the runway length is assumed to be 3050 meters.

Table B.1

Straight-In Approach for DME/DME Navigation Mode

	LAT	LON	ALTITUDE
Waypoint WP_1	39°00'00"	73°27'11.3"	2073 meters
Waypoint WP_2	39°00'00"	73°30'24.3"	2073 meters
Waypoint WP_3	39°99'00"	73°57'57.4"	0 meters
Facility a_1	38°56'10.4"	73°22'23.3"	0 meters
Facility a_2	38°56'10.4"	73°46'09.2"	0 meters
Facility b_1	39°07'04.3"	73°43'09.2"	0 meters
Facility b_2	38°52'55.7"	73°43'22.7"	0 meters

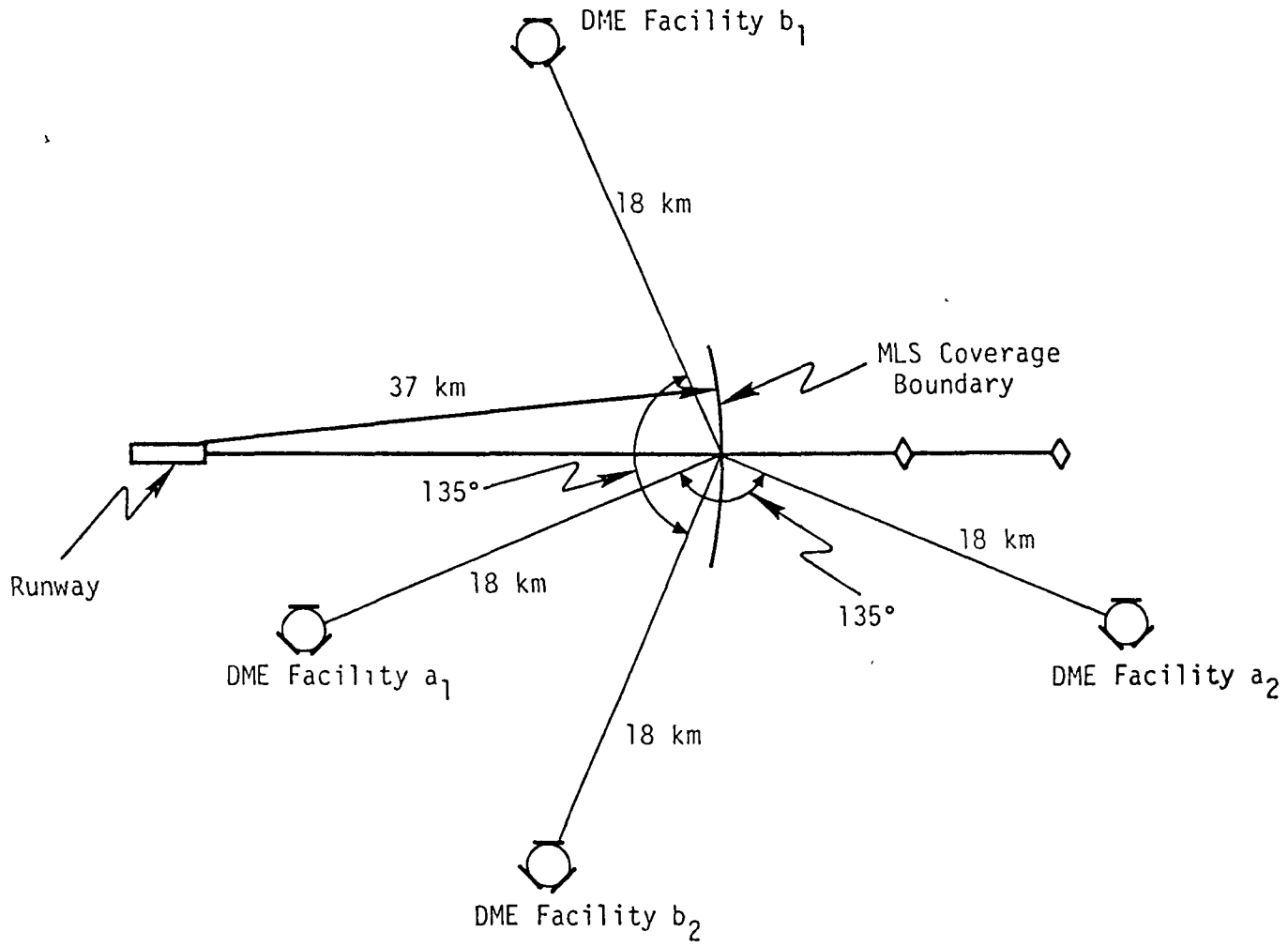

Figure B.1 Straight-In Approach for DME/DME Navigation Mode

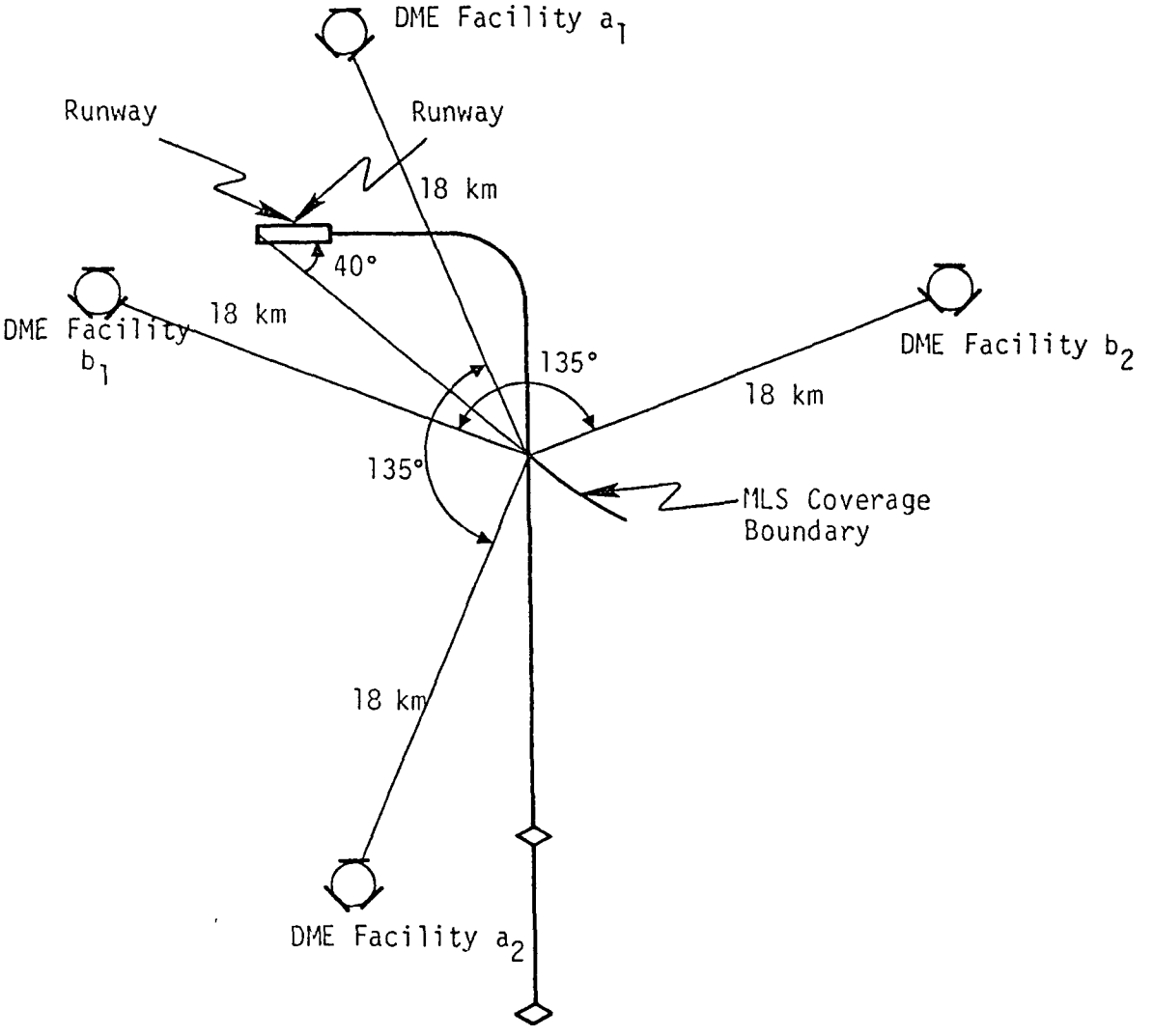

Figure B.2 90° Turn to Final Approach for DME/DME Navigation Mode

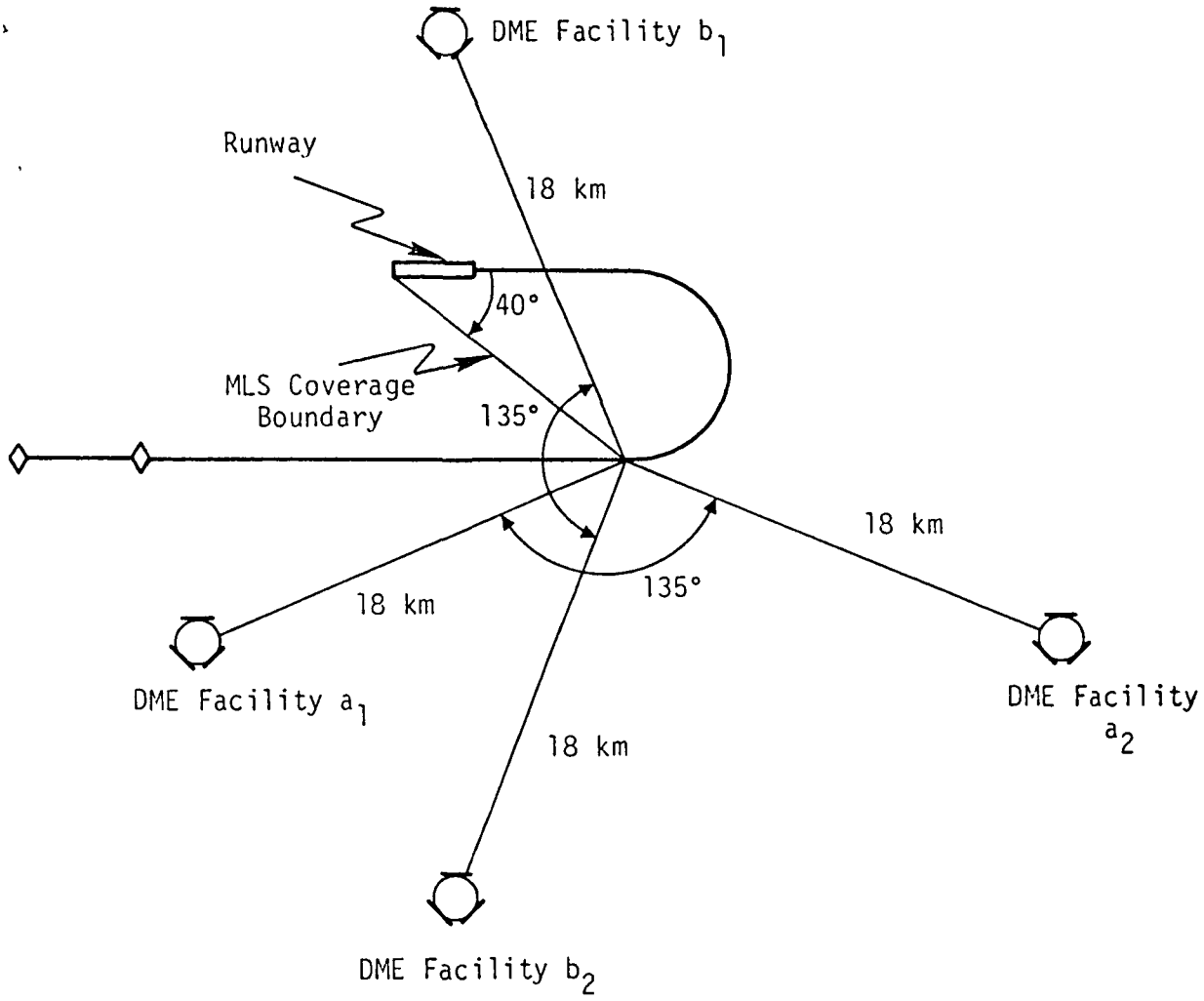

Figure B.3 180° Turn to Final Approach for DME/DME Navigation Mode

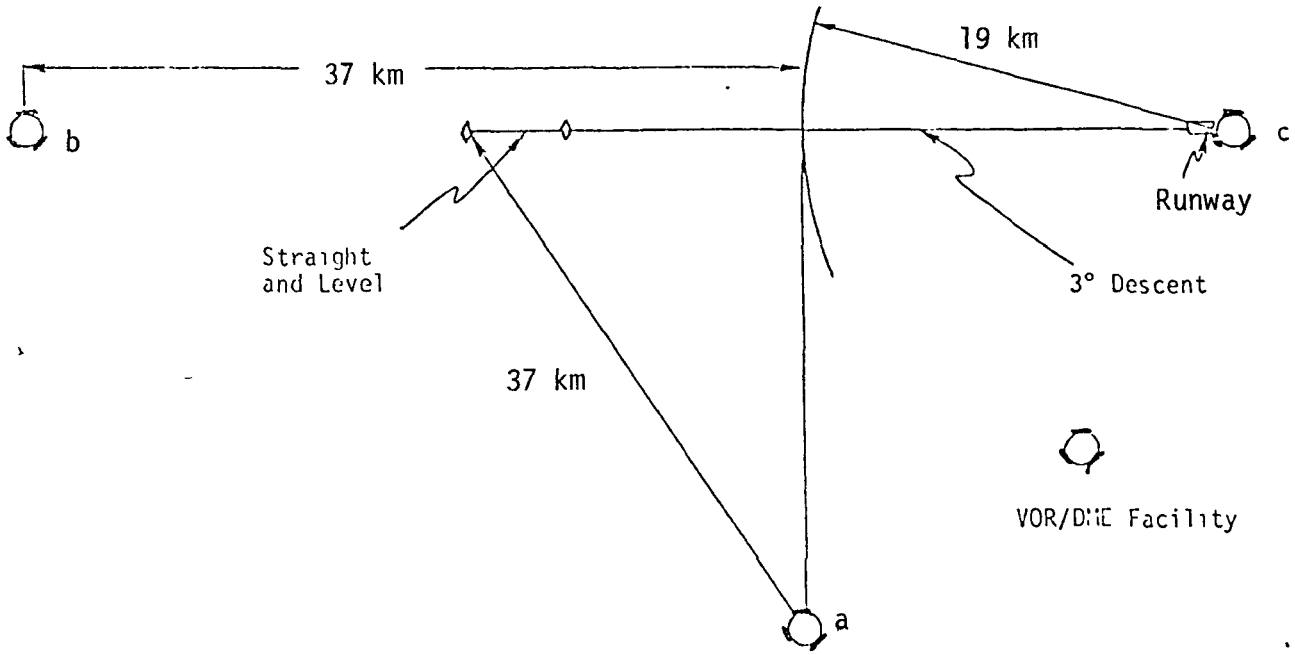

Figure B.4 Straight-In Approach for VOR/DME Navigation Mode

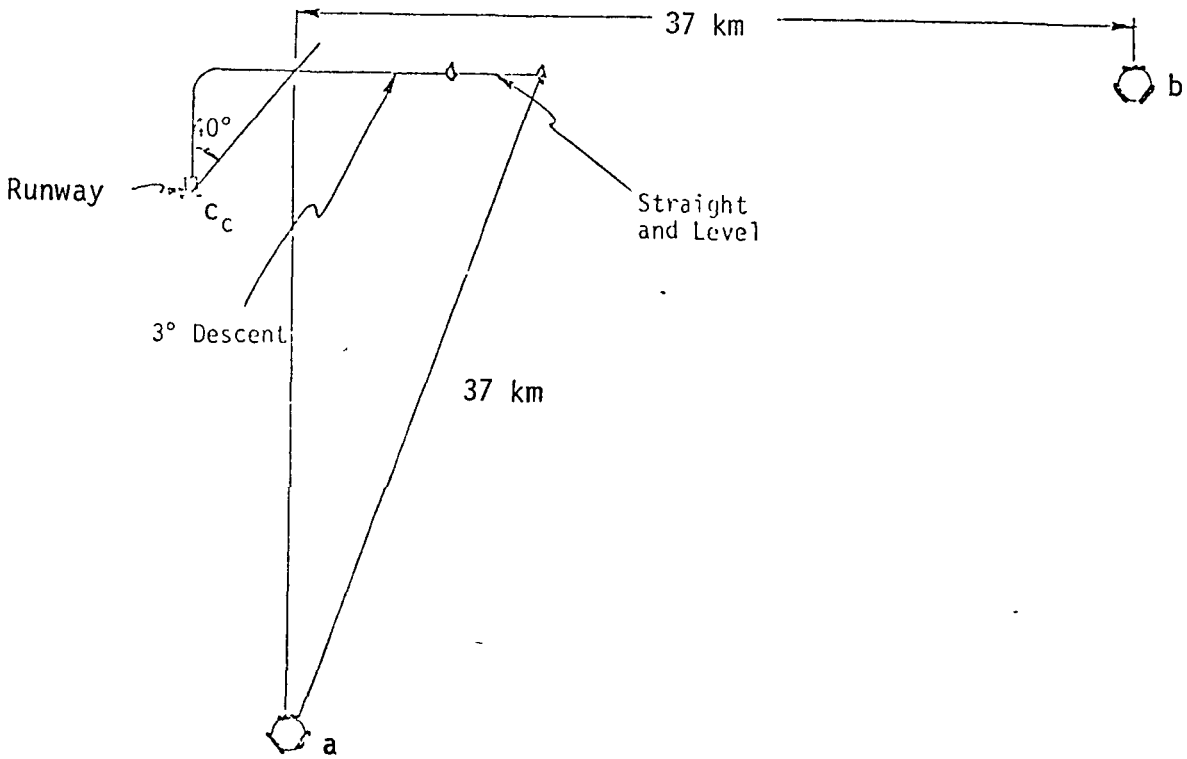

Figure B.5 90° Turn to Final VOR/DME Navigation Mode

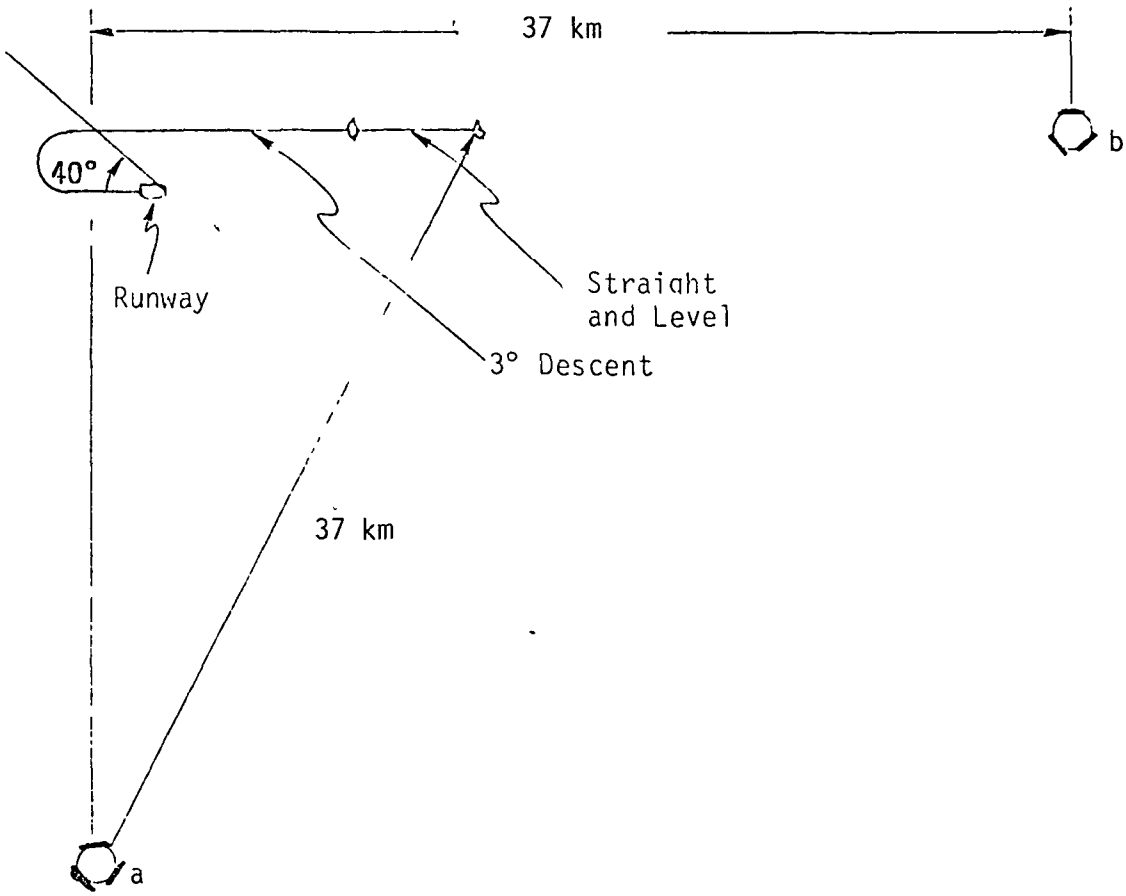

Figure B.6 180° Turn to Final for VOR/DME Navigation Mode

Table B.2

'90° Turn-to-Final Approach for DME/DME Navigation Mode

	LAT	LON	ALTITUDE
Waypoint WP_1	38°49'24.4"	73°52'11.1"	1165 meters
Waypoint WP_2	38°51'54.4"	73°52'11.1"	1165 meters
Waypoint WP_3	38°58'46.0"	73°52'11.1"	499 meters
Waypoint WP_4	39°00'00"	73°53'46.3"	311 meters
Waypoint WP_5	39°00'00"	73°57'53.4"	0 meters
Facility a_1	39°04'08.7"	73°57'07.5"	0 meters
Facility a_2	38°45'40.1"	73°57'07.5"	0 meters
Facility b_1	38°58'44.0"	74°04'04.2"	0 meters
Facility b_2	38°58'44.0"	73°40'18.0"	0 meters

Table B.3

180° Turn-to-Final Approach for DME/DME Navigation Mode

	LAT	LON	ALTITUDE
Waypoint WP_1	38°56'42.6"	74°00'50.3"	853 meters
Waypoint WP_2	38°56'42.6"	73°57'37.4"	853 meters
Waypoint WP_3	38°56'42.6"	73°53'45.9"	526 meters
Waypoint WP_4	39°00'00"	73°53'45.9"	311 meters
Waypoint WP_5	39°00'00"	73°57'53.4"	0 meters
Facility a_1	38°52'53.0"	74°05'38.0"	0 meters
Facility a_2	38°05'56.9"	73°58'41.8"	0 meters
Facility b_1	39°05'56.9"	73°58'41.8"	0 meters
Facility b_2	38°47'28.3"	73°58'41.8"	0 meters

Table B.4

Straight-In Approach for VOR/DME Navigation Mode

	LAT	LON	ALTITUDE
Waypoints WP_1, WP_2, WP_3		Same as Table B.1	
Facility A	38°40'00"	73°34'15.9"	0 meters
Facility B	39°00'00"	73°08'31.8"	0 meters

Table B.5

90° Turn-to-Final Approach for VOR/DME Navigation Mode

	LAT	LON	ALTITUDE
Waypoints WP_1, WP_2, WP_3, WP_4, WP_5		Same as Table B.2	
Facility A	38°54'54.9"	74°41'21.0"	0 meters
Facility B	38°34'54.9"	73°52'11.1"	0 meters

Table B.6

180° Turn-to-Final Approach for VOR/DME Navigation Mode

	LAT	LON	ALTITUDE
Waypoints WP_1, WP_2, WP_3, WP_4, WP_5		Same as Table B.3	
Facility A	39°33'49.6"	73°53'45.9"	0 meters
Facility B	38°56'42.6"	74°19.28.9"	0 meters

REFERENCES

1. "SST Technology Follow-On Program, Phase II, ADEDS Functional/Software Requirements," FAA=SS-73-19, Dec. 1973.

2. "737-TCV Computer Program Listing," - NASA-Langley Research Center, Oct. 28, 1975.

3. McKinstry, R. Gill, "Guidance Algorithms and Non-Critical Control Laws for ADEDS and AGCS," the Boeing Company, Renton, Washington, March 18, 1974.

4. "Instrument and Navigation Equipment for the NASA-737," Appendix I-2-1, Boeing Aircraft Company, No Date.

5. Bobick, J.C. and Bryson, A.E., Jr., "Improved Navigation by Combining VOR/DME Information with Air or Inertial Data," SUDAAR No. 442, Stanford University, Stanford, California, May 1972.

6. Heine, W., "NAVAID Simulation," Technical Memorandum TM 5988-01, Systems Control, Inc. (Vt), Palo Alto, Calif., July 30, 1973.

7. Burrous, C.N., et al., "Preliminary Assessment of the Microwave Landing System Requirements for STOL Operations," NASA TM X-62,310, NASA Ames Research Center, Moffett Field, Calif., Oct. 1973.

8. Bryson, A.E., Jr., and Ho, Y.C., Applied Optimal Control, Blaisdell Publishing Co., Waltham, Mass., 1969.

9. "A New Guidance System for Approach and Landing," prepared by the SC-117 Radio Technical Commission for Aeronautics, Dec. 18, 1970.

10. "Approval of Area Navigation Systems for Use in the U.S. National Airspace System," FAA Advisory Circular AC 90-45A, Feb. 21, 1975.

NASA CR-145107
NASA CR-145108

DISTRIBUTION LIST
NAS1-14144

	No. Copies
NASA Langley Research Center Hampton, VA 23665	
Attn: Report & Manuscript Control Office, Mail Stop 180A	1
William D. Mace, Mail Stop 476	1
Robert L. Kenimer, Mail Stop 473	1
Dr. Thomas M. Walsh, Mail Stop 473	1
H. J. E. Reid, Jr., Mail Stop 494	1
James H. Schrader, Mail Stop 490	1
Billy L. Dove, Mail Stop 477	1
A. O. Lupton, Mail Stop 477	1
Terminal Configured Vehicle Program Office, MS 265	3
Terry A. Straeter, Mail Stop 125	1
John E. Hogge, Mail Stop 125	1
Dr. Roland L. Bowles, Mail Stop 125B	1
Robert T. Taylor, Mail Stop 246A	1
Lawrence R. Shultz, Mail Stop 473	5
NASA Ames Research Center Moffett Field, CA 94035 Attn: Mail Stop 202-3	1
NASA Dryden Flight Research Center P. O. Box 273 Edwards, CA 93523 Attn: Library	1
NASA Goddard Space Flight Center Greenbelt, MD 20771 Attn: Library	1
NASA Lyndon B. Johnson Space Center 2101 Webster Seabrook Road Houston, TX 77058 Attn: Library/JM6	1
NASA Marshall Space Flight Center Huntsville, AL 35812 Attn: Library, AS61L	1
NASA Lewis Research Center 21000 Brookpark Road Cleveland, OH 44135 Attn: Library, Mail Stop 60-3	1
Jet Propulsion Laboratory 4800 Oak Grove Drive Pasadena, CA 91103 Attn: Library, Mail 111-113	1

NASA CR-145107
NASA CR-145108

DISTRIBUTION LIST
NAS1-14144

	No. Copies
NASA John F. Kennedy Space Center Kennedy Space Center, FL 32899 Attn: Library, IS-DOC-1L	1
National Aeronautics & Space Administration Washington, DC 20546 Attn: KSA-10/Library RO/Lee D. Goolsby	1 3
U. S. Department of Transportation Federal Aviation Administration 800 Independence Avenue, SW Washington, DC 20591 Attn: ARD	1
NASA Scientific & Technical Information Facility P. O. Box 8757 Baltimore/Washington International Airport Maryland 21240	7 plus reproducible